The influence of incident waves on runup

A comparison between a phase-averaged and a phase-resolving XBeach model

A.F. de Beer

The influence of incident waves on runup

A comparison between a phase-averaged and a phase-resolving XBeach model

by

Anne de Beer

in partial fulfillment of the requirements for the degree of

Master of Science

in Hydraulic Engineering

at the Delft University of Technology,
to be defended publicly on Thursday October 26, 2017 at 3:00 PM.

Abstract

Wave runup is generated by energy which remains after wave breaking and travels farther to the coast in the form of a bore. It can be seen as a thin wedge of water running up the beach face (Brocchini and Baldock, 2008). Under storm conditions runup is responsible for beach and dune erosion and accurate runup predictions are therefore required (Ruggiero et al., 2001; Stockdon et al., 2005). For runup and its components, the time-mean setup component and the time-varying swash component, empirical parameterizations have been developed in the past, but they cannot be validated for storm conditions due to a lack of data (Stockdon et al., 2005). The data gap can be filled by numerically simulated runup, for example with the process-based XBeach model. XBeach is a depth-averaged model which predicts nearshore hydrodynamics and can be used in a phase-averaged or a phase-resolving mode. However, both the significant incident and infragravity swash is underpredicted by the phase-averaged XBeach Surfbeat model (Palmsten and Splinter, 2016; Stockdon et al., 2014), which does not resolve incident wave motions.

In order to predict runup under storm conditions with confidence the performance of XBeach under mild conditions should be assessed. Here runup simulated with XBeach Surfbeat and the phase-resolving XBeach Non-hydrostatic for the intermediate reflective beach of Duck was compared to measurements of the SandyDuck'97 experiment, where mild offshore conditions were present. A 2DH model was set up using measured bathymetry and forced with measured frequency-directional spectra. The hydrodynamics responsible for a difference in runup predictions between the two XBeach models were investigated and their origin in the cross shore was identified. It was shown that the prediction of significant incident and infragravity swash can be improved by using the phase-resolving XBeach Non-hydrostatic model instead of the XBeach Surfbeat model, while performance for setup remains similar. Incident swash predictions are improved by resolving the incident wave motions. The major part of the improvement in infragravity swash predictions is driven by differences in infragravity wave transformation between the two XBeach models. A small part also originates within the swash zone, for which incident bore merging can be a possible explanation. The difference in infragravity wave height predictions between the two XBeach models mainly develops in the surf zone where a different response to directional spreading and different degrees of shoaling most likely can explain the difference in infragravity wave height. Against expectations no correlation with the groupiness of the incident waves or with the phase difference between wave group and infragravity wave was found. A small part of the difference in infragravity wave height predictions is already present near the offshore boundary and probably results from interaction processes between high and low frequency wave boundary conditions.

It can thus be said that on intermediate reflective beaches, where both incident and infragravity waves play a role, the resolving of incident wave motions is a necessity to predict runup accurately. In these situations the phase-resolving XBeach Non-hydrostatic model should therefore be used, instead of the phase-averaged XBeach Surfbeat model. Here only an intermediate reflective beach and a small range of energetic conditions were included. More types of beaches and storm condition forcing should be investigated to be able to validate the empirical parameterizations but also to further indicate applicability ranges of the two XBeach models. Also, more attention should be paid to hydrodynamic differences at the boundary and in the surf zone in order to find more conclusive reasons for differences between the two XBeach models.

Acknowledgements

Contents

List of Figures

xi

List of Tables

Nomenclature

$\bar{A(t)}$	Mean of the wave envelope timeseries	m
α	Shoaling exponent	-
β	Normalized bed slope	-
β_f	Foreshore beach slope	-
$\Delta\psi$	Phase difference between the bound infragravity wave and the wave group	-
Δx	Grid size in x-direction	m
$\hat{\zeta}$	Amplitude variation of bound infragravity wave	m
η	Setup at the waterline	m
η_{hi}	High frequency water level timeseries generated at the XBeach boundary	m
η_{lo}	Low frequency water level timeseries generated at the XBeach boundary	m
η_{in}	Incoming water level timeseries	m
η_{out}	Reflected water level timeseries	m
$\frac{\sigma}{\mu}$	Measure of alongshore variability	-
γ	Breaker parameter	-
ω	Radial frequency	rad/s
ψ	Phase of frequency component	-
$\rho_{lf,hf}$	Coefficient of correlation between the bound infragravity wave and the wave group	-
σ_A	Standard deviation of the wave envelope timeseries	m
θ_{spread}	Directional spreading of the wave field	degrees
ξ	Iribarren parameter	-
A	Wave envelope timeseries	m
a	Amplitude of frequency component	m
B	Bias	m
b	Slope of the line of linear regression	-
C	Chezy coefficient	$m^{1/2}/s$
c_g	Group velocity	m/s
D	Difference-interaction coefficient	-
D_p	Direction at the peak frequency	degrees
$E_{f,\theta}$	Spectral density at frequency f and direction θ	$m^2/Hz/degree$
E_f	Spectral density at frequency f	m^2/Hz
E_{swash}	Spectral density of the swash spectrum	m^2/Hz
eps	Threshold water depth above which cells are considered wet	m
$f_{1,2,3}$	Frequency components in a triad wave-wave interaction	Hz
f_p	Peak frequency	Hz
f_{spread}	Frequency spreading of a wave field	Hz
g	Gravitational acceleration	m/s^2
GF	Groupiness factor	-
h	Water depth	m
H_0	Offshore wave height	m
$H_{m0,ig}$	Significant infragravity wave height	m
$H_{m0,in,ig}$	Incoming significant infragravity wave height	m
$H_{m0,in,inc}$	Incoming significant incident wave height	m
$H_{m0,in,tot}$	Incoming significant wave height	m
$H_{m0,inc}$	Significant incident wave height	m

H_{m0}	Significant wave height	m
$H_{rms,inc}$	Incident root mean square wave height	m
h_x	Bed slope	-
k	Wave number	m^{-1}
L_0	Offshore wave length	m
$maxbrsteep$	Maximum wave steepness upon breaking	-
n	Manning coefficient	-
R	Phase-averaged rate of transfer of energy from incident to infragravity waves	W/m^2
R^2	Coefficient of determination	-
$R_{2\%}$	2% runup level	m
$RMSE$	Root mean squar error	m
$rugdepth$	Runup gauge depth	m
S	Significant swash	m
S_{ig}	Significant infragravity swash	m
S_{inc}	Significant incident swash	m
$secbrsteep$	Secundary wave steepness upon breaking	-
$T_{m01,ig}$	Mean infragravity wave period	s
T_p	Peak period	s
u	Depth-averaged cross shore velocity	m/s

1

Introduction

1.1. Background

When incident waves travel from the ocean to the coast, they start breaking when the depth becomes limited. Most of their energy is dissipated in that process but a part is converted to potential energy in the form of a bore which propagates farther to the coast (Brocchini and Baldock, 2008). When the bore reaches the coastline, it collapses and its potential energy is converted to kinetic energy in the form of uprush on the beach. This can be seen as a thin wedge of water whose tip propagates up the beach face (Brocchini and Baldock, 2008). Besides incident waves also infragravity waves travel to the coast and either break or reflect, in both ways making a contribution to the wedge of water running up the beach (Baldock et al., 1997). The maximum height the thin wedge of water reaches on the beach face (above still water level) is called runup (Stockdon et al., 2005). The part of the beach in which this process takes place is called the swash zone, in between the surf zone and the beach.

Runup delivers much energy to the coast (Stockdon et al., 2005). This energy is, especially under storm conditions, responsible for beach and dune erosion (Ruggiero et al., 2001), but also for overtopping of structures (van der Meer and Stam, 1992), eventually leading to inundation of the areas behind. As a large part of the world's population lives in areas near the coast, these effects are very relevant and will become even more relevant due to sea level rise and climate change (Senechal et al., 2011). Therefore, runup is an important parameter for coastal planners and coastal engineers (Stockdon et al., 2005) and it is important to predict it accurately.

Much research has already been done into the nature of wave runup, and especially into predicting it. However, it still proves to be difficult to predict runup accurately. In this light Stockdon et al. (2005) has come up with an empirical parameterization to simply predict the maximum runup elevation based on a large set of data from a range of beaches, from reflective to dissipative. It was shown that runup is best parameterized when seperating it into its two dynamically different components: setup and swash. Setup is the time-averaged waterlevel elevation at the shoreline (Holthuijsen, 2007) and swash is the variation in time of vertical water level around the temporal mean level of the setup (Stockdon et al., 2005). Swash can be decomposed into an incident frequency and an infragravity frequency component. It seems that usually runup is dominated by energy in the infragravity band, as the incident band is saturated due to incident wave breaking. This happens especially on dissipative beaches and to a lesser extent on reflective beaches (Ruessink et al., 1998; Senechal et al., 2011; Stockdon et al., 2005; Thornton and Guza, 1982).

The parameterization developed by Stockdon et al. (2005) is based on results from low to intermediate energetic conditions as measurements of runup in storm conditions are not abundantly available, leading to unknown skill of the parameterization in storm conditions (Stockdon et al., 2014). Stockdon et al. (2014) addressed this by using the process-based numerical model XBeach Surfbeat to generate wave runup predictions for storm events. However, for an intermediate reflective beach (Duck, field experiment SandyDuck'97) runup is underestimated by XBeach Surfbeat: both incident and infragravity

swash are underestimated and setup is slightly overestimated. Similar trends were seen by Palmsten and Splinter (2016). The underestimation of the incident swash was expected, as XBeach Surfbeat does not resolve incident waves and incident swash, but the reason why setup and especially infragravity swash are not predicted accurately is not well known yet. Regardless of this, XBeach shows promising results for predicting runup.

Besides XBeach Surfbeat, the phase-averaged XBeach model, also XBeach Non-hydrostatic can be used to simulate runup. XBeach Non-hydrostatic is a phase-resolving XBeach model and solves all wave and swash components. The performance of XBeach for predicting runup might be improved by using XBeach Non-hydrostatic instead of XBeach Surfbeat. The fact that incident waves and swash are resolved, will probably increase the performance for incident swash significantly. Also, the phase relationship between the individual wave components is included in XBeach Non-hydrostatic, which is an important parameter influencing nonlinear interactions between different wave compontents (de Bakker et al., 2015). The nonlinear interactions transfer energy between wave components and in the surf zone a significant amount of energy is expected to go from incident to infragravity frequencies (Battjes et al., 2004; de Bakker et al., 2016). However, van Thiel de Vries (2009) showed that the phase difference between the incident wave group and the forced infragravity wave is overestimated by XBeach Surfbeat. It is expected that resolving phase information with XBeach Non-hydrostatic will lead to a more accurate representation of the nonlinear energy transfers. Generally, inclusion of the incident waves in XBeach Non-hdyrostatic is expected to lead to a more accurate prediction of setup, incident swash and infragravity swash.

1.2. Research objective

This research continues on work by Stockdon et al. (2005), Stockdon et al. (2014) and Palmsten and Splinter (2016). It is not well known why XBeach Surfbeat underestimates infragravity swash and overestimates setup and where in the cross shore this mismatch originates. Including incident waves will result in solving more processes and added phase information. This leads to the following research question:

Does phase-resolved modelling of incident waves with XBeach increase the predictive skill for wave runup and why (not)?

This question is split up in different subquestions:

- Is XBeach Non-hydrostatic capable of reproducing the runup data, specifically setup and infragravity swash, from an intermediate reflective beach better than XBeach Surfbeat?

- Does the difference in runup (mainly) originate from differences in hydrodynamics of the surf zone, the swash zone or the offshore boundary?

- What are the dominant processes leading to a difference in runup predictions?

1.3. Approach

To determine whether XBeach Non-hydrostatic is capable of reproducing runup data on an intermediate reflective beach better than XBeach Surfbeat a validation of the SandyDuck'97 data was performed. SandyDuck'97 is a field experiment on the beach of Duck, North Carolina, an intermediate reflective beach with mild to intermediate energetic conditions. A validation of wave height transformation, setup, incident swash, infragravity swash and the 2% runup level is done for both XBeach models. A 2DH model of Duck is used, the model grid generated with measured bathymetry and forced with measured frequency-directional spectra. From the validation of both XBeach models differences in runup prediction can be identified.

On the swash zone border the correlation is determined between the difference in runup and the difference in certain parameters between the two XBeach models likely to cause the difference, such as wave height, groupiness of the incident waves and the phase difference between the wave groups and the infragravity waves. This gives an indication of relevant processes leading to the difference in runup

predictions and whether the difference originates within the swash zone or outside of it.

From the above the hydrodynamic processes causing the runup difference between the XBeach models are identified. Their development at the offshore model boundary, in the surf zone and in the swash zone are followed in order to identify the exact location where and reason why XBeach Non-hydrostatic and XBeach Surfbeat deviate from each other. The approach followed is visualised in figure 1.1.
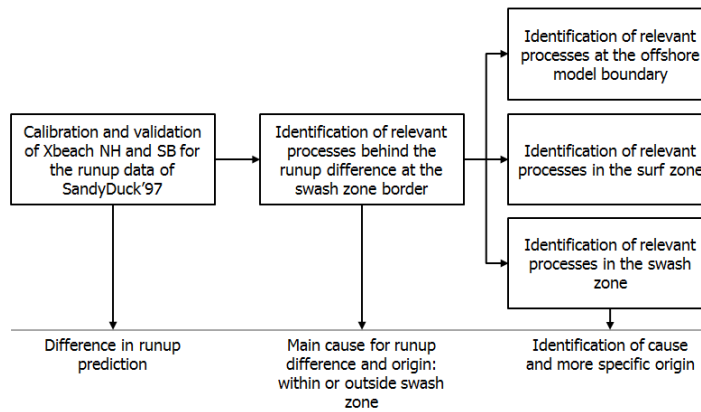
Figure 1.1: Overview of the approach followed.

1.4. Report outline

This thesis report is build up as follows:

Chapter 2: gives background information about hydrodynamics relevant for runup
Chapter 3: explains the methodology used
Chapter 4: contains an overview of the results of the XBeach validation of SandyDuck'97
Chapter 5: identifies causes for the runup difference and their origin in the cross shore
Chapter 6: investigates causes for the runup difference originating at the offshore model boundary
Chapter 7: looks into causes for the runup difference originating within the model domain
Chapter 8: gives the conclusions and recommendations to this thesis

Additional information can be found in the appendices A till M.

Background

2.1. Introduction

In this chapter background information is given which is necessary to understand the methods and concepts in this report. It is however assumed that the reader already has some prior knowledge about important concepts in coastal engineering. The swash zone and other zones in the cross shore will be briefly explained in section 2.2, followed by the definition of wave-induced runup in section 2.3. Not only the runup itself is important but also the mechanisms through which it is forced, which are discussed in section 2.4. Finally, the ways to predict runup and especially predicting runup numerically with XBeach is discussed in section 2.5.

2.2. The swash zone and the rest of the cross shore

Waves are generated offshore and travel towards shore. The cross shore they travel along can be divided into multiple parts. Offshore waves are generated by wind (Bosboom and Stive, 2015). The nearshore region can be subdivided into the shoaling zone, where waves grow in amplitude and become asymmetric towards the point of breaking, and the surfzone, where waves are breaking. Finally the swash zone is the part where waves lose their last energy in the form of runup on the beach (Brocchini and Baldock, 2008). This subdivision can be seen in figure 2.1.
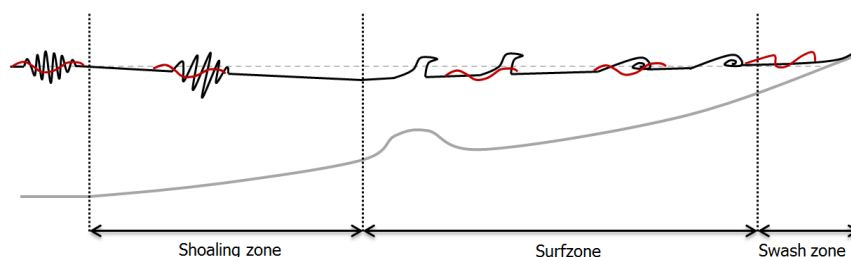
Figure 2.1: The cross shore subdivided in its regions and the relevant wave processes for each part. Black indicates the short waves and wave groups, red indicates the long waves.

The swash zone is the upper part of the beach, in between surfzone and back beach (Brocchini and Baldock, 2008). Exact definitions of the swash zone differ between authors. By Short (1999) it is defined as the area in between the lower limit of rundown and the upper limit of runup. The location of the swash zone can therefore change in time, due to for instance the tide. Puleo and Butt (2006) define the seaward border of the swash zone as the location of bore collapse. However, on steep beaches this works better than on mild beaches as there often is a pronounced point of bore collapse. Also, on mild slopes there always is a thin layer of water on the foreshore, making it difficult to define where the swash zone actually begins. The swash zone can be characterised by intermittency: the moving shoreline leads to regions which are alternating wet and dry (Brocchini and Baldock, 2008). In

this report the definition of Short (1999) is followed, as this is relatively easy to determine from the XBeach model output.

The behaviour of wave and runup processes on a beach is determined by its relative steepness (Battjes, 1974; Ruessink et al., 1998; Stockdon et al., 2005; Wright and Short, 1984) (the slope of the beach relative to the steepness of the incoming waves, indicated by the Iribarren parameter ξ). The two extremes are a reflective beach or a dissipative beach. A reflective beach is characterized by a relatively steep beach face and waves of low steepness (long waves with a small amplitude) (Bosboom and Stive, 2015). Dissipative beaches, on the other end, have a wide and flat beach face. This is the result of high and short waves which start breaking far offshore. The surfzone is thus wide. The beach considered in this research is Duck (North Carolina), which is an intermediate reflective beach (in between the two end states).

2.3. Wave-induced runup

Runup is defined as the maximum vertical extent of wave uprush on a beach above still water level (Stockdon et al., 2005) and is caused by the fact that waves still have energy left when reaching the shoreline. Runup can be divided into two dynamically different processes: a mean part and a oscillating part, setup η and swash S respectively (Stockdon et al., 2005), see figure 2.2.

The arrival of waves at the shoreline results in a cyclic pattern of runup and rundown (van Rooijen, 2011), swash, around the mean setup. This can be seen as a thin wedge of water whose tip propagates up and down the beach face (Brocchini and Baldock, 2008). The cycle caused by one single wave is referred to as the swash cycle, consisting of two phases: uprush and backwash (Brocchini and Baldock, 2008). During the uprush phase the flow velocity of the water wedge decreases until reaching zero (due to bottom friction and gravity). This is the moment the water has reached its maximum height, referred to as the maximum runup, flow reversal takes place and the water starts moving back: the backwash phase. During the backwash the flow diverges, reducing the runup height further. The backwash flow velocity increases, until the next wave arrives and thus the next swash cycle starts.
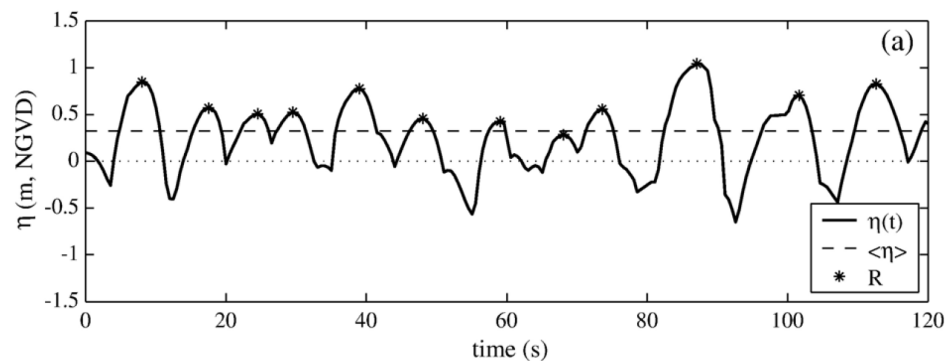
Figure 2.2: Water level elevation at the shoreline, subdivided into setup and swash (Stockdon et al., 2005). $<\eta>$ indicates the setup, R the individual runup maxima and η the swash. The water level elevation is in vertical direction, relative to NGVD.

Setup is the elevation of the mean water level at the waterline (Stockdon et al., 2005) and is driven by the breaking of waves and the resulting cross-shore gradient in radiation stress (Holthuijsen, 2007). Swash is the time-varying location of the border between the sea and the beach, so the local instanteneous shoreline (Stockdon et al., 2005). When a single wave is approaching the coast the swash motion follows a parabolic trajectory (Brocchini and Baldock, 2008). However, always a train of waves approaches the beach, leading to interaction between the uprush and backwash. Swash can be subdivided into an incident and an infragravity frequency part, or a fast and slow oscillating part. They are forced by incident and infragravity waves respectively. Depending on the steepness of the beach the swash is either dominated by incident or infragravity energy (Ruessink et al., 1998). On dissipative beaches, most of the incident waves have broken in the surfzone and the shoreline is dominated by

infragravity energy. At reflective beaches, there is still much incident energy left at the shoreline and this is dominant. At intermediate beaches, such as Duck, both incident and infragravity energy play a role.

$$S = \sqrt{S_{inc}^2 + S_{ig}^2} \qquad\qquad (2.1)$$

2.4. The forcing of wave-induced runup

2.4.1. High frequency, or incident, waves

On the ocean relatively short irregular waves are generated by local wind fields (Holthuijsen, 2007). This wave field consists of an infinite amount of wave components: one individual harmonic wave component can be defined by a sine curve with a certain phase and amplitude. Together all these wave components form a irregular high frequency wave field (Holthuijsen, 2007). These high frequency waves can travel long distances across the ocean to the coast and deliver their energy there. In that process they become more regular due to frequency and directional dispersion: wave fields spread out as different wave components travel with different speeds (depending on their frequency) and different directions (Holthuijsen, 2007). In this report high frequency waves, defined here as waves with a frequency larger than 0.05 Hz, will be referred to as incident waves.
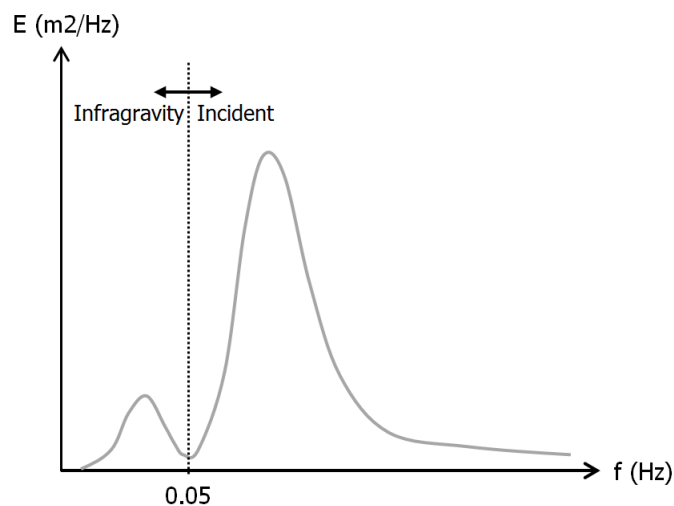
Figure 2.3: An example of a frequency spectrum. A division can be made between the low frequency (infragravity) part of the spectrum and the high frequency (incident) part. In this report the split frequency used is f = 0.05 Hz.

A wave field can be represented by its frequency-directional spectrum. This spectrum indicates how much variance (or energy) is contained in each frequency and directional component (Holthuijsen, 2007). Basically the wave field is split up in its harmonic components and the variance is defined for each component. The narrower the spectrum, the more regular the waves are. Also, for shorter waves (with a higher frequency) the spectrum will be shifted to the right while for longer waves with a lower frequency the spectrum will be shifted to the left (Bosboom and Stive, 2015). An example of a frequency spectrum can be seen in figure 2.3. The same can be done for a directional spectrum.

Between wave components of a slightly different frequency interference can occur, strengthening each other at some points and weakening each other at others and a wave group is formed, see figure 2.4 a (Bosboom and Stive, 2015). The energy of the waves is carried by the group, not by the individual waves. The wave groups propagate with the group velocity c_g which is slower than the individual wave celerity in deep water. For regular waves as in figure 2.4 a a clear wave group can be distinguished
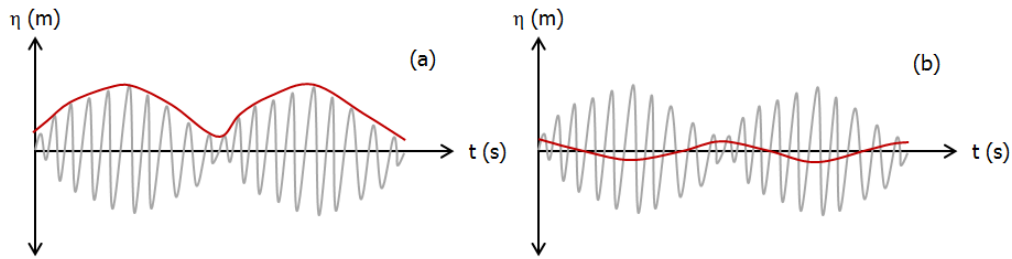
Figure 2.4: Example of a wave group and its bound infragravity wave. (a) Wave group (in grey) and its envelope (red). (b) Wave group (in grey) and its bound infragravity wave (in red).

but for irregular waves the wave groups are less clear.

When the waves come closer to shore the depth becomes smaller and the waves start feeling the bottom. The speed and the length of the waves decreases and they become higher, called shoaling (Holthuijsen, 2007). Besides shoaling waves also become skewed and asymmetric close to shore: the wave crest becomes peaked while the trough flattens and the wave face becomes steeper (Holthuijsen, 2007). This goes on until the wave becomes too steep and breaks, at the point where the wave height is a certain portion of the water depth defined by the breaker index γ (Bosboom and Stive, 2015). γ generally is around 0.8.

2.4.2. Low frequency, or infragravity waves

In the shoaling zone the wave components in a wave group can interact with each other through difference interactions to create a bound infragravity wave (de Bakker et al., 2015). This bound infragravity wave has the same length as the wave group but a much smaller amplitude (Longuet-Higgins and Stewart, 1962). The fact that it is bound means that it travels with the speed of the wave group, c_g. The bound infragravity wave is out of phase with the wave group: its crest is aligned with the trough of the wave group, see figure 2.4 b. The shoaling rate of infragravity waves is much higher than for incident waves (Battjes et al., 2004) and during shoaling the bound infragravity wave lags behind in time with the wave group (Battjes et al., 2004). When the incident waves start to break the groupiness disappears. The bound infragravity wave is released and travels further to shore as a free infragravity wave (with a wave celerity according to the dispersion relationship) (Longuet-Higgins and Stewart, 1962).

Just as the energy of the incident waves can be dissipated, the energy of infragravity waves can be dissipated. Three mechanisms are known: dissipation through enhanced effects of bottom friction in shallow water, nonlinear interactions between infragravity and incident waves and breaking of infragravity waves. On sandy beaches dissipation through bottom friction is assumed not to be dominant (van Dongeren et al., 2007). Infragravity wave breaking is induced by energy being transferred to higher infragravity frequencies forming higher infragravity harmonics (infragravity-infragravity interactions), which causes them to steepen and break (de Bakker et al., 2016). Infragravity energy can also be transferred to incident frequencies (infragravity-incident interactions), resulting in dissipation of the infragravity wave. These last two mechanisms both are the result of nonlinear interactions, which will be discussed extensively in the next section. The dominant mechanism again depends on site characteristics (de Bakker et al., 2016): on dissipative beaches infragravity wave breaking dominates (Inch et al., 2017). On reflective beaches, where incident energy dominates, nonlinear incident-infragravity interactions are dominant (Henderson et al., 2006; Thomson et al., 2006).

Not all infragravity energy is dissipated and part reflects from the coast. The degree of reflection depends on the relative steepness of the beach. The longest infragravity waves reflect the most but the reflection coefficient is always smaller than 1 (Battjes et al., 2004; Guedes et al., 2013). For large reflection coefficients a standing wave structure develops for the infragavity waves (Inch et al., 2017).

This usually happens on a reflective beach, while on a dissipative beach most infragravity energy is dissipated.

2.4.3. Contribution of incident and infragravity waves to swash

After incident waves have broken in the surf zone, their remaining energy travels farther towards the shoreline in the form of a bore (Brocchini and Baldock, 2008). When the bore meets the local instantaneous shoreline the bore front and the water behind it quickly accelerate and the bore collapses. Its potential energy is transferred to kinetic energy of a thin wedge of water, whose tip progagates up the beach, creating incident swash. During the uprush phase the energy is transferred back to potential energy. Infragravity swash can either be caused by the water surface level excursion of a reflected infragravity wave (can be a cross shore standing infragravity wave) or due to infragravity wave breaking (infragravity bores) (Baldock et al., 1997; Raubenheimer et al., 1995). On reflective beaches dominated by incident energy the main driver of swash is the collapsing of incident bores, while on dissipative beaches dominated by infragravity energy swash is driven by infragravity motions (Ruessink et al., 1998).

2.4.4. Interaction between incident and infragravity waves

Wave components of different frequencies, such as the incident and infragravity waves, can interact with each other through nonlinear interactions, transferring energy to each other (Holthuijsen, 2007). In the nearshore the most relevant nonlinear interactions are the triad interactions, occuring between three wave components. Interactions can occur either through sum or difference interactions. Sum interactions transfer energy to higher harmonics ($f_3 = f_1 + f_2$) and difference interactions transfer energy to lower frequencies ($f_3 = f_1 - f_2$, responsible for generating the bound infragravity wave). The magnitude of the energy transfer depends on the phase and directional differences of the three wave components involved.

The nonlinear interactions are important for transferring energy either between multiple incident wave components, between incident and infragravity wave components or between multiple infragravity components (de Bakker et al., 2015). According to Battjes et al. (2004) net time-averaged energy fluxes between bound infragravity waves and the primary incident waves are only possible when they are not completely out op phase, but an additional phase lag is present ($\Delta \psi$). When a larger phase lag is present more energy can be transferred. In direction of the shore the additional phase lag increases.

The different kinds of interactions as described above occur at different locations in the nearshore (de Bakker et al., 2015), see also figure 2.5:

- Shoaling zone: sum interactions transfer energy from the peak frequency to multiples of the peak frequency ($2f_p$), creating higher harmonics. These higher harmonics are linked to the generation of wave skewness and asymmetry during shoaling and breaking. Difference interactions create bound infragravity waves.
- Outer surf zone: energy is transferred from the peak frequency to its higher harmonics and to the infragravity band.
- Inner surf zone: the peak at $2f_p$ decreases and its energy is transferred to the infragravity peak. Also weak infragravity-infragravity interactions can be seen here.
- Near the shoreline: interactions between infragravity components transfer energy to higher frequencies, creating higher infragravity harmonics which eventually lead to breaking of the infragravity waves. No interactions between incident waves can be seen anymore.

Above holds for a mild sloping beach. For steeper slopes infragravity-infragravity interactions can only occur near the shoreline (de Bakker et al., 2016). Near the shoreline also interactions between incident and infragravity frequencies can occur, transferring energy to the incident band, instead of infragravity wave breaking. The degree of nonlinear interactions increases for higher energetic conditions (Inch et al., 2017), a narrower spectrum (de Bakker et al., 2015) or a smaller directional spread (Herbers et al., 1994). Another indication that in the surf zone energy is transferred to the infragravity waves is the shoaling rate of infragravity waves: this is much higher than for incident waves. This is only

possible when energy is transferred to the infragravity waves (Battjes et al., 2004).
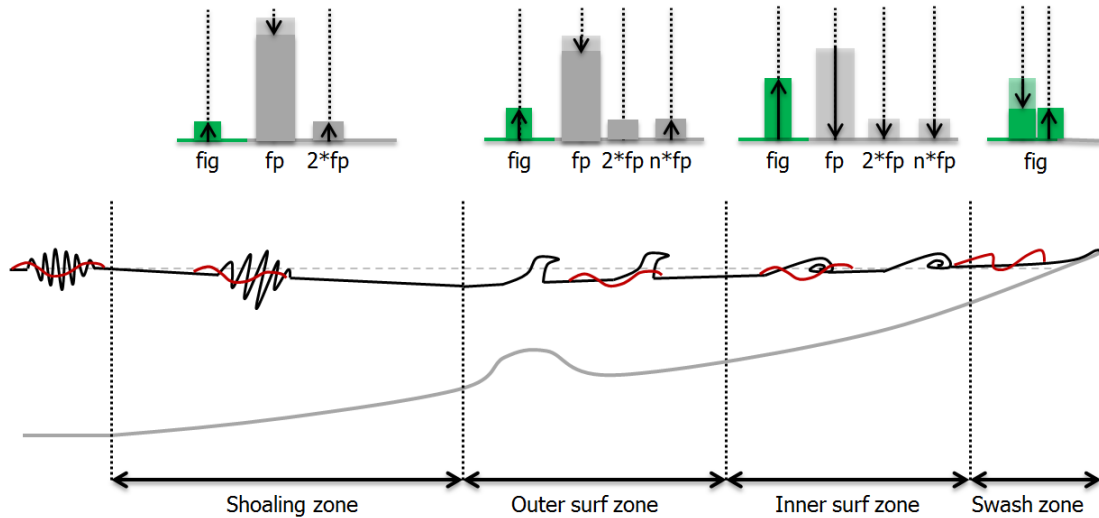
Figure 2.5: Location of different nonlinear interactions in the cross shore (for a mild sloping beach). For each part of the cross shore the changes in the spectrum due to nonlinear interactions are schematically depicted, with fig the infragravity frequencies and fp the peak frequency. Incident wave (-groups) are indicated in black, infragravity waves in red.

2.5. Predicting runup

2.5.1. Empirical formulations

Many empirical relations for predicting runup have been developed in the past, mainly linking runup to offshore wave height H_0 or the Iribarren number ξ_0. Stockdon et al. (2005) has improved former empirical relationships by using a data set of 10 field experiments representing a wide range of beach and wave conditions and by seperately parameterizing setup and swash. The beaches examined ranged from dissipative to reflective and the wave conditions were in the range of low to intermediate energetic conditions. One of the beaches in the data set is Duck. Stockdon et al. (2005) showed that runup could not be parameterized only using the offshore wave height H_0, but that also offshore wave length L_0 and the foreshore beach slope β_f should be included. The general bulk formula for runup on all beaches in the data set is the following (built up out of seperate parameterizations for setup, incident swash and infragravity swash):

$$R_{2\%} = 1.1(0.35\beta_f(H_0L_0)^{1/2} + \frac{(H_0L_0(0.563\beta_f^2 + 0.004)^{1/2}}{2}) \tag{2.2}$$

A clear dependence on $\beta_f(H_0L_0)^{1/2}$ can be seen. The parameterization performs well for the full range of beaches but its performance under storm conditions can not be validated due to a lack of runup data under storm conditions. A more general form of the equation above is shown below and indicates that the 2% runup level consists of the setup and the swash (Stockdon et al., 2005).

$$R_{2\%} = 1.1(\bar{\eta} + \frac{S}{2}) \tag{2.3}$$

2.5.2. Numerical modelling

A solution for the lack of runup data under storm conditions is to numerically simulate runup using a process-based model like XBeach. In Stockdon et al. (2014) and Palmsten and Splinter (2016) runup simulations with XBeach were compared to data, with the ultimate goal to improve the parameterization of Stockdon et al. (2005) and make it suitable for storm conditions.

The XBeach model XBeach is an open-source process-based numerical model which simulates hydrodynamic and morphodynamic processes and impacts on sandy coasts (Roelvink et al., 2009 2010). Hydrodynamic processes such as incident wave transformation (refraction, shoaling and breaking) infragravity wave transformation (generation, propagation and dissipation) and wave-induced setup are included. The included morphodynamic processes are not relevant for this research. The model can be used in 1D and 2D and is depth-averaged (1DH and 2DH). XBeach has multiple modes of which the relevant ones for this study are XBeach Surfbeat and XBeach Non-hydrostatic. In figures and tables XBeach Non-hydrostatic is referred to as NH, XBeach Surfbeat as SB.
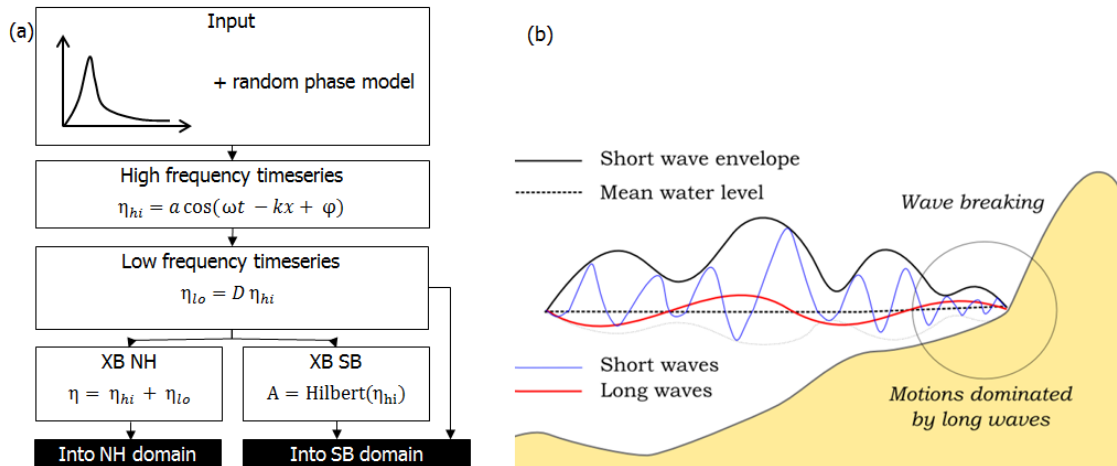
Figure 2.6: The XBeach models. (a) Process of boundary condition generation for both XBeach models (van Dongeren et al., 2003). (b) Relevant wave processes in XBeach Non-hydrostatic and XBeach Surfbeat (Roelvink et al., 2010). XBeach Surfbeat solves the short wave envelope and the long waves while XBeach Non-hydrostatic solves the short and long waves.

XBeach Surfbeat is a phase-averaged model and solves the incident wave energy variation (on wave group scale) seperately from infragravity waves (Roelvink et al., 2010). The variations on wave group scale drive infragravity waves through radiation stress gradients. The incident wave energy variation is solved with the wave action balance while the infragravity water level elevation is solved with the nonlinear shallow water equations. Individual incident waves and their phase are thus not solved. Only infragravity swash is solved. XBeach Surfbeat is fully valid on dissipative beaches, where the incident waves almost all break in the surf zone.

XBeach Non-hydrostatic does solve the individual incident waves and is a phase-resolving model (Roelvink et al., 2010). Both incident and infragravity waves are solved with the nonlinear shallow water equations including non-hydrostatic pressure (Roelvink et al., 2010). The hydrostatic front approximation is used to improve the location of wave breaking, where the pressure under breaking bores is assumed to be hydrostatic (Smit et al., 2013). Both incident and infragravity swash are solved by XBeach Non-hydrostatic.

There is a small difference in the generation of the boundary conditions between XBeach Non-hydrostatic and XBeach Surfbeat (van Dongeren et al., 2003), see figure 2.6 a. From the input spectrum a high frequency water level timeseries η_{hi} is constructed with a random phase model. From η_{hi} a low frequency timeseries η_{lo} is constructed with help of the difference-interaction coefficient D of Herbers et al. (1994). For XBeach Non-hydrostatic η_{hi} and η_{lo} are added together and sent into the domain. In the case of XBeach Surfbeat the envelope A of η_{hi} is constructed with the Hilbert transformation and sent into the domain along with η_{lo}.

Performance of XBeach for runup So far only XBeach Surfbeat has been used for predicting runup. Stockdon et al. (2014) has validated XBeach Surfbeat for the runup data of SandyDuck'97,

an intermediate reflective beach under low to intermediate energetic conditions. XBeach Surfbeat predicts the wave height transformation over the surfzone well, although a lot of scatter is present. The model performs well for setup, but significantly underestimates significant incident and infragravity swash. The underestimation of incident swash by XBeach Surfbeat is expected, as the incident frequency motions are not resolved. These findings are confirmed by Palmsten and Splinter (2016), who compared a 1D XBeach Surfbeat model with a flume test with storm condition forcing. However, infragravity wave heights were overestimated near shore while infragravity swash was underestimated.

<div align="right">

3

</div>

Methodology

3.1. Introduction

The methodology used to answer the research question is described in this chapter. A desciption of the field data set from SandyDuck'97 is given in section 3.2, followed by the way the XBeach Non-hydrostatic and XBeach Surfbeat model were set up in section 3.3, and calibrated and validated in section 3.4. After that the methods used to identify important parameters for explaining the runup differences are layed out in section 3.5.

3.2. Description of SandyDuck'97

3.2.1. The FRF site at Duck

As explained in chapter 1 the data set which has been used in this research is that of SandyDuck'97. This is the same data set as was used in the validation of XBeach Surfbeat by Stockdon et al. (2014). Duck is a beach in North Carolina, USA bordering the Atlantic Ocean. It is located at the outer side of a small strip of land, see figure 3.1 a. As can be seen in the figure Duck is a fairly alongshore uniform beach. It is an intermediate reflective beach, with an average foreshore beach slope β_f of 0.10 (Stockdon et al., 2005). At Duck the Field Research Facility (FRF) is based, a coastal observatory, and multiple nearshore field experiments have been carried out there (besides SandyDuck'97 also DELILAH and Duck94), with the goal of improving fundamental understanding and modeling of surf zone physics (FRF, 2004). The FRF site can be seen in figure 3.1 b. The measurements for SandyDuck'97 started on September 22th 1997 and lasted for 6 weeks. The data used in this report is from the period October 3-31.
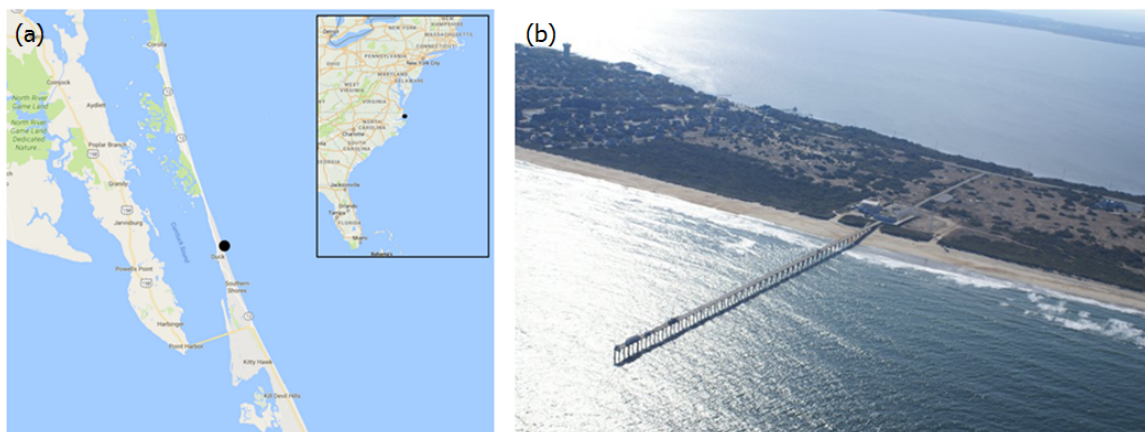
Figure 3.1: (a) Location of Duck. (b) FRF site at Duck (FRF, 2004).

3.2.2. Methods & locations

Over 30 experiments were carried out during SandyDuck'97. The data of the experiments relevant in this report are:

- Offshore frequency-directional spectrum measurements
- Measured tidal waterlevels
- Measured bathymetry
- Waveheight transformation over the surfzone
- Runup measurements

Some of the data listed above were used to force the XBeach models with, others were used to compare the model output with. Below a short description is given of how the data was gathered, for more information one is referred to FRF (2004). In figure 3.2 the location of the measurements is shown.
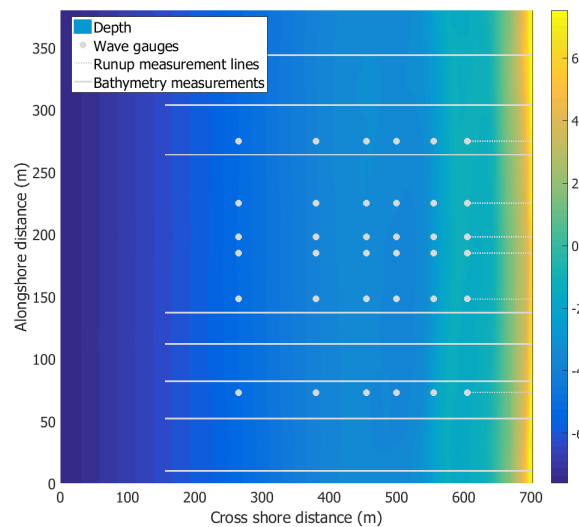
Figure 3.2: Locations of different output locations in XBeach, which are the same as measurement locations during SandyDuck'97. 36 pressure gauges and 6 runup gauges were present, resulting in 36 point output locations and 6 runup gauges in XBeach. In this figure also the location of the bathymetry measurements is shown. Note that the coordinates are in XBeach coordinates (x-coordinate increasing towards shore) while originally measurements were done in FRF coordinates (x-coordinates increasing when going offshore).

Offshore waves   Offshore wind wave frequency-directional spectra were measured at the 8m array (an array of 15 bottom mounted pressure gauges at the 8-m contour). 8 spectra are available for each day. The spectra were measured between frequencies of 0.044 and 0.318 Hz. They are characterized by low to medium energetic conditions and fairly shore normal incidence. The mean significant wave height H_{m0} is 0.96 m with a σ of 0.60 m. The mean direction D_p at the peak frequency is 3.83 degrees from shore normal with a σ of 19.19 degrees. The mean peak frequency f_p is 0.11 Hz with a σ of 0.041 Hz. The change of the above described parameters over the full month of October can be seen in figure 3.3. A small storm with wave heights up to 3.5 m occured around October 18. A positive angle of incidence indicates waves coming in from the North.

Tide   The tide was measured at a tide gauge located at the seaward end of the FRF pier (see figure 3.1 b) at a depth of approximately 8 m. The tide heights were measured every 6 minutes relative to NGVD (NGVD 29, the vertical datum used to measure elevation and depression relative to mean sea level, established in the United States in 1929 (Wikipedia, 2016)). In figure 3.4 b the tide as measured at the pier in about 8 meters depth is shown. The tidal range is about 1 m.
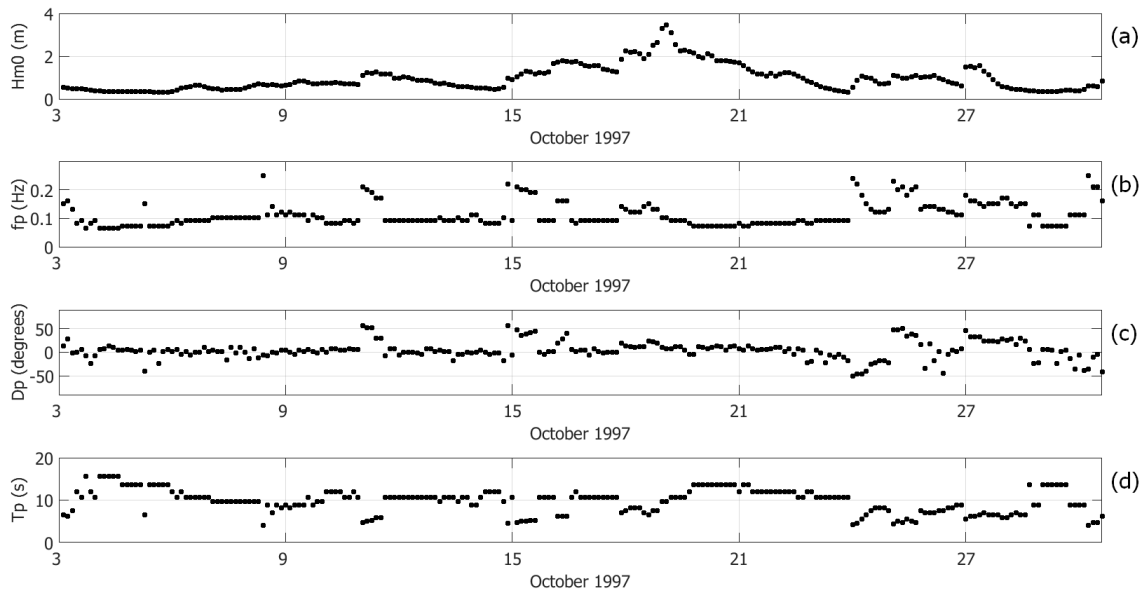
Figure 3.3: Observed offshore wave conditions during the SandyDuck'97 field experiment. (a) The significant wave height. (b) The peak frequency. (c) The peak direction. (d) The peak period. A positive angle of incidence indicates that waves are coming from the North.
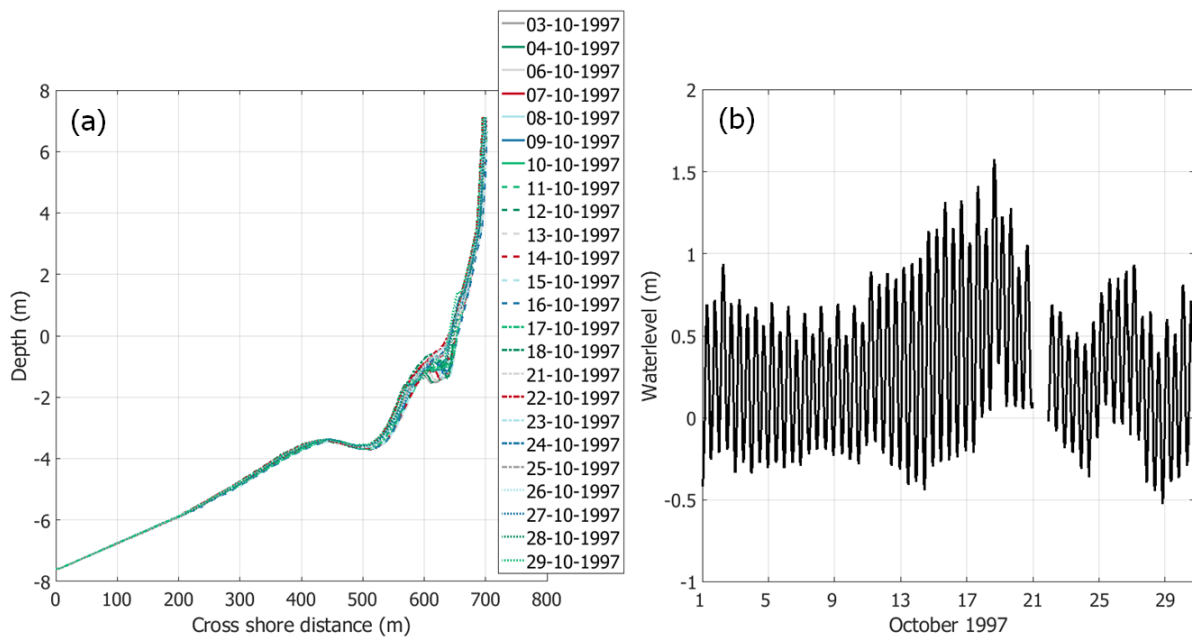
Figure 3.4: (a) The measured bathymetry between October 3 and October 30 during the SandyDuck'97 field experiment. The measurements are relative to NGVD. (b) The measured tidal waterlevels during the field experiment. The measurements are relative to NGVD. Half the days of October 21 and 22 no measurements are available.

Bathymetry   The CRAB, an instrumented sled, was used to measure the bathymetry around the area in which all the measuring instruments were situated (called the minigrid). For this minigrid the XBeach Surfbeat model in Stockdon et al. (2014) and the XBeach Non-hydrostatic and Surfbeat model in this research were set up. The bathymetry was measured daily in 20 cross shore lines, of which 8 fall within the XBeach domain. It was measured in local FRF coordinates (approximately from $x = 50$ to 500 m, with $x = 50$ at the dune base).The bathymetry measured during the field experiment showed a barred

system with one bar at about 50 meters from the waterline and a second bar at about 200 m from the waterline, see figure 3.4 a. The second bar is of fairly constant shape during the experiment, while the nearshore bar shows some variation in bar height and crest location. For example, the nearshore bar moved offshore during the storm of October 18-22. The bathymetry was measured once a day but not for all days the bathymetry data is complete.

Wave height transformation Significant incident wave heights in the surfzone were computed from sea surface elevations in the frequency band 0.05 to 0.25 Hz measured at 36 pressure gauges (6 transects in the alongshore with six points in the cross shore each, ranging from a mean depth of 5.3 m to a mean depth of 1.5 m (FRF, 2004)) for record lengths of 17 min. This was already done by Stockdon et al. (2014). For the significant infragravity wave height the pressure timeseries at the 36 pressure gauges were transformed into water level timeseries, see appendix K, and the significant infragravity wave height was computed in the frequency band 0 to 0.05 Hz.

Runup measurements Runup measurements were performed at 6 alongshore locations using video (Stockdon et al., 2005), see figure 3.5. At the 6 cross shore transects pixel intensity was sampled over 17 minutes record lengths. The leading edge of runup was digitized from these pixel intensities and converted to a timeseries of water level elevation relative to mean sea level. Data timeseries of 17 minutes were used to minimise the effect of changing tide on the location of wave breaking and the area of the foreshore over which swash propagates. The runup timeseries were converted to runup statistics, such as the setup and the significant swash, by Stockdon et al. (2005). In this research the runup statistics data has been used, not the raw timeseries. The runup statistics data is available for every hour between noon and 9 PM at 6 alongshore locations but not everyday at all times and all locations.
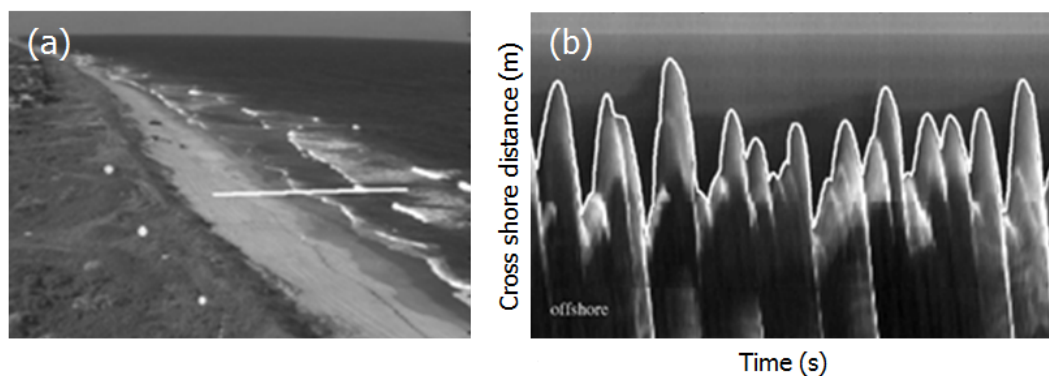
Figure 3.5: (a) One of the cross shore transects at Duck (Stockdon et al., 2005). (b) The digitized leading edge of the swash in one of the cross shore transects (Stockdon et al., 2005)

3.3. XBeach model setup

The measured bathymetry, tide and offshore frequency-directional spectra were used to set up a XBeach Non-hydrostatic and a XBeach Surfbeat model of Duck (about 700 meters in the cross shore and 350 meters in the alongshore). A short description of the model setup is given below, in appendix A more information can be found.

As explained earlier, the significant wave height and the runup statistics were computed from data timeseries of 17 minutes duration. To be able to compare model output and post processed data well, all XBeach simulations were set up with a duration of 17 minutes as well, each simulation of 17 minutes matching a data timeseries of 17 minutes at a specific day and a specific time. 5 minutes were added to the run time to give the model time to spin up. These five minutes were later removed from the output.

Grid & bathymetry   For each day the bathymetry data was complete the bathymetry data were transformed into bathymetry files for XBeach (a x-grid, a y-grid and a depth file). The x- and y-grid were kept constant for all days, to make postprocessing of the model output easier.

The bathymetry was measured in local FRF coordinates, meaning the x-coordinate increases when going offshore. A grid which is suitable for XBeach should be defined the other way around, with x-coordinates increasing towards shore. Therefore, the bathymetry data had to be flipped in order to generate a XBeach bathymetry. Also, the resolution in x-direction on which the bathymetry was measured varied for the different cross shore transects. A varying x-grid was generated which was then kept constant for all cross shore transects. The varying x-grid was mainly based on considerations about numerical diffusion:

- Numerical diffusion: in order to limit numerical diffusion at least 20 points per wave length should be used (Zijlema, 2015). The minimum T_{m01} of all measured spectra was used to calculate the wave length and 30 points per wave length were used to account for shorter waves. The resulting grid size is the maximum grid size which can be used.

- The miminum grid size was set to 0.10 m.

From these considerations a x-grid with a resolution ranging from Δx of 1 m offshore to 0.25 m near the waterline resulted. This was combined with a y-grid of constant resolution of 5 m. On this grid the measured depth was interpolated. The maximum depth of the measurements was -5.7 m relative to MSL. The grid for the XBeach Surfbeat model as used by Stockdon et al. (2014) was extended until a depth of -7.8 m, therefore the grid in this research was also extended until that depth. In this way the depth at the offshore model boundary approximately coincides with the depth at which the frequency-directional spectra were measured. The first three grid cells have a constant depth and also in alongshore direction the depth is uniform close to the offshore boundary.

Tide   The tidal water levels at relevant times were isolated from the full tidal water level timeseries. Each 17 minute XBeach simulation was matched with the tide at that specific time. During the simulation a constant tidal waterlevel was used, as the tidal difference in 17 minutes is very limited (1-2 cm).

Waves   The measured frequency-directional spectra are available every 3 hours while runup measurements are available every hour. To be able to force each XBeach simulation with the closest wave spectrum, the measured spectra were linearly interpolated. For example, runup data is available at 11 AM while measured spectra are available at 10 AM and 1 PM. The spectra are represented by a matrix of 29 frequencies and 91 directions and their respective spectral density $E_{f,\theta}$ (the spectral density at frequency f and direction θ). The interpolated spectra can be constructed by linearly interpolating the spectral densities at each frequency and each direction between consecutive measurement times:

$$E_{f,\theta-1100} = E_{f,\theta-1000} + \frac{E_{f,\theta-1300} - E_{f,\theta-1000}}{3} \qquad (3.1)$$

The performance of the linear interpolation was checked by computing the root mean square error between significant wave height at the 8m array and the most offshore pressure gauges, resulting in a root mean square error of 0.064 m for the original frequency-directional spectra and 0.067 m for the interpolated frequency-directional spectra. Also, the statistics as presented in section 3.2.2 are similar for the original and the interpolated frequency-directional spectra. More details can be found in appendix A.

Output locations   The output locations in the XBeach models were chosen such that they coincide with the measurement locations as in the experiment. During SandyDuck'97 significant wave heights were measured at 36 locations (a 6 by 6 grid of pressure gauges) and runup was measured at 6 alongshore locations. As the x-coordinates are defined positive the other way in XBeach than in local FRF coordinates also the locations of the output locations had to be flipped. Their location in the XBeach grid can be seen in figure 3.2. To check whether the conversion of the output locations to

XBeach coordinates went well the distance from the output location to the waterline was computed for both coordinate systems, resulting in equal distances, see appendix A.

Output processing   Significant wave height was calculated from the water level timeseries at the 36 output locations. From the water level timeseries a spectrum was made and the variance m_0 was calculated using the same integration bounds as were used for the data processing (for incident wave height 0.05 - 0.25 Hz and for infragravity wave height 0 - 0.05 Hz).

$$H_{m0,inc} = 4 \cdot \sqrt{\int_{0.05}^{0.25} E(f)df} \tag{3.2}$$

$$H_{m0,ig} = 4 \cdot \sqrt{\int_{0}^{0.05} E(f)df} \tag{3.3}$$

The setup η was computed from the water level timeseries at the waterline, removing the tide to exclude effects of changing tide on the runup statistics. From the waterlevel timeseries relative to the tidal water level the mean is taken, which is equal to the setup in that simulation of 17 minutes.

To compute the swash again the tide is removed from the water level timeseries at the waterline. The swash spectrum is generated and integrated between 0 and 0.05 Hz to get the significant infragravity swash S_{ig} and from 0.05 Hz onwards to get the significant incident swash S_{inc}. This border between incident and infragravity energy is the same as used in Stockdon et al. (2014).

$$S_{inc} = 4 \cdot \sqrt{\int_{0.05}^{\infty} E_{swash}(f)df} \tag{3.4}$$

$$S_{ig} = 4 \cdot \sqrt{\int_{0}^{0.05} E_{swash}(f)df} \tag{3.5}$$

To compute the 2% runup level the cumulative probability density function is taken of the local maxima in the water level timeseries at the waterline. Only maxima which lie above the still water level (in this case the tidal water level) are taken into account. The 2% runup level is the runup level with an exceedence probability of 2%.

The output processing for XBeach Surfbeat is slightly different as incident and infragravity waves are outputted seperately. Calculation of the infragravity wave height is the same as for XBeach Non-hydrostatic. For the incident wave height the incident root mean square wave height can be computed from the incident wave energy to which the high frequency tail of the infragravity water level timeseries has to be added:

$$H_{m0,inc} = \sqrt{(\int_{0.05}^{0.25} E(f)df)^2 + (\sqrt{2}H_{rms,inc})^2} \tag{3.6}$$

3.4. Calibration & validation of the XBeach models
3.4.1. Calibration
The XBeach Non-hydrostatic model was calibrated with bottom friction, breaking parameters and runup gauge depth. The aim in the calibration was to get the wave height transformation in the surfzone as good as possible, assuming this is the most important parameter for predicting runup accurately. The runup itself was not extensively calibrated for, as this is the parameter of interest. However, some parameters such as the bottom friction may have a big influence on the runup and therefore their influence was investigated. Also, in Stockdon et al. (2014) it was shown that the XBeach Surfbeat model is sensitive to the choice of the runup gauge depth, the minimum depth which is used to determine the last wet point in the runup gauge (Roelvink et al., 2010). Therefore the model was calibrated for

this parameter as well. For XBeach Surfbeat a briefer calibration was done, as parameter values were taken from Stockdon et al. (2014). An overview of the steps in the calibration for both models can be found in figure 3.6 and 3.7. A top-down approach was adopted with consecutive calibration of bottom friction and breaking parameters. The bottom friction calibration then was repeated to check whether the formulation and parameter value found before are still the best ones. Three XBeach simulations were used to calibrate the models with. The simulations were chosen such that they represent a variety of wave conditions based on wave height and wave steepness:

- Average wave height with a small wave period: $H_{m0} = 1.19$ m and $T_p = 5.83$ s
- Average wave height with a large wave period: $H_{m0} = 1.16$ m and $T_p = 10.72$ s
- Large wave height: $H_{m0} = 2.11$ m and $T_p = 8.16$ s

In the XBeach model different bottom friction formulations are available of which some are depth independent and some are depth dependent. In the calibration three different bottom friction formulations were used: Chezy, Manning and White-Colebrook. Chezy is depth independent, while Manning and White-Colebrook are depth dependent. It is expected that the choice for either a depth dependent or independent bottom friction formulation will have a large influence on the runup, as a depth dependent formulation will lead to enhanced friction in the shallow waters of the swash zone. The effect of this depth dependency was investigated and a choice for either a depth dependent or independent bottom friction was made based on which one stirs the setup and significant swash in the right direction. For both the Chezy and the Manning formulation 11 values of their respective bottom friction parameter (C and n) were tested, for White-Colebrook only one as this already showed no significant improvement. The performance of the different values and formulations was indicated with the root mean square error in the significant wave height over all 36 output locations. After the wave breaking parameters were calibrated all bottom friction values were tested again, to see if the value found at first is still the best one.

The breaking parameters used in the calibration of XBeach Non-hydrostatic are maxbrsteep and secbrsteep. These parameters influence the performance of the hydrostatic front approximation, in which the pressure distribution under breaking bores is assumed to be hydrostatic (Roelvink et al., 2010; Smit et al., 2013). Maxbrsteep gives the wave steepness from which on a grid point is considered to be hydrostatic and wave breaking is initiated. Grid points neighboring the hydrostatic grid point can be considered hydrostatic already at a lower wave steepness, enhancing wave breaking. This secondary wave steepness is given by secbrsteep. The breaking parameter used in the calibration of XBeach Surfbeat is γ. The values for the respective breaker parameters are varied. For XBeach Non-hydrostatic first the optimum maxbrsteep is chosen, after which secbrsteep is calibrated. As the breaking parameters will only influence the wave height transformation near the shore, the performance of the different values of maxbrsteep, secbrsteep and γ are judged by taking the root mean square errors in the significant wave height in the output locations closest to shore.

The parameter rugdepth indicates the minimum depth which is used to determine the last wet point in the runup gauge (Roelvink et al., 2010). The runup measurements of SandyDuck'97 also have a kind of runup gauge depth: the video measurements of runup do not measure the waterline at a depth of exactly 0 but always at a certain small depth. Calibrating the runup gauge depth in the XBeach model makes sure the waterline is considered at a comparable depth, indicated by the best performance of the model for runup. For XBeach Non-hydrostatic three values of the runup gauge depth were tested. This means that for an increasing value of rugdepth the predicted waterline lies lower and thus values for setup and swash are lower. The value of rugdepth which performs best (smallest root mean square error) for setup and significant swash together is chosen.

For more information about the calibration of the XBeach models one is referred to appendix B and C.
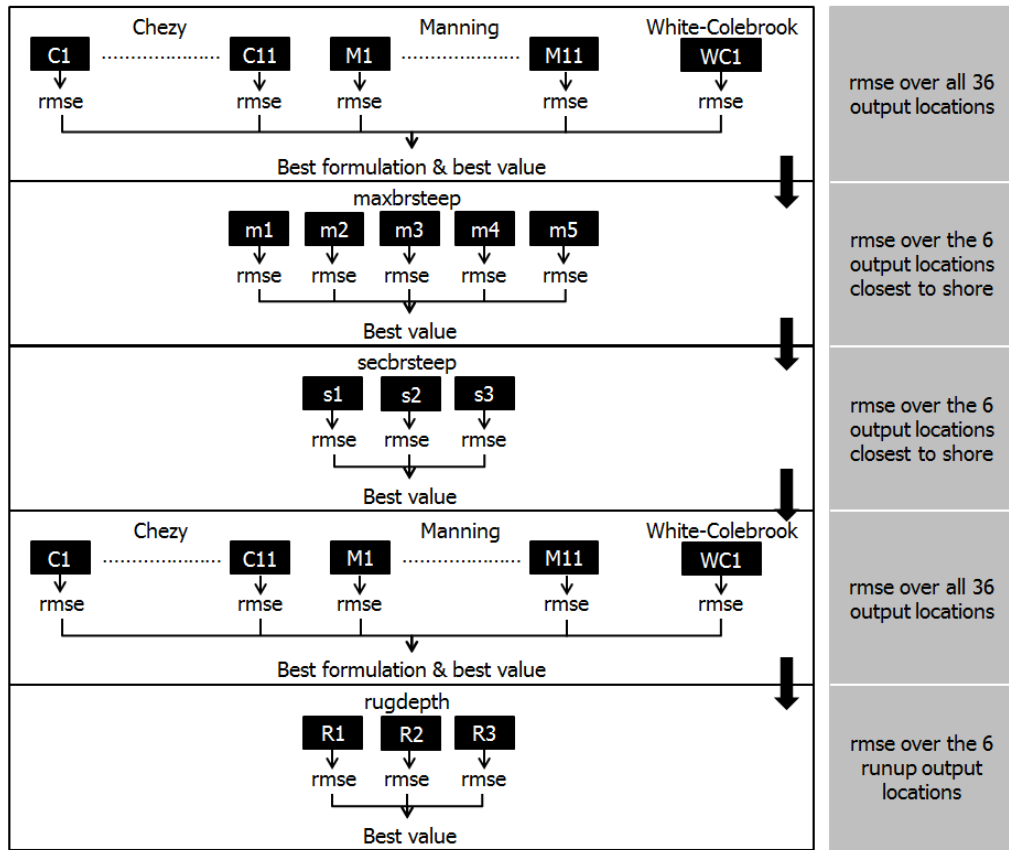
Figure 3.6: Steps in the calibration of the XBeach Non-hydrostatic model.
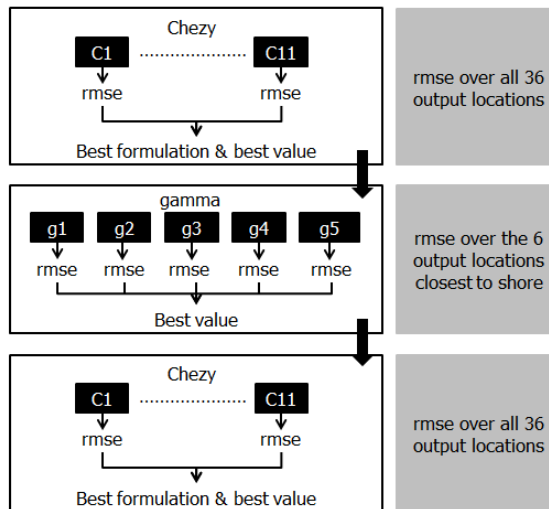
Figure 3.7: Steps in the calibration of the XBeach Surfbeat model.

3.4.2. Validation

After calibrating both XBeach models a validation is done for incident and infragravity wave height transformation over the surf zone, setup, significant incident swash, significant infragravity swash and the 2% runup level. In total 156 XBeach simulations were used for both models, of which 105 were used to validate wave height transformation and 89 to validate runup (as not for each moment in time both wave height and runup data are available). This means that 3780 wave height and 534

runup measurements were compared to model output. The following statistics are used to describe the performance of the XBeach models:

- Root mean squared error (RMSE)
- Coefficient of determination (R^2)
- Slope of best-fit linear regression line (b)
- Bias (B)

These specific statistics were chosen as they were used to describe the performance of the XBeach Surfbeat model in Stockdon et al. (2014). The formulations used for the statistics can be found in appendix D. Two comparisons are made in the validation: between the XBeach Non-hydrostatic and the XBeach Surfbeat model set up in this study and between the XBeach Surfbeat model set up here and the XBeach Surfbeat model of Stockdon et al. (2014). As different runup gauge depths were used for the XBeach Non-hydrostatic model here and the XBeach Surfbeat model of Stockdon et al. (2014) two XBeach Surfbeat models were used: one with the runup gauge depth equal to the XBeach Non-hydrostatic model and one with a runup gauge depth equal to the XBeach Surfbeat model of Stockdon et al. (2014). Relevant differences between the XBeach Surfbeat model set up here and the XBeach Surfbeat model used by Stockdon et al. (2014) are the use of single dir (propagating wave energy over the mean direction, thereby preserving groupiness (Roelvink et al., 2010)) and the use of less validation cases here due to missing bathymetry data. The results of the validation can be found in chapter 4.

3.5. Identification of driving processes behind the runup difference

From the validation of the XBeach models a difference in runup prediction can be seen. This difference can originate at the boundary, in the surf zone or in the swash zone. Outside the swash zone the following parameters could cause the difference:

- A difference in wave height transformation between the models, both the incident and the infragravity wave height transformation.
- A difference in the groupiness of the incident waves.
- A difference in the predicted phase difference between the incident wave group and the forced infragravity wave (important for the nonlinear energy transfers).

To determine which of these parameters plays a role in explaining the difference between the two XBeach models the following is done:

1. At the edge of the swash zone the difference in the respective parameter between XBeach Non-hydrostatic and XBeach Surfbeat is determined. This is done for one alongshore location as there is little alongshore variability. The swash zone border is chosen as it will indicate whether the largest differences in the model occur within the swash zone or outside of it.
2. At the same alongshore location the difference in runup (setup, significant incident swash and significant infragravity swash) is determined between XBeach Non-hydrostatic and XBeach Surfbeat.
3. The difference in respective parameter is plotted against the difference in runup for all the validation simulations. If a large coefficient of correlation is found between them, it indicates that this parameter is an important one for explaining the difference between XBeach Surfbeat and XBeach Non-hydrostatic.

One alongshore location is selected approximately in the middle of the domain and where both wave height and runup data are available. It was chosen to look at only one alongshore location as the coast is fairly alongshore uniform. The alongshore variability in wave height ($\frac{\sigma}{\mu}$, following the approach of Stockdon et al. (2005)) is small and stays constant over the cross shore: 0.07 for XBeach Non-hydrostatic and 0.05 for XBeach Surfbeat. Besides, alongshore variability is not the topic of this reseach.

3.5.1. Definition of the swash zone border

The location of the swash zone is different for all XBeach simulations due to the changing tide, making it impossible to define a swash zone border position fixed in space. For each XBeach simulation, both Non-hydrostatic and Surfbeat, the location of the swash zone border is determined as follows (assuming the swash zone border is at the point of maximum rundown):

- At all gridpoints in x-direction at the chosen alongshore location the minimum water level elevation during the simulation is determined. For XBeach Non-hydrostatic this follows directly from the water level timeseries. For XBeach Surfbeat the water level timeseries is only the result of the infragravity waves. However, the swash is usually dominated by infragravity swash and therefore the use of the infragravity swash zone border will be sufficient. Also, as setup is predicted similar but swash predicted larger by XBeach Non-hydrostatic, see chapter 4, the point of maximum rundown for XBeach Non-hydrostatic always has a smaller x-coordinate than for XBeach Surfbeat.
- The bottom level at the grid point is subtracted, this results in the minimum water depth during the simulation.
- At each grid point it is checked whether the minimum water depth is larger or smaller than the value of eps (0.005 m, the threshold water depth above which cells are considered wet (Roelvink et al., 2010)). If the minimum water depth is larger than eps, the grid point is wet during the entire simulation. If the minimum water depth is smaller than eps, the grid point is alternating wet and dry during the simulation.
- The swash zone border is considered to be the grid point x_i which is wet during the entire simulation with the next grid point x_{i+1} being alternating wet and dry. The gridpoint which is wet all the time is chosen because otherwise output will only be generated by the XBeach models part of the time.

The determination of the swash zone border is visualized in figure 3.8. The x-coordinate of the XBeach Surfbeat swash zone border is slightly larger than the x-coordinate of the XBeach Non-hydrostatic swash zone border (average difference of 2.68 m). Therefore the XBeach Non-hydrostatic swash zone border is used for both models, such that the respective grid point is always wet in both models.
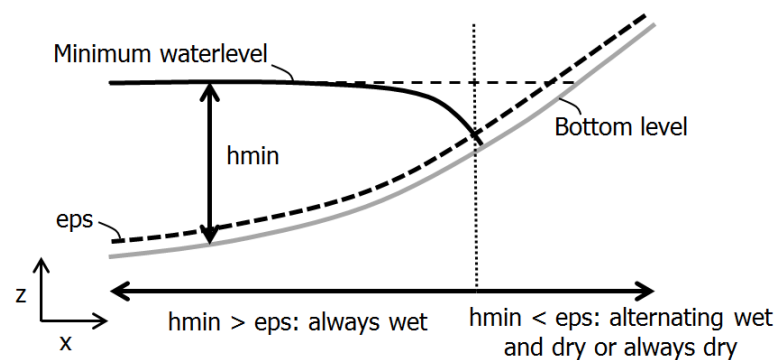
Figure 3.8: Visualisation of the determination of the swash zone border. The minimum depth during a simulation is determined as the difference between the minimum water level and the bottom level. When this value is larger than eps, the grid point is wet during the entire simulation. When it is smaller than eps the grid point is alternating wet and dry or always dry.

3.5.2. Splitting in- and outgoing waves

Only incoming waves are considered, as it is expected that reflected waves do not influence runup anymore. The method of Guza is used to seperate incoming and reflected waves (Guza et al., 1984), which is a method suitable for a 1D wave field. However, a 2D method for seperating waves is complicated and introduces errors of unknown size. It is expected that the Guza method will give fairly good results close to shore where waves are mainly cross shore dominated while leading to larger errors

offshore. Incoming and reflected water level timeseries can be computed as follows:

$$\eta_{in} = \frac{\eta c_{out} + uh}{c_{in} + c_{out}} \tag{3.7}$$

$$\eta_{out} = \frac{\eta c_{out} - uh}{c_{in} + c_{out}} \tag{3.8}$$

The Guza method can either be executed in time space or in Fourier space. In time space yields the most exact results while in Fourier space some smoothing errors are introduced. To be able to use the method in time space requires the waves to be in shallow water with a group speed of $\sqrt{gh}$. When taking the shallow water limit as $h < \frac{L}{20}$ and defining L with the zero down crossing method, it shows that for the XBeach Non-hydrostatic model 35% of the waves at the swash zone border are not yet in shallow water. This means the seperation of the incoming and reflected waves at the swash zone border (and further offshore) should be done in Fourier space, instead of in time space. A full description of the Guza method is given in appendix E. From the incoming water level timeseries the incoming infragravity wave height, the incoming incident wave height and the incoming total wave height are computed:

$$H_{m0,in,total} = 4 \cdot \sqrt{\int_0^\infty E(f)df} \tag{3.9}$$

$$H_{m0,in,inc} = 4 \cdot \sqrt{\int_{0.05}^\infty E(f)df} \tag{3.10}$$

$$H_{m0,in,ig} = 4 \cdot \sqrt{\int_0^{0.05} E(f)df} \tag{3.11}$$

3.5.3. Groupiness of the incident waves

The groupiness of the incident waves is determined as suggested by List (1990) with the groupiness factor GF:

$$GF = \frac{\sqrt{2}\sigma_A}{\bar{A(t)}} \tag{3.12}$$

σ_A is the standard deviation of the incident wave envelope timeseries and $\bar{A(t)}$ is its mean. GF is a number between 0 and 1, with a value of 1 indicating much groupiness and a value of 0 no groupiness at all. Usually an Hilbert transformation is used to get the envelope, but close to shore the waves are too nonlinear for the Hilbert transformation to give good results. Instead, a Hilbert-Huang transformation is used, a method suitable for nonlinear and non-stationary processes (Huang and Chen, 2005; Veltcheva and Soares, 2016). Besides the groupiness at the swash zone border, the transformation of the groupiness over the cross shore is computed. For a description of the Hilbert-Huang transformation one is referred to appendix F. The Hilbert-Huang transformation has to be used on the incoming incident water level timeseries, which is retrieved from the total incoming water level timeseries by low-pass filtering the infragravity waves (below f = 0.05 Hz) out of it. For XBeach Surfbeat it is not necessary to perform a Hilbert-Huang transformation as the model directly outputs the wave height envelope. To compare it to results of the Hilbert-Huang transformation for XBeach Non-hydrostatic it should be divided by two to get the wave amplitude envelope. In the infragravity water level output a small high frequency tail is present but it was shown that this has a negligible effect on the total envelope (on average a difference of less than 0.01 m on the total envelope).

3.5.4. Phase difference between the wave group and the infragravity wave

The phase difference between the wave group and its forced infragravity wave is an indicator of the intensity of nonlinear energy transfers between them. According to van Thiel de Vries (2009) the phase difference can be indicated by the coefficient of correlation between the wave envelope timeseries and

the infragravity water level timeseries, which will hereafter be referred to as $\rho_{lf,hf}$. A $\rho_{lf,hf}$ of -1 indicates the two are exactly out of phase, which should be the case offshore when the infragravity waves are bound to the incident waves. However, offshore $\rho_{lf,hf}$ will be slightly larger than -1 due to free infragravity waves. Towards the shore the incident waves break and the wave group forcing disappears. The infragravity waves are released and propagate faster than incident waves. $\rho_{lf,hf}$ increases towards the shore and becomes positive around the point of incident wave breaking. Close to shore a positive $\rho_{lf,hf}$ indicates that the highest incident waves travel on top of the infragravity wave crests. The approach as described above was tested by comparing it to the phase difference as defined by Battjes et al. (2004) for a theoretical wave envelope and forced infragravity wave timeseries, see figure 3.9 and 3.10 a. Battjes et al. (2004) defined the phase difference $\Delta\psi$ as the lag of the trough of the infragravity wave behind the crest of the wave envelope: offshore this results in $\Delta\psi = 0$ and close to shore in $\Delta\psi = \pi$. From the figures it can be seen that the method of van Thiel de Vries (2009) not only works for the extreme ends of completely in or out of phase: also in between there is a gradual increase of $\rho_{lf,hf}$. Using the envelope of the incident wave group, as described in the previous section, and the incoming infragravity water level timeseries, the coefficient of correlation between these two timeseries can easily be computed.
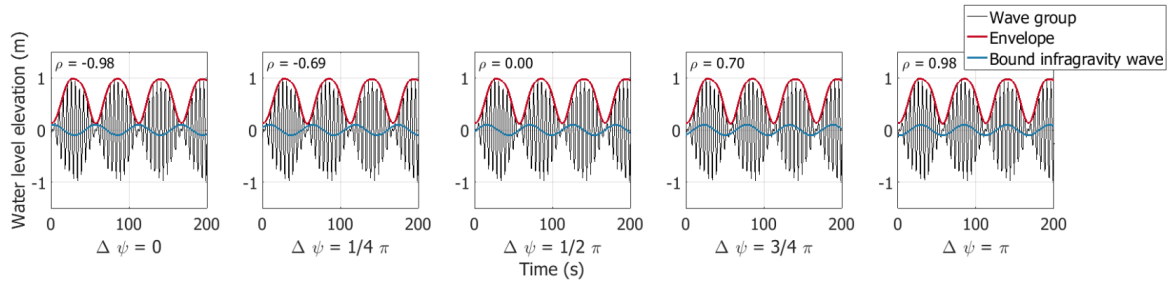
Figure 3.9: Comparison of two definitions of the phase difference. For different values of $\Delta\psi$ ρ indicates the value of $\rho_{lf,hf}$ between the envelope of the wave group and the bound infragravity wave.
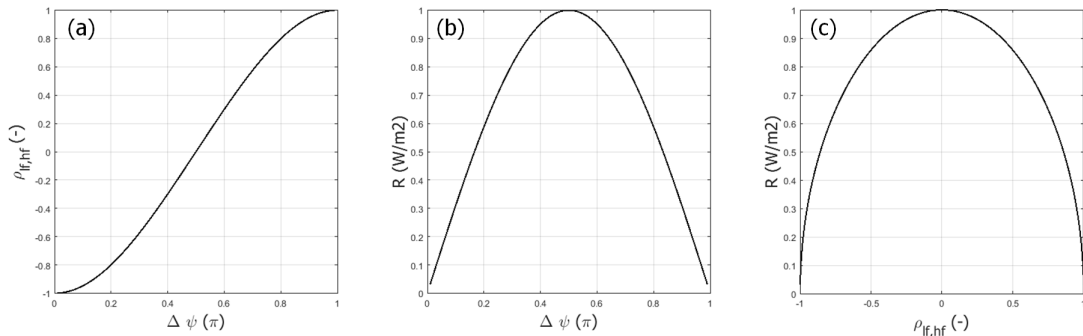
Figure 3.10: The relation between different definitions of the phase difference and the energy transfer into infragravity waves. (a) Relation between $\Delta\psi$ and $\rho_{lf,hf}$. (b) Relation between $\Delta\psi$ and R. (c) Relation between $\rho_{lf,hf}$ and R.

Also according to Battjes et al. (2004) the phase difference $\Delta\psi$, and thus $\rho_{lf,hf}$ can be related to the energy transfer R from the incident waves into the infragravity waves through the following relation:

$$R = \frac{1}{2}\kappa\hat{U}\hat{S}\sin\Delta\psi \sim \sin\Delta\psi \tag{3.13}$$

The theoretical relation between R and $\Delta\psi$ can be seen in figure 3.10 b and with the relation between $\Delta\psi$ and $\rho_{lf,hf}$ also the relation between R and $\rho_{lf,hf}$ can be drawn, see figure 3.10 c. Over the part of

the cross shore where $\rho_{lf,hf}$ is negative (offshore of the point of incident wave breaking) theoretically a positive correlation should be found between $\rho_{lf,hf}$ and R, and thus between $\rho_{lf,hf}$ and the growth in infragravity wave height.

3.5.5. Isolation of the swash zone

At the swash zone border the correlation between the difference in parameters such as wave height, groupiness and the phase difference and the difference in runup was computed. To prove that a parameter with a high correlation is the cause of a difference in runup, an isolated model of the swash zone is made and forced with different values of the parameter in question, see figure 3.11. Also hydrodynamic differences developing within the swash zone can be identified in this way. A 1D XBeach Non-hydrostatic model of the swash zone is made, by isolating grid cells from the swash zone border onwards on one cross shore transect from the large XBeach Non-hydrostatic model. The isolated model has to be forced with water level and velocity timeseries, as forcing with a spectrum in that shallow water is not possible. The boundary conditions for the isolated model are generated as follows:

1. A 1D XBeach model of the full cross shore is forced with measured frequency-directional spectra. Water level and velocity timeseries are extracted at the swash zone border.
2. These timeseries are adapted such that they represent different values of the parameter in question.
3. The adapted water level and velocity timeseries are used to force the isolated model of the swash zone with.

A 1D model of the swash zone is used, as forcing a 2D XBeach model with timeseries is not easily done and on the swash zone border everything is cross shore dominated. A full description of the isolation of the swash zone can be found in appendix J.
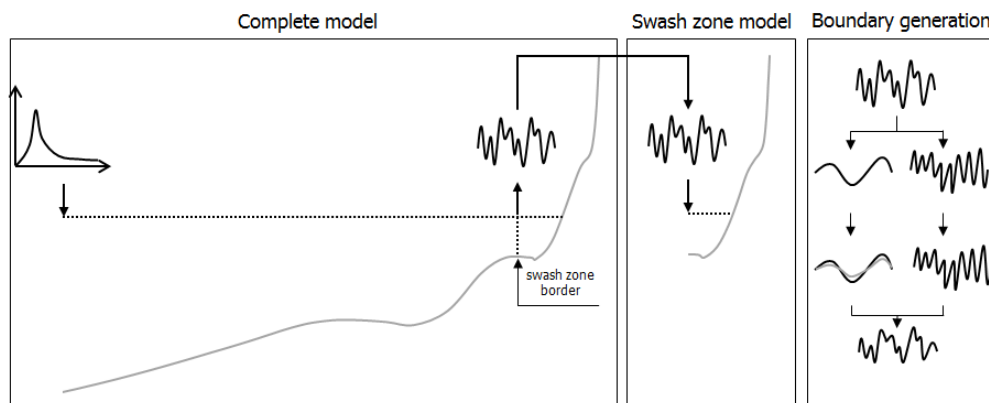
Figure 3.11: Visualisation of the isolation of the swash zone. A large 1D model is forced with a measured frequency-directional spectrum. At the swash zone border water level and velocity timeseries are extracted, which are used to force the swash zone model with.

3.5.6. Directional and frequency spreading

The directional and frequency spreading of the wave field, θ_{spread} and f_{spread} respectively, are determined from the frequency-directional spectrum. A simple definition of the spreading is adopted, following Long (2017). The full frequency-directional spectrum is integrated either over all frequencies or over all directions to create a single directional or frequency spectrum. The peak of the spectrum and its half power, half of the peak, are determined. The spreading is defined as the distance between the two intersection points of the spectum with its half power. The same approach is used for directional and frequency spreading. An example can be seen in figure 3.12 and more information can be found in appendix G.
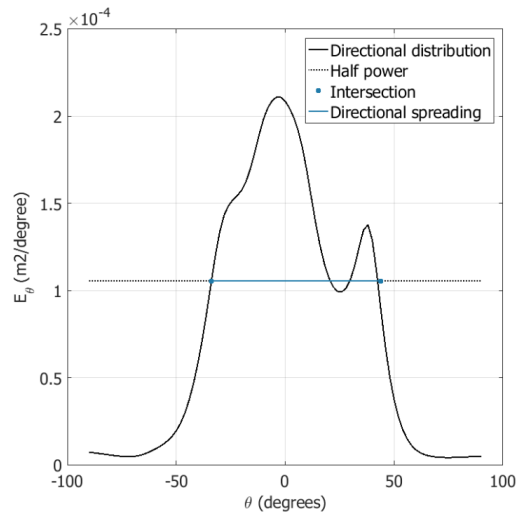
Figure 3.12: Approach used to determine directional spreading.

3.5.7. Generation of boundary conditions

Differences between the XBeach Non-hydrostatic and Surfbeat model can also be caused by a difference in boundary condition generation. As explained in section 2.5.2 XBeach Non-hydrostatic generates a water level timeseries from the forcing spectrum which is then sent into the domain, while XBeach Surfbeat generates the wave envelope timeseries of the incident waves and a water level timeseries of the infragravity waves. Whether differences in hydrodynamics originate from these different methods is investigated in two ways. A write statement is added to the XBeach code, which writes the high and low frequency water level timeseries generated at the boundary to a file, such that they can be compared for the two XBeach models. Also, simple test cases are performed to check for differences in hydrodynamics close to the boundary. These test cases consist of a 1D grid or an alongshore uniform 2D grid and a narrow JONSWAP spectrum with different degrees of directional spreading. A full list of the test cases used and their goal and setup can be found in appendix L.

Performance of XBeach Non-hydrostatic and XBeach Surfbeat for SandyDuck'97

4.1. Introduction

In this chapter the results of the calibration and validation of the XBeach Non-hydrostatic and XBeach Surfbeat model for the field data set of SandyDuck'97 are presented. The models are validated for incident and infragravity wave height transformation over the cross shore and runup: setup, significant incident swash, significant infragravity swash and the 2% runup level. A full description of the results of the calibration can be found in appendix B and C. Two comparisons are made: between the XBeach Non-hydrostatic and the XBeach Surfbeat model set up in this research and between this XBeach Surfbeat model and the one used by Stockdon et al. (2014). To be able to do that most parameters in the XBeach Surfbeat model are kept the same as in Stockdon et al. (2014). However, the runup gauge depth resulting from the calibration of XBeach Non-hydrostatic is different from the one used in Stockdon et al. (2014). Therefore two XBeach Surfbeat models were used: one with a runup gauge depth similar to the XBeach Non-hydrostatic model and one with a runup gauge depth similar to the XBeach Surfbeat model of Stockdon et al. (2014).

`
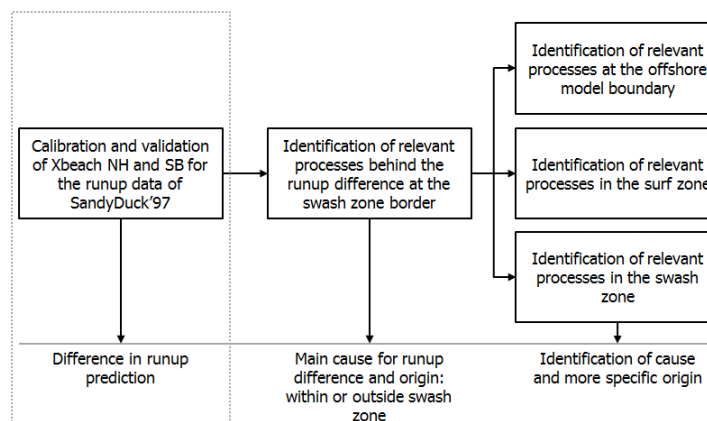
4.2. Calibration of the XBeach models

4.2.1. XBeach Non-hydrostatic

The XBeach Non-hydrostatic model was calibrated for bottom friction, breaker parameters and the runup gauge depth. For the bottom friction the depth independent bottom friction formulation of Chezy was chosen, with a value of C of 57 $m^{1/2}/s$. The depth dependent formulations of Manning and White-Colebrook were investigated but they resulted in a lower prediction of the significant swash

than a depth independent formulation. As XBeach Surfbeat already underestimated significant swash (Stockdon et al., 2014), these were not preferred.

It proved difficult to find one value for the maximum wave steepness upon breaking which performed well for all three calibration simulations and all locations in the cross shore. For example, one value of the maximum wave steepness might give a very good performance in the array of output locations closest to shore but a bad performance in one output location further from shore (where the waves are just breaking or just not). Another value of the maximum wave steepness might do it the other way around. The value of the maximum wave steepness which performed best for the output locations closest to shore was chosen. In this point the waves are usually breaking and the value of the maximum wave steepness has the most influence on the model performance. The same was done for the value of the secundary wave steepness.

In Stockdon et al. (2014) it was shown that XBeach Surfbeat is sensitive to the choice of runup gauge depth, which is the case for XBeach Non-hydrostatic as well. Predictive capability of the model for setup increased with a higher runup gauge depth, while the predictive capability for significant swash went down. The best value for the three runup statistics overall was chosen. The calibration resulted in a value of C of 57 $m^{1/2}/s$, a value for the maximum wave steepness upon breaking of 0.4, for the secondary wave steepness of 0.2 and for the runup gauge depth of 0.05 m.

4.2.2. XBeach Surfbeat

As explained in chapter 3 one of the aims of the XBeach Surfbeat model is to check whether the results as presented by Stockdon et al. (2014) can be reproduced. In order to be able to do this, most parameters are kept equal to those used in that model. Parameters which were either not reported in Stockdon et al. (2014) or were known to be a source of insecurity, were calibrated here. For example, the value of the Chezy parameter was not reported and the calibration of the breaker parameter γ was difficult, just as it was for the calibration of the breaker parameters in the XBeach Non-hydrostatic model.

For the bottom friction the depth independent bottom friction formulation of Chezy was chosen, as this was also used in the XBeach Surfbeat model used by Stockdon et al. (2014). A value of 56 $m^{1/2}/s$ resulted in the lowest errors over all 36 measuring locations. The value of γ was chosen in the same way as the maximum wave steepness in the XBeach Non-hydrostatic model: the value which resulted in the lowest errors at the array of output locations closest to shore ($\gamma = 0.42$, equal to the value of γ used in Stockdon et al. (2014)).

For the runup gauge depth the same value as the one used in Stockdon et al. (2014) was taken, 0.10 m. However, to be able to compare the runup predictions of the XBeach Non-hydrostatic model well with the XBeach Surfbeat model the runup gauge depth in both models should be the same. For that reason a second validation of XBeach Surfbeat was done with a runup gauge depth of 0.05 m.

4.3. Validation of the XBeach Non-hydrostatic and XBeach Surfbeat model

4.3.1. Incident wave height transformation

In figure 4.1 the results of the incident wave height validation are shown. Only the results for the XBeach Surfbeat model with a runup gauge depth of 0.10 m are shown, as the runup gauge depth does not influence the wave height. Model output at 36 locations (an array of six alongshore locations with six points in the cross shore each) was compared to the wave height data at the same locations. Generally XBeach Non-hydrostatic and XBeach Surfbeat have a similar performance for incident wave height transformation.

The significant incident wave heights in the surfzone simulated by XBeach Non-hydrostatic compare well to the surfzone measurements, see figure 4.1 a and table 4.1, with an overall root mean square error of 0.085 m. The performance decreases somewhat towards the shore, with root mean square
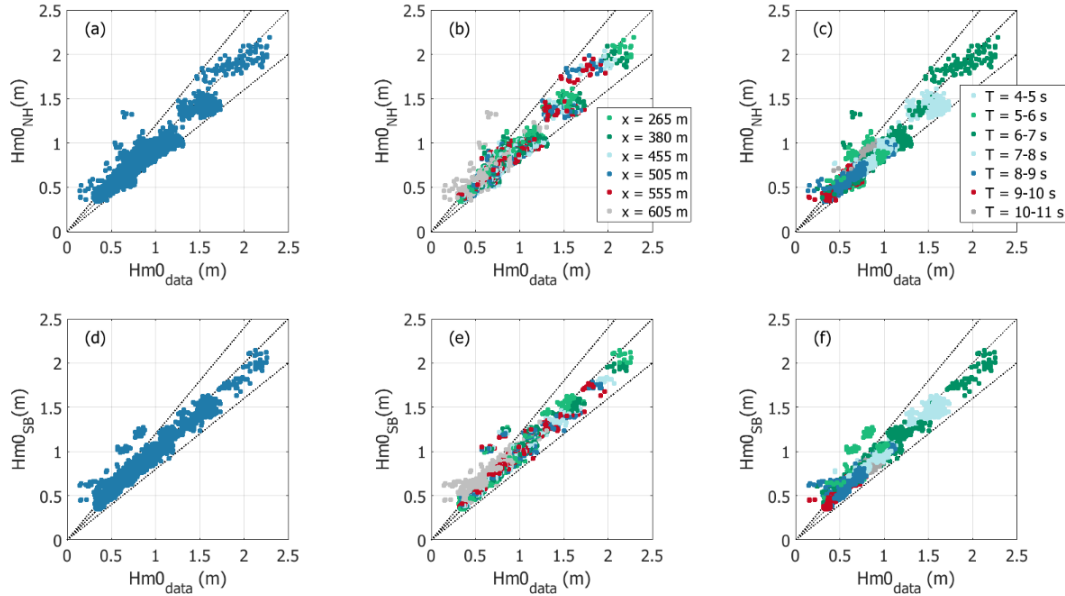
Figure 4.1: Comparison of modeled and observed significant incident wave heights for both XBeach models. (a-c) Results for XBeach Non-hydrostatic. (d-f) Results for XBeach Surfbeat. (a & d) Normal scatter plot. (b & e) Distinction between different cross shore locations. (c & f) Distinction between offshore representative wave periods.

Table 4.1: Root mean square errors and bias, describing the fit between observations and model results for $H_{m0,inc}$, for both XBeach models. Overall indicates that the root mean square error or bias has been taken over all 36 output locations.

Location	XBeach Non-hydrostatic		XBeach Surfbeat	
	RMSE (m)	Bias (m)	RMSE (m)	Bias(m)
Overall	0.085	-0.032	0.085	0.003
x = 265	0.068	-0.014	0.068	-0.010
x = 380	0.086	-0.053	0.070	-0.024
x = 455	0.083	-0.048	0.070	-0.013
x = 505	0.080	-0.043	0.067	-0.013
x = 555	0.083	-0.044	0.072	0.004
x = 605	0.079	-0.008	0.108	0.073

errors increasing from the most offshore location to the most nearshore location from 0.068 m to 0.079 m. This can be caused by two things:

- The waves close to shore are too nonlinear for the model to capture well.

- There is uncertainty with respect to the bathymetry close to shore. The models are ran without morphogical updates, just as the XBeach Surfbeat model of Stockdon et al. (2014). The measured bathymetry is used as a bottom profile but this was only measured once a day. The variations of the nearshore bar may not be captured well when updating the bottom only once a day.

XBeach Non-hydrostatic generally underestimates significant wave height slightly, which can be seen from the bias values. However, this underestimation decreases towards shore. The same is seen from figure 4.1 b where the same scatter plot as in a is shown but with a distinction made between the location in the cross shore: almost all overestimated wave heights visible in the figure are at the point closest to shore. From figure 4.1 c, where a distinction is made between offshore wave period, it becomes clear that the overestimation of nearshore wave heights is not dependent on wave period. The

performance of the model for incident wave height transformation is thus mainly determined by the location in the cross shore. This might be improved by running the model with morphological updates.

The significant incident wave heights simulated by XBeach Surfbeat also compare well to surfzone measurements, with the same overall root mean square error as XBeach Non-hydrostatic, see figure 4.1 d and table 4.1. The performance decreases towards shore, with the root mean square error increasing from 0.068 offshore to 0.108 m nearshore. Part of the overestimated wave heights, positioned above the 20% error line in figure 4.1 e are at the most nearshore location. However, also a fair amount of overestimated wave heights is from different locations in the cross shore, which can also be seen from a positive bias at some cross shore locations. Overestimated wave heights can be seen in all wave period bins, meaning the wave period does not have an influence on the overestimation. Again the performance of the XBeach Surfbeat model mainly depends on the location in the cross shore.

Comparing XBeach Non-hydrostatic and XBeach Surfbeat, it seems that the performance of XBeach Non-hydrostatic is slightly more constant over the cross shore (increase in root mean square error of 16% against an increase of 23% for XBeach Surfbeat). However, at locations 1 to 5 XBeach Surfbeat actually performs better, only at the most nearshore location XBeach Surfbeat's performance drops while the performance of the Non-hydrostatic model remains constant. XBeach Non-hydrostatic generally underpredicts incident wave height while XBeach Surfbeat generally overestimates it.

4.3.2. Infragravity wave height transformation

The results from the validation of the significant infragravity wave height can be seen in figure 4.2 and table 4.2. Modeled infragravity wave heights by XBeach Non-hydrostatic correspond better with measured infragravity wave heights but both models underestimate significant infragravity wave height.
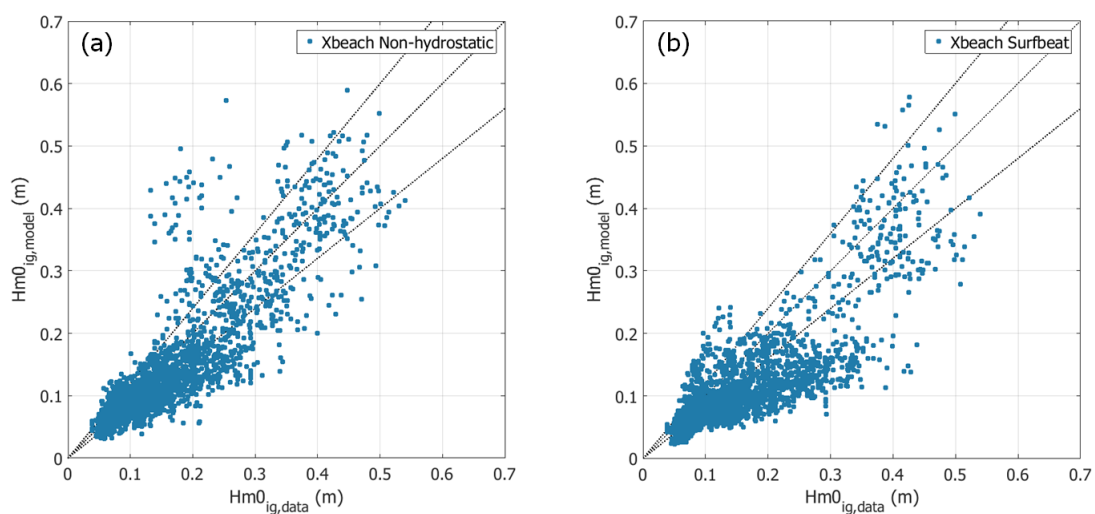
Figure 4.2: Observed and modeled infragravity wave heights for XBeach Non-hydrostatic and XBeach Surfbeat. (a) XBeach Non-hydrostatic. (b) XBeach Surfbeat.

Both XBeach models underpredict the significant infragravity wave height at every location in the cross shore, which can be seen from figure 4.2 and the negative bias values. However, the underestimation by XBeach Surfbeat is larger than that of XBeach Non-hdyrostatic, also at every location. From the root mean square errors it can be seen that XBeach Non-hydrostatic predicts infragravity wave height better, not only overall but at every location in the cross shore. For both models a decrease in performance towards shore can be seen, with root mean square errors increasing from 0.033 to 0.056 m for XBeach Non-hydrostatic and from 0.044 to 0.076 m for XBeach Surfbeat.

Table 4.2: Root mean square errors and bias, describing the fit between observations and model results for $H_{m0,ig}$, for both XBeach models. Overall indicates that the root mean square error and bias has been taken over all 36 output locations.

Location	XBeach Non-hydrostatic		XBeach Surfbeat	
	RMSE (m)	Bias (m)	RMSE (m)	Bias(m)
Overall	0.046	-0.019	0.059	-0.045
x = 265	0.033	-0.009	0.044	-0.037
x = 380	0.039	-0.017	0.052	-0.043
x = 455	0.042	-0.017	0.056	-0.048
x = 505	0.041	-0.008	0.055	-0.047
x = 555	0.048	-0.027	0.060	-0.045
x = 605	0.056	-0.034	0.076	-0.051

4.3.3. Runup

Both the XBeach Non-hydrostatic and the XBeach Surfbeat model were validated for setup at the waterline $\bar{\eta}$, significant incident swash S_{inc}, significant infragravity swash S_{ig} and the 2% runup level $R_{2\%}$. An overview of the results of the validation of both models can be seen in figure 4.3. An overview of the statistics describing the fit between data and model output can be found in table 4.3. XBeach Non-hydrostatic and XBeach Surfbeat perform comparable for setup, but XBeach Non-hydrostatic predicts significant incident swash, significant infragravity swash and the 2% runup level better than XBeach Surfbeat.
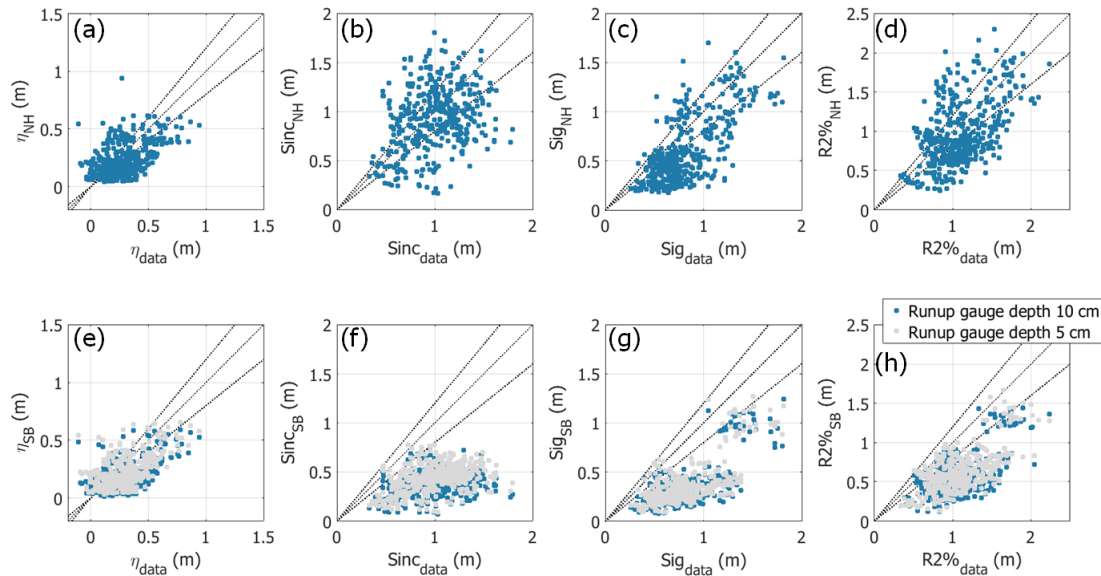
Figure 4.3: Comparison of modeled and observed runup statistics for both XBeach models. (a-d) Results for XBeach Non-hydrostatic: setup at the waterline $\bar{\eta}$, significant incident swash S_{inc}, significant infragravity swash S_{ig} and the 2% runup level $R_{2\%}$. (e-h) Results for both XBeach Surfbeat models (with two values of the runup gauge depth).

Setup   In figure 4.3 a and e the results of the validation of both XBeach models for setup are shown. The root mean square errors for the XBeach Non-hydrostatic and XBeach Surfbeat models are very similar, just as the coefficient of determination R^2 and the slope of the line of linear regression b, see table 4.3. b is smaller than 1 indicating that, when assuming that higher energetic conditions result in more setup, setup is overestimated in the low energetic conditions, while being underestimated

Table 4.3: Statistics describing the fit between observations and model results for setup $\bar{\eta}$, significant incident swash S_{inc}, significant infragravity swash S_{ig} and the 2% runup level $R_{2\%}$, for the XBeach models. The statistics used are the root mean square error RMSE, the coefficient of determination R^2, the slope of the line of linear regression b and the bias B. NH indicates the XBeach Non-hydrostatic model and SB10 and SB5 the XBeach Surfbeat models with a runup gauge depth of 0.10 and 0.05 m respectively.

Parameter	RMSE (m)			R^2 (-)			b (-)			Bias (m)		
	NH	SB10	SB5	NH	SB10	SB5	NH	SB10	SB5	NH	SB10	SB5
$\bar{\eta}$	0.16	0.16	0.14	0.47	0.43	0.42	0.40	0.36	0.36	-0.04	-0.11	-0.06
S_{inc}	0.31	0.63	0.58	0.41	0.46	0.45	0.37	0.09	0.14	-0.07	-0.61	-0.55
S_{ig}	0.34	0.46	0.46	0.60	0.48	0.48	0.77	0.40	0.38	-0.17	-0.46	-0.44
$R_{2\%}$	0.35	0.57	0.49	0.53	0.48	0.51	0.41	0.24	0.31	-0.13	-0.52	-0.45

for increasing energetic conditions. This effect is strongest for the XBeach Surfbeat model with a runup gauge depth of 0.05 m and weakest for the XBeach Non-hydrostatic model. Generally, both XBeach Non-hydrostatic and XBeach Surfbeat underestimate setup, as can be seen from the negative bias values. The XBeach Surfbeat model with a runup gauge depth of 0.10 m results in a larger underestimation than the XBeach Surfbeat model with a runup gauge depth of 0.05 m. From figure 4.3 e it can also be seen that the setup for a runup gauge depth of 0.10 is slightly lower.

Significant swash   In figure 4.3 b and f the results of the validation of both XBeach models for significant incident swash are shown. XBeach Non-hydrostatic predicts the incident swash better than the XBeach Surfbeat models, with a root mean square error of about half the ones of XBeach Surfbeat. The lines of linear regression for the XBeach Surfbeat models are close to 0, indicating that incident swash is underestimated more for higher energetic conditions (again assuming swash increases for increasing energetic conditions). XBeach Non-hydrostatic slightly underestimates incident swash, seen from the negative bias, and the underestimation is much worse for XBeach Surfbeat. The XBeach Surfbeat model with a runup gauge depth of 0.10 m underestimates incident swash more than with a runup gauge depth of 0.05 m. The R^2 values for all models are similar, as the XBeach Surfbeat models give a large underestimation while there is a lot of scatter for the XBeach Non-hydrostatic model.

In figure 4.3 c and g the results of the validation of both XBeach models for significant infragravity swash are shown. XBeach Non-hydrostatic is a better predictor of infragravity swash but the difference is smaller than for incident swash. The root mean square error for XBeach Non-hydrostatic is about two third of what it is for XBeach Surfbeat. The slope of the line of linear regression is much closer to 1 for XBeach Non-hydrostatic than for XBeach Surfbeat. From the negative bias values it can be seen that generally XBeach Non-hydrostatic slightly underestimates infragravity swash (mostly in the lower energetic conditions), which is worse for XBeach Surfbeat. Again the XBeach Surfbeat model with a runup gauge depth of 0.10 m results in a larger underestimation, but the effect is smaller than for incident swash.

2% Runup level   In figure 4.3 d and h the results of the validation of both XBeach models for the 2% runup level are shown. Again XBeach Non-hydrostatic is a better predictor of $R_{2\%}$ than XBeach Surfbeat, the root mean square error is about two third of what it is for XBeach Surfbeat. XBeach Non-hydrostatic slightly underestimates $R_{2\%}$ while the underestimation by XBeach Surfbeat is much larger and increases for increasing energetic conditions. The trends visible for $R_{2\%}$ are similar to the trends in setup and significant swash, which is to be expected as those are the components of $R_{2\%}$. Again the XBeach Surfbeat model with a runup gauge depth of 0.10 m gives a larger underprediction than the one with a runup gauge depth of 0.05 m.

4.4. Comparison with the XBeach Surfbeat model of Stockdon et al. (2014)

4.4.1. Wave height transformation

For the incident wave height transformation over the surfzone Stockdon et al. (2014) reports root mean square errors ranging from 0.21 m at the most offshore location to 0.41 m at the most nearshore location and a bias of 0.08 m. These results are very different from the results found here for the XBeach Surfbeat model, where root mean square errors range from 0.07 to 0.11 m. The difference in the model setup is that here the single dir option has been used, which propagates the wave energy over the mean direction. This results in an increased groupiness (Roelvink et al., 2010). Another reason for the large difference could be the fact that some of the higher wave conditions were not simulated here as the bathymetry measurements were not complete at that day. It was therefore chosen not to use these bathymetry data. However, these wave conditions were simulated by Stockdon et al. (2014), probably making use of bathymetry data interpolation. The larger error could have resulted from these higher wave conditions, leading to a better performance here. Not only the total root mean square reported in Stockdon et al. (2014) is much larger, but also the decrease in performance towards shore. Ranging from 0.21 m offshore to 0.41 m nearshore means an decrease in performance of 95%, while the XBeach Surfbeat model here results in a decrease in performance of 23%. Stockdon et al. (2014) did not look at infragravity wave height, so no comparison can be made for that.

4.4.2. Runup

The XBeach Surfbeat model as used by Stockdon et al. (2014) gives similar root mean square errors for the setup as the XBeach model used here. The XBeach Surfbeat model overestimated the setup somewhat for increasing energetic conditions, while the XBeach Surfbeat model used here underestimates it with increasing energetic conditions. The missing higher wave conditions can also be seen in the setup: the maximum value of setup predicted by Stockdon et al. (2014) is around 0.8 while the maximum value of setup predicted here is around 0.6.
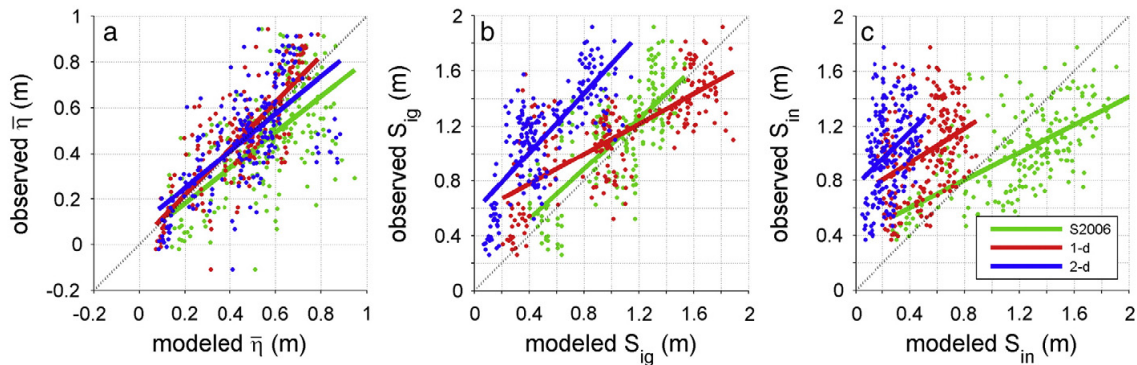
Figure 4.4: Observed and modeled setup $\bar{\eta}$, significant infragravity swash S_{ig} and significant incident swash S_{in} (Stockdon et al., 2014). Scatterplots for the parameterization of Stockdon et al. (2005), the 1D Surfbeat model and the 2D Surfbeat model are shown. The results of the 2D Surfbeat model are relevant in this case, as the XBeach models uses here are also 2D.

In the case of significant incident swash the XBeach Surfbeat model used here and the XBeach Surfbeat model used by Stockdon et al. (2014) give similar trends. They both underpredict the significant incident swash significantly. The difference is that the significant swash is equally underpredicted for the full range of energetic conditions in the XBeach Surfbeat model used by Stockdon et al. (2014), while the underprediction increases for higher energetic conditions here. Also, the root mean square error reported here is smaller than reported in Stockdon et al. (2014): 0.63 versus 0.82 m. For the significant infragravity swash both XBeach Surfbeat models result in a consistent underprediction, but again this underprediction is equal for all energetic conditions in the Surfbeat model used by Stockdon et al. (2014) while increasing for the XBeach Surfbeat model used here. Also, the XBeach Surfbeat

model here performs slightly better in terms of the root mean square error (0.46 versus 0.66 m).

4.5. Conclusion & Discussion

From the validation of the XBeach Non-hydrostatic and XBeach Surfbeat model for the SandyDuck'97 data set it can be concluded that XBeach Non-hydrostatic and XBeach Surfbeat perform similarly for incident wave height transformation over the surfzone, but the performance of XBeach Non-hydrostatic is more constant over the cross shore. The performance of the XBeach Surfbeat model used here is much better than that of the XBeach Surfbeat model used by Stockdon et al. (2014). Also the decrease in performance is much lower. This can be due to the use of the single dir option (propagation of wave energy over the mean wave direction which increases groupiness (Roelvink et al., 2010)) or due to the fact that some of the higher wave conditions were not modeled here due to missing bathymetry data. To be able to compare well with the XBeach Surfbeat model of Stockdon et al. (2014) exactly the same XBeach simulations should be used and single dir should not be used. While there only is a small difference in predictive capability for incident wave height transformation, there is a larger difference for infragravity wave height transformation. Both models underpredict infragravity wave height, but XBeach Non-hydrostatic does this to a smaller extent. The decrease in performance towards shore is similar for both models but much larger than for incident wave height transformation. It can be concluded that on an intermediate reflective beach such as Duck resolving incident waves does not contribute much to predicting the incident wave height transformation accurately. Only close to the shore, where the waves become highly nonlinear, the effect is noticed and only solving the incident wave envelope is an approximation which is too rough. Solving the incident waves does have a positive effect on the prediction of infragravity wave height transformation. This could be due to added phase information and energy transfers between incident and infragravity waves which are captured better by the XBeach Non-hydrostatic model.

It was noted that the decrease in performance of wave height predictions towards shore can be due to uncertainty with regard to the bathymetry close to shore. In this study the XBeach models were ran without morphology and the bathymetry was updated once a day with the measured bathymetry. However, the local morphology can have a large influence on the runup according to Ahrens and Seelig (2001). The actual influence of the morphology on runup can be tested first by forcing the XBeach models with the same boundary conditions but on different bathymetries. If the influence is significant, the morphological transformation should be validated for the XBeach models before including morphological updates in the study.

XBeach Non-hydrostatic and XBeach Surfbeat perform comparable for setup. Together with the comparable performance for incident wave height this suggests that the setup is mainly driven by time-averaged radiation stress gradients resulting from breaking of the incident waves and to a minor degree of the infragravity waves. Also, setup is clearly mainly influenced by a correct incident wave height prediction and not much by other aspects of the incident waves. Contradicting is that the performance of this Surfbeat model and the Surfbeat model of Stockdon et al. (2014) is similar, while the performance for incident wave height transformation is much better.

The XBeach Non-hydrostatic model is a far better predictor of significant incident swash than XBeach Surfbeat. This improvement was expected, as XBeach Non-hydrostatic solves the incident waves and swash while XBeach Surfbeat does not.

Also for significant infragravity swash XBeach Non-hydrostatic is a better predictor, though the improvement is smaller and the infragravity swash is still underpredicted, especially in the lower energetic conditions. In this specific case it could be explained by the fact that the offshore frequency-directional spectra are only measured between 0.044-0.318 Hz. The XBeach model generates the bound infragravity wave from the frequency-directional spectra in the incident band, but in this way free infragravity energy is not taken into account. However, the underprediction of significant infragravity swash has now been seen three times: in the 1D XBeach Surfbeat model of a flume experiment of Palmsten and Splinter (2016), in the XBeach Surfbeat model of Duck of Stockdon et al. (2014) and in this study.

The fact that even in a controlled environment of a flume experiment the significant infragravity swash is underestimated, while in that experiment infragravity wave heights were even overestimated (in this research also infragravity wave height is underestimated) near the shore and no free infragravity energy is present, is strange and indicates that the lack of free infragravity energy is most likely not the cause of the underprediction of infragravity swash. Overall, solving incident waves has a positive effect on the prediction of infragravity swash, just as it has a positive effect on infragravity wave height transformation.

The 2% runup level shows the same trends as its components: XBeach Non-hydrostatic gives a better prediction than XBeach Surfbeat. As there is hardly any difference in setup, this means that the 2% runup level is dominated by the swash. As the 2% runup level shows the same trends as its components the different runup components and their respective energy do not compensate for each other. The underprediction of total runup for a phase-averaged model was also seen by Casella et al. (2014) for the phase-averaged CSHORE model.

Besides XBeach also the numerical model SWASH can be used to simulate runup. A validation of a two-layered SWASH model for runup data of a highly dissipative beach and high energetic conditions was reported by Lerma et al. (2017), which yielded good results. Setup and infragravity swash were well predicted, while incident swash was overpredicted. Lerma et al. (2017) states that the SWASH model is a significantly better predictor of runup than the XBeach Surfbeat model of Stockdon et al. (2014), based on statistics. However, the statistics for the XBeach Non-hydrostatic model are much closer to the ones of the SWASH model and the statistics for incident swash are even better. This would indicate that the performance for runup of a depth-averaged XBeach Non-hydrostatic model is comparable to a SWASH model with two layers. However, to make a proper comparison both models should be validated for the same data set.

Overall, the results of the validation are promising for the performance of XBeach Non-hydrostatic for runup. The reason why the predictive capability for significant incident swash has improved speaks for itself, but the reason for the improvement in significant infragravity swash does not. This question will be addressed in chapters 5, 6 and 7.

Source of runup differences between XBeach Surfbeat and Non-hydrostatic

5.1. Introduction

There is a difference in significant incident and infragravity swash predictions between XBeach Non-hydrostatic and XBeach Surfbeat, which was described in chapter 4. The difference in incident swash was expected but the reason and driving processes behind the difference in infragravity swash are not known. Multiple parameters can be the cause, such as a difference in wave height transformation between the models, a difference in the groupiness of the incident waves or a difference in the predicted phase difference between the incident wave group and the forced infragravity wave. In this chapter the relevance of each of these parameters for explaining the runup difference between the two XBeach models is discussed. In order to do that the difference in the respective parameter between the two XBeach models is considered on the swash zone border and compared to the difference in runup between the two models. Only incoming waves are considered for this. In the last part of this chapter relevant processes within the swash zone are considered.
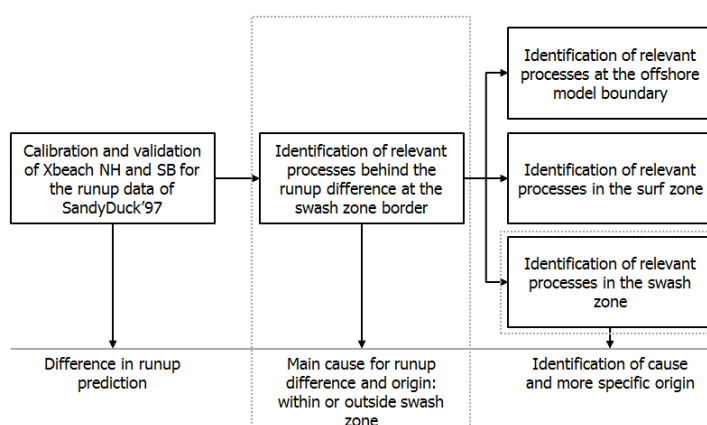
5.2. Influence of the incoming wave height

5.2.1. Transformation of infragravity wave height over the cross shore

In chapter 4 a difference in infragravity wave height prediction between XBeach Non-hydrostatic and XBeach Surfbeat was found, while the models perform similarly for incident wave height transformation. The transformation of the incoming infragravity wave height over the cross shore is considered in this section. Over the entire cross shore there is a difference in incoming infragravity wave height between the XBeach models and this difference is already present near the offshore model boundary.
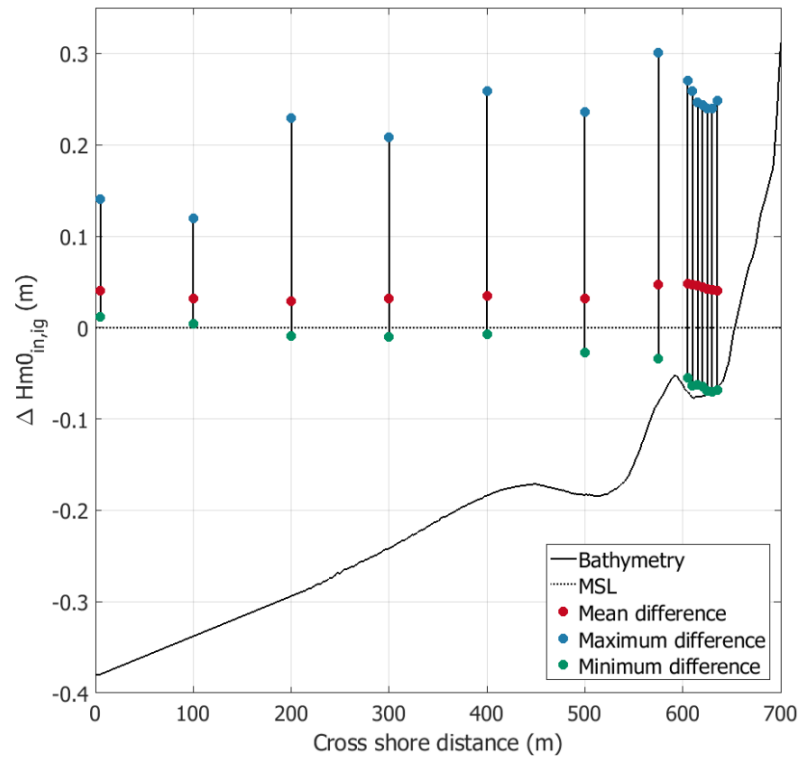
Figure 5.1: Difference in incoming infragravity wave height between XBeach Non-hydrostatic and XBeach Surfbeat over the cross shore. The change of the minimum, mean and maximum difference are shown. A positive difference indicates that XBeach Non-hydrostatic predicts a larger value.
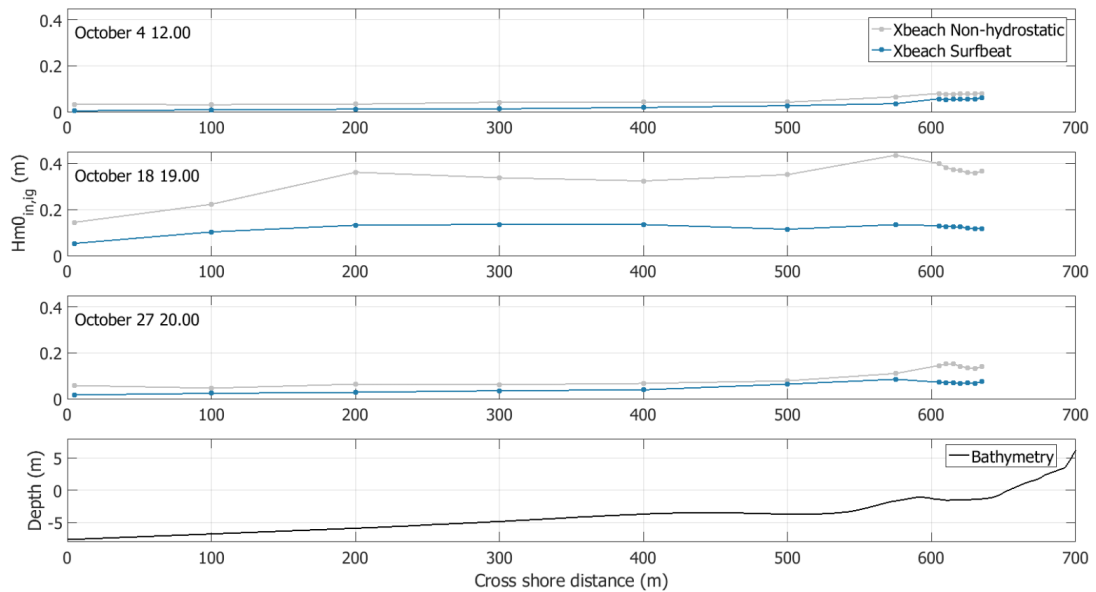
Figure 5.2: Transformation of incoming infragravity wave height for XBeach Non-hydrostatic and XBeach Surfbeat over the cross shore for three wave conditions (low offshore wave height at October 4, intermediate offshore wave height at October 27, high offshore wave height at October 18).

In figure 5.1 the transformation of incoming infragravity wave height differences between the XBeach models over the cross shore is shown. The mean, minimum and maximum difference are depicted, which are determined from all the XBeach simulations used in the validation. The mean difference

is positive everywhere, indicating that XBeach Non-hydrostatic predicts a higher incoming infragravity wave height over the entire cross shore. It is constant until x = 500, where it slightly increases. Both the minimum and the maximum difference increase shoreward in absolute value, leading to a larger range in differences close to shore. Close to shore XBeach Surfbeat predicts a higher incoming infragravity wave height in some cases, seen from the negative minimum difference. There already is a difference in the incoming infragravity wave height at x = 5 m, very close to the boundary.

The fact that XBeach Non-hydrostatic generally predicts a higher infragravity wave height can also be seen from figure 5.2. For three specific simulations, representing three different wave conditions (low offshore wave heights on October 4 12.00, high offshore wave heights on October 18 19.00 and intermediate offshore wave heights on October 27 20.00) the transformation of the incoming infragravity wave height over the cross shore is shown for both XBeach Non-hydrostatic and XBeach Surfbeat. The following trend can be seen: when offshore wave heights increase the difference in infragravity wave height prediction between XBeach Non-hydrostatic and XBeach Surfbeat increases too. In chapter 7 more attention is paid to this observation. For intermediate and high offshore wave heights XBeach Non-hydrostatic also predicts a stronger increase in infragravity wave height towards shore. This could be caused by a mechanism also suggested in chapter 1: in XBeach Non-hydrostatic the nonlinear transfers transferring energy from the incident to the infragravity frequencies might be better captured, leading to higher infragravity wave heights and therefore leading to a better prediction of the infragravity swash. The last thing which should be noted from figure 5.2 is that the difference in infragravity wave height close to the boundary is visible here too, with a larger difference for higher offshore waves. This is investigated further in chapter 6.

To indicate the effect of splitting incoming and reflected waves with the Guza method, which is a 1D method applied on a 2D wave field, the same analyses have been carried out for the total infragravity wave field. These figures can be found in appendix M. The same trends can be seen: generally XBeach Non-hydrostatic predicts a higher infragravity wave height and there already is a difference present close to the boundary. The differences between the two models are slightly larger for the total wave field: there are not only differences in incoming infragravity wave height but also in transformation and reflection.

5.2.2. Correlation between wave height and runup

At the swash zone border the correlation is determined between the difference in incoming wave height and the difference in runup between XBeach Non-hydrostatic and XBeach Surfbeat. This is done not only for incoming infragravity wave height, but also for incoming incident and total wave height and for setup, significant incident swash and significant infragravity swash. A strong correlation is found between incoming infragravity wave height and significant infragravity swash.

In figure 5.3 the scatter plots for every wave height and runup statistic can be seen. A positive difference indicates that XBeach Non-hydrostatic predicts a larger value and the ρ-value in each plot indicates the correlation. Setup is mainly influenced by infragravity wave height, see figure 5.3 a, d and g. A larger difference in infragravity wave height leads to a larger difference in setup, with a coefficient of correlation of 0.41. Larger differences in incoming incident wave height and incoming total wave height do lead to larger differences in setup but to a smaller degree, which can be seen from the lower coefficients of correlation. However, the differences in setup are very small. The fact that setup mainly correlates with the infragravity wave height indicates that the breaking of infragravity waves contributes to the creation of setup.

The significant incident swash is approximately equally influenced by the incoming infragravity wave height, the incoming incident wave height and the total incoming wave height, see figure 5.3 b, e and h. A larger difference in wave height leads to a larger difference in significant incident swash but there is a lot of scatter and a low coefficient of correlation. This means that the incoming wave height is not an interesting parameter when trying to explain the difference in significant incident swash between XBeach Non-hydrostatic and XBeach Surfbeat. This was already seen in chapter 4: the XBeach models perform similar for incident wave height transformation while performing differently for incident swash.
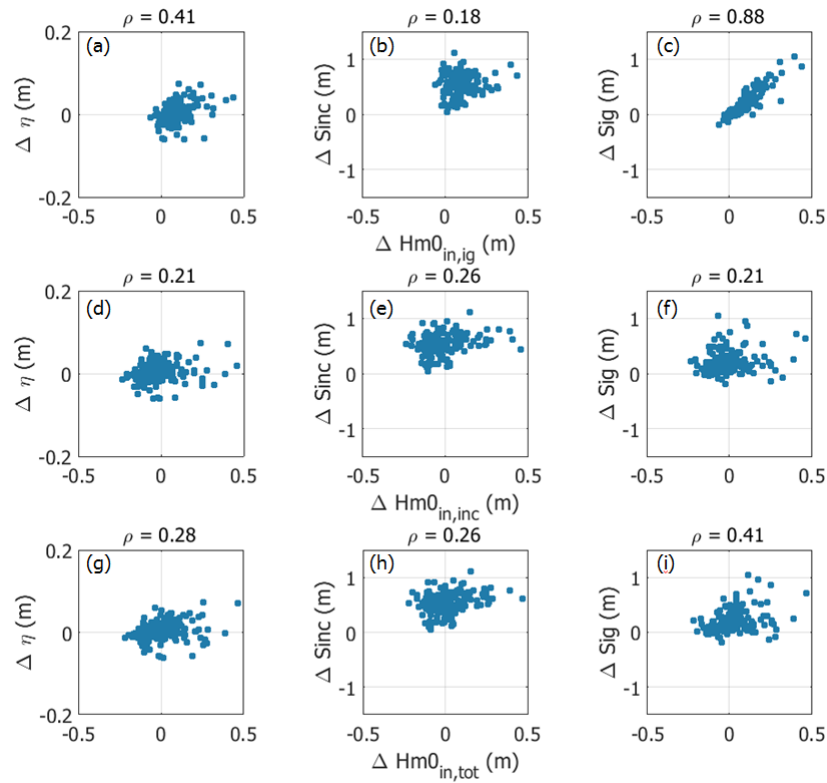
Figure 5.3: Influence of the difference in incoming waveheight ($Hm0_{in,ig}$, $Hm0_{in,inc}$ and $Hm0_{in,tot}$) between the XBeach models on the difference in runup (η, S_{inc} and S_{ig}). (a-c) The difference in incoming infragravity wave height against the difference in runup. (d-f) The difference in incoming incident wave height against the difference in runup. (g-i) The difference in total incoming wave height against the difference in runup. ρ gives the coefficient of correlation. A positive difference indicates XBeach Non-hydrostatic predicts a larger value.

Significant infragravity swash is clearly influenced by the infragravity wave height, see figure 5.3 c, f and i. This can be seen from the high correlation of 0.88 between the difference in infragravity wave height and the difference in significant infragravity swash. The incoming incident waves hardly influence the infragravity swash. The fact that for the total incoming wave height a coefficient of correlation of 0.38 is found is probably caused by the high coefficient of correlation for the infragravity wave height.

A strong correlation between $\Delta Hm0_{in,ig}$ and ΔSig is not only found at the swash zone border but also offshore of that: at x = 5 a correlation of 0.39 is found, increasing to 0.52 at x = 100, 0.58 at x = 200, 0.67 at x = 300 and 0.74 at x = 400. At the location of the pressure gauges closest to the swash zone border, x = 605, the correlation is 0.84. The increase in correlation over the cross shore is due to differences in infragravity wave height propagation, but the differences close to the boundary are already relevant.

5.3. Influence of the groupiness of the incoming waves

5.3.1. Transformation of the groupiness over the cross shore

An increased groupiness of the incoming incident waves is expected to lead to more forcing of the infragravity waves and therefore to more setup and/or infragravity swash. The groupiness is indicated by the groupiness factor GF. In this section the transformation of the groupiness factor GF over the cross shore is considered for both XBeach models. XBeach Surfbeat generally predicts a higher groupiness factor and a difference in the decrease in groupiness at breaking is seen.
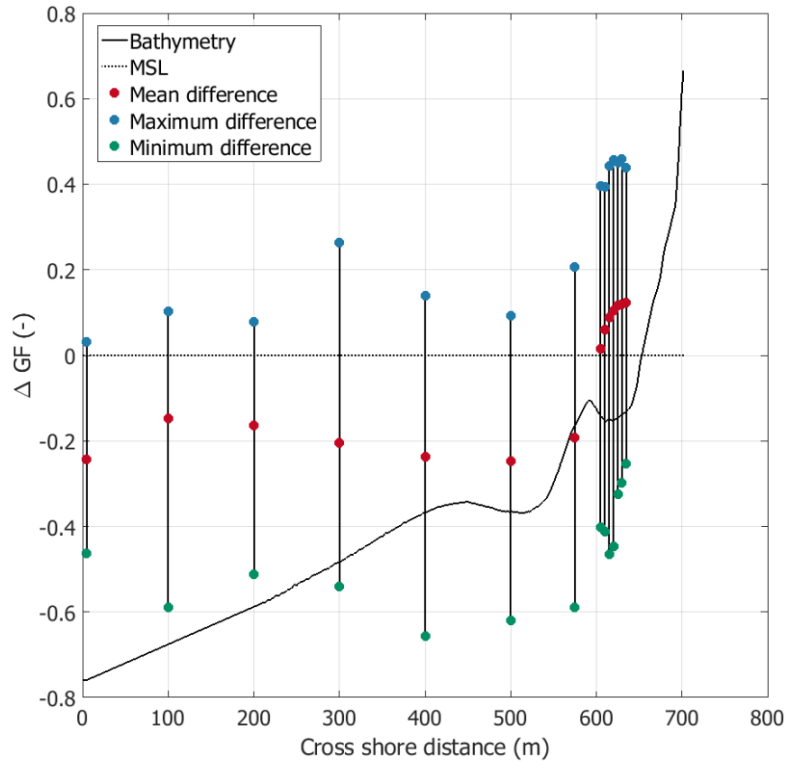
Figure 5.4: Difference in groupiness factor GF between XBeach Non-hydrostatic and XBeach Surfbeat over the cross shore. The change of the minimum, mean and maximum difference over the cross shore are shown. A positive difference indicates that XBeach Non-hydrostatic predicts a larger value.
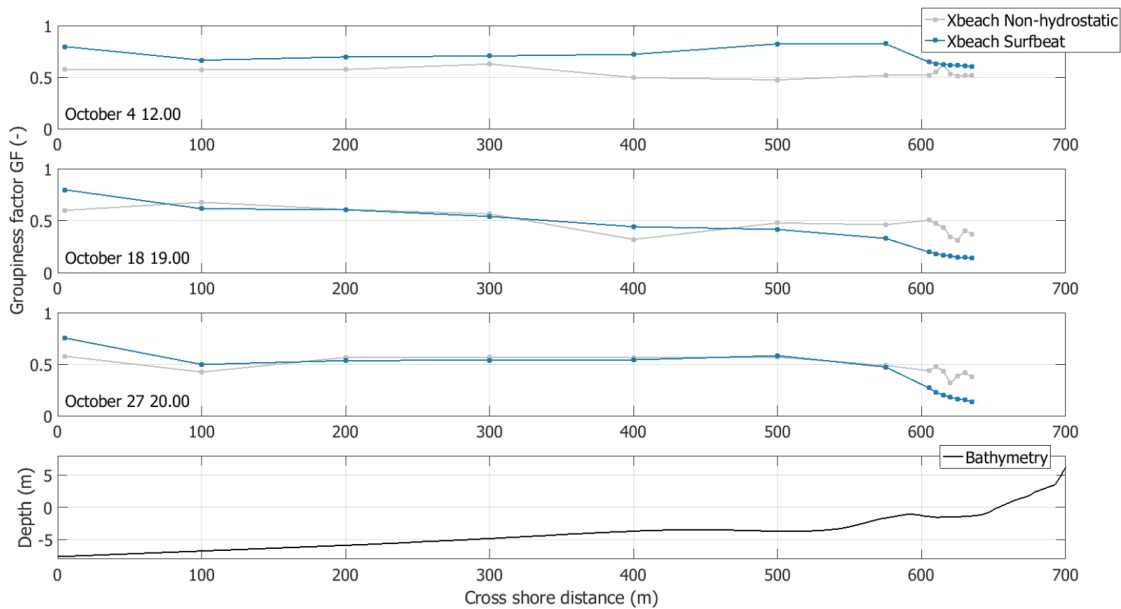
Figure 5.5: Transformation of the groupiness factor GF for XBeach Non-hydrostatic and XBeach Surfbeat over the cross shore for three wave conditions (low offshore wave height on October 4 12.00, high offshore wave height on October 18 19.00, intermediate offshore wave height on October 27 20.00).

Figure 5.4 shows the transformation of the mean, minimum and maximum difference in GF between XBeach Non-hydrostatic and XBeach Surfbeat over the cross shore. The mean difference is negative

until x = 575: XBeach Surfbeat generally predicts a larger GF in that part of the cross shore. This makes sense as XBeach Surfbeat only solves the wave groups. The mean difference increases after x = 575, indicating that XBeach Non-hydrostatic predicts a larger GF close to shore. The maximum difference also increases towards shore, while the minimum difference first increases in absolute value and then decreases again. The spread in results thus first increases towards shore and then decreases again close to shore.

For three simulations, representing a range in wave conditions, the transformation of the groupiness factor over the cross shore is shown in figure 5.5 for both XBeach Non-hydrostatic and XBeach Surfbeat. For all three cases GF near the offshore boundary is larger for XBeach Surfbeat. Between x = 100 and x = 575 (the breaking point in most cases), GF is fairly similar for XBeach Non-Hydrostatic and XBeach Surfbeat and remains approximately constant. From x = 575 onwards a decrease in GF can be seen, due to breaking of the incident waves. The decrease in GF is stronger for XBeach Surfbeat than for XBeach Non-hydrostatic, hence the higher values of GF for XBeach Non-hydrostatic near the shore visible in figure 5.4. This could be caused by breaking of the wave group as a whole in XBeach Surfbeat while some individual incident waves in XBeach Non-hydrostatic have not broken yet.

Splitting the wave field with the Guza method hardly has any influence on the prediction of GF. The incident waves outputted by XBeach Surfbeat are already split into incoming and reflected waves and the transformation of GF over the cross shore for XBeach Non-hydrostatic is similar for the incoming and total wave field.

5.3.2. Correlation between groupiness and runup
At the swash zone border the correlation between the difference in groupiness factor GF and the difference in runup is determined. An intermediate correlation was found between the difference in groupiness factor and the difference in significant infragravity swash but not high enough to mark the groupiness as a clear cause for the difference in significant infragravity swash.
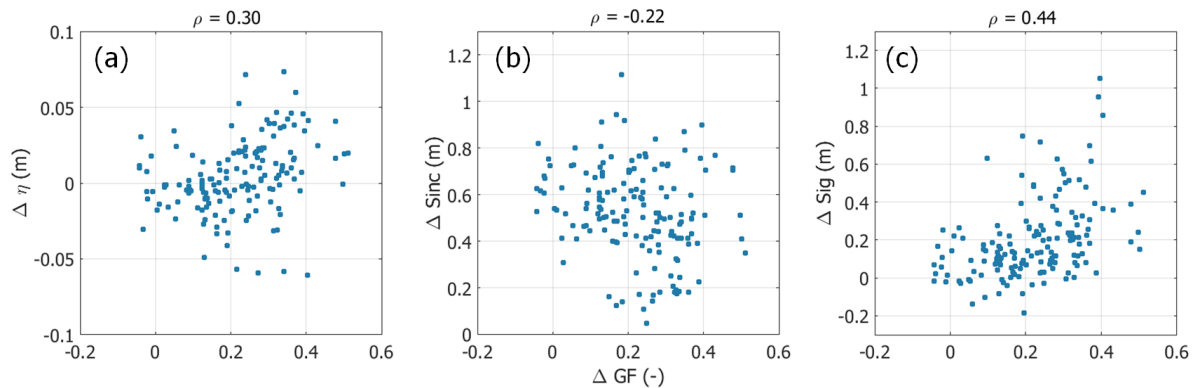
Figure 5.6: Influence of the difference in groupiness factor between XBeach Non-hydrostatic and XBeach Surfbeat on the difference in runup. (a) Difference in GF against difference in setup. (b) Difference in GF against difference in incident swash. (c) Difference in GF against difference in infragravity swash. ρ indicates the coefficient of correlation. A positive difference indicates XBeach Non-hydrostatic predicts a larger value.

In figure 5.6 the relation between the difference in GF and the difference in setup, significant incident and significant infragravity swash is shown. The coefficient of correlation for the setup and the infragravity swash is positive, meaning that a larger difference in GF leads to a larger difference in setup/infragravity swash, as a larger GF results in more infragravity wave forcing. A larger difference in GF leads to a smaller difference in significant incident swash. However, the coefficients of correlation are relatively small. This was expected as on the swash zone border almost all waves have broken, reducing the groupiness.
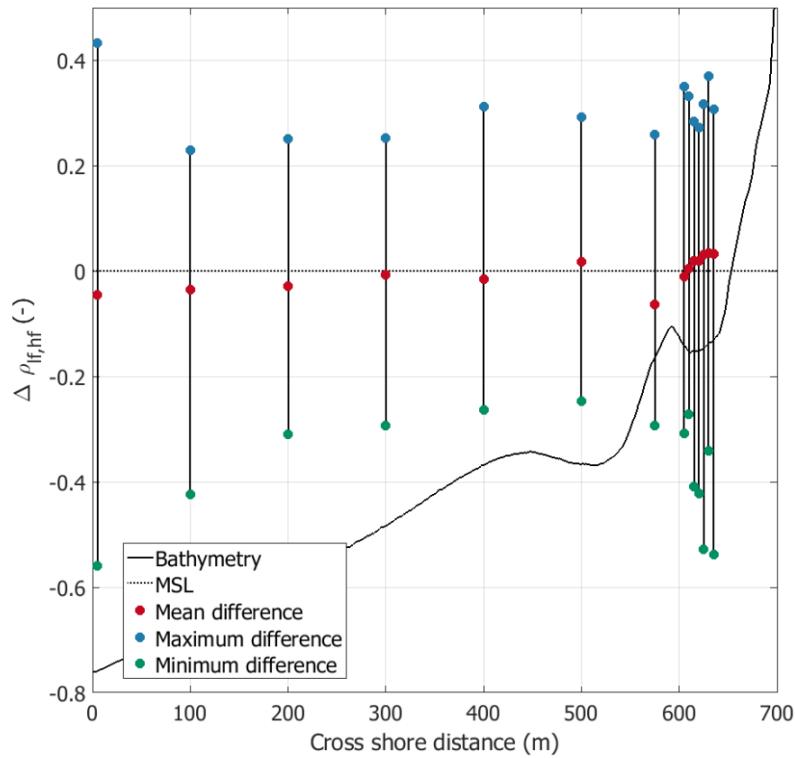
Figure 5.7: Difference in $\rho_{lf,hf}$ between XBeach Non-hydrostatic and XBeach Surfbeat over the cross shore. The change of the minimum, mean and maximum difference over the cross shore is shown. A positive difference indicates that XBeach Non-hydrostatic predicts a larger value.
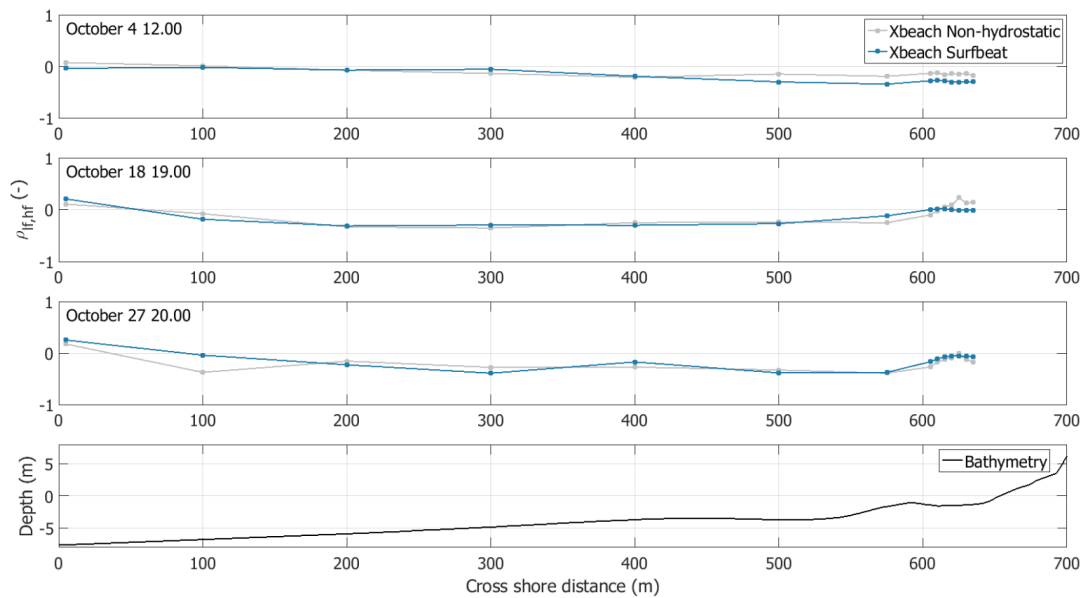
Figure 5.8: Transformation of $\rho_{lf,hf}$ for XBeach Non-hydrostatic and XBeach Surfbeat over the cross shore for three wave conditions (low offshore wave height on October 4 12.00, high offshore wave height on October 18 19.00, intermediate offshore wave height on October 27 20.00).

5.4. Influence of the phase difference between the infragravity waves and the incident wave groups

5.4.1. Transformation of the phase difference over the cross shore

The phase difference between wave groups and infragravity waves is one of the parameters influencing energy transfers between them. Here an indication of the phase difference is given by the coefficient of correlation between the incident wave envelope and the infragravity waves, called $\rho_{lf,hf}$. The transformation of $\rho_{lf,hf}$ over the cross shore is considered for both XBeach models. There are small differences in $\rho_{lf,hf}$ between XBeach Non-hydrostatic but the behaviour of $\rho_{lf,hf}$ is not as expected.

In figure 5.7 the transformation of the mean, minimum and maximum difference in $\rho_{lf,hf}$ between XBeach Non-hydrostatic and XBeach Surfbeat is shown. The mean difference is very small and generally negative, indicating that at most locations in the cross shore XBeach Surfbeat predicts a larger value of $\rho_{lf,hf}$. Close to shore XBeach Non-hydrostatic predicts a larger value of $\rho_{lf,hf}$. The maximum difference remains fairly constant over the cross shore while the minimum difference first decreases and then increases towards shore. The spread in results thus first decreases after which it increases again.

For three simulations, representing a range in wave conditions, the transformation of $\rho_{lf,hf}$ over the cross shore is shown in figure 5.8 for both XBeach models. For these three cases the two models predict similar values of $\rho_{lf,hf}$ over the cross shore. $\rho_{lf,hf}$ near the offshore boundary is close to zero, which is against expectations: theoretically $\rho_{lf,hf}$ should be most negative offshore, stay negative until the point of incident wave breaking and become positive close to shore. From x = 0 to x = 100 $\rho_{lf,hf}$ decreases and stays approximately constant until x = 575, which is the breaking point in most cases. $\rho_{lf,hf}$ then increases slightly towards shore, becoming positive for XBeach Non-hydrostatic but staying negative for XBeach Surfbeat.

The strange results offshore could be the result of using the Guza method for splitting the incoming and outgoing waves. For XBeach Surfbeat the transformation of $\rho_{lf,hf}$ can not be computed for the total wave field, as its incident wave output only contains the incoming signal. However, the transformation of $\rho_{lf,hf}$ for XBeach Non-hydrostatic remains similar when considering the total wave field. The transformation of $\rho_{lf,hf}$ was also computed for a simple 1D test case where no directional spreading was present, see figure 5.9. In this case the transformation of $\rho_{lf,hf}$ over the cross shore does behave according to theory: a negative $\rho_{lf,hf}$ offshore where the wave envelope and the infragravity wave are out op phase, which stays negative until the incident waves start to break around x = 575 m and becomes positive after. $\rho_{lf,hf}$ as predicted by XBeach Surfbeat stays negative close to shore though, just as in the results for the 2D simulations of Duck. In 1D the used method of indicating $\rho_{lf,hf}$ thus works.
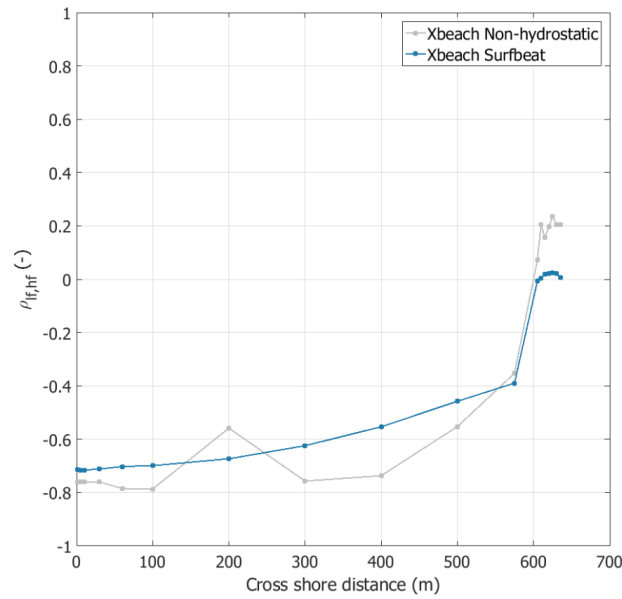
Figure 5.9: Transformation of $\rho_{lf,hf}$ over the cross shore for a simple 1D test case (narrow JONSWAP spectrum without directional spreading) for both XBeach models.

5.4.2. Correlation between the phase difference and runup

At the swash zone border the correlation between the difference in $\rho_{lf,hf}$ and the difference in runup (setup, significant incident and significant infragravity swash) is computed. Very small coefficients of correlation were found and the difference in $\rho_{lf,hf}$ is not the driver of the difference in runup.
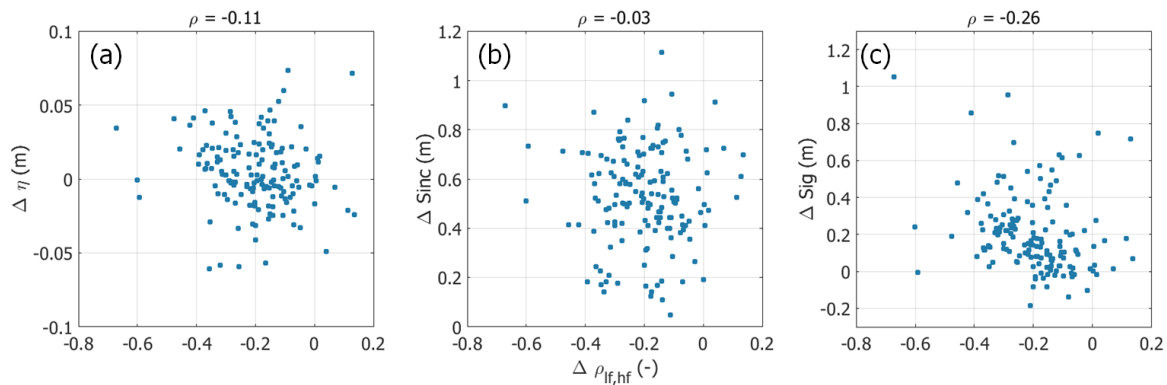
Figure 5.10: Influence of the difference in $\rho_{lf,hf}$ between XBeach Non-hydrostatic and XBeach Surfbeat on the difference in runup. (a) Difference in $\rho_{lf,hf}$ against the difference in setup. (b) Difference in $\rho_{lf,hf}$ against the difference in incident swash. (c) Difference in $\rho_{lf,hf}$ against the difference in infragravity swash. ρ gives the coefficient of correlation. A positive difference indicates XBeach Non-hydrostatic predicts a larger value.

In figure 5.10 the relation between the difference in $\rho_{lf,hf}$ and the difference in runup is shown. A positive difference indicates XBeach Non-hydrostatic predicts a larger value and the value of ρ gives the coefficient of correlation for each plot. All three plots show a negative coefficient of correlation, indicating that a larger difference in $\rho_{lf,hf}$ results in a smaller difference in runup, and the coefficients of correlation are small: $\rho_{lf,hf}$ on the swash zone border is not an important parameter for explaining the model difference in runup. On average $\rho_{lf,hf}$ at the swash zone border is -0.16 for XBeach Non-hydrostatic and -0.04 for XBeach Surfbeat. According to the theoretical relationship between $\rho_{lf,hf}$

and the energy transfer into the infragravity waves of Battjes et al. (2004), see section 3.5.4, a larger negative $\rho_{lf,hf}$ (closer to -1) results in a smaller energy transfer into the infragravity waves. The fact that XBeach Surfbeat predicts a larger energy transfer into the infragravity waves but does not predict higher infragravity waves or infragravity swash again indicates that $\rho_{lf,hf}$ is not an important parameter for explaining the model difference in runup. The influence of the tide on $\rho_{lf,hf}$ was checked: for both models $\rho_{lf,hf}$ decreases for larger tidal water levels. For a larger tidal water level less incident waves have broken and the infragravity wave is still bound (or closer to being bound), resulting in a smaller $\rho_{lf,hf}$. This relation is stronger for XBeach Non-hydrostatic than for XBeach Surfbeat (correlation of -0.31 versus -0.21 between the tidal water level and $\rho_{lf,hf}$).

5.5. Isolation of the swash zone

5.5.1. Forcing the swash zone with infragravity wave height

The importance of the incoming infragravity wave height for the significant infragravity swash is proven by forcing an isolated 1D XBeach Non-hydrostatic model of the swash zone with different infragravity wave heights. This was done for multiple cases of which three are shown here: the October 18 case (high offshore wave heights), the October 4 case (low offshore wave heights) and the October 27 case (intermediate offshore wave heights). For all cases a positive relation between the incoming infragravity wave height at the swash zone border and the infragravity swash was found, but the strength of this relation differs.
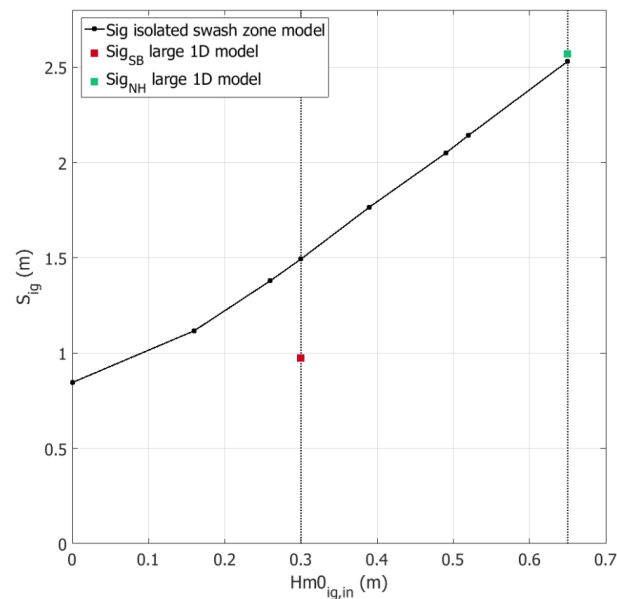
Figure 5.11: Relationship between the incoming infragravity wave height at the border of the isolated model of the swash zone of October 18 and the significant infragravity swash.

Swash zone model of October 18: high offshore wave heights   As explained in section 3.5.5 and appendix J a 1D XBeach Non-hydrostatic and a 1D XBeach Surfbeat simulation of the full cross shore of Duck are used to generate the infragravity wave height at the swash zone border. The isolated XBeach Non-hydrostatic model is forced with the respective infragravity wave heights of the full 1D simulations ($H_{m0,ig,in,NH} = 0.64$ m and $H_{m0,ig,in,SB} = 0.30$ m) and other evenly distributed infragravity wave heights. The result for the isolated swash zone model of October 18 is an almost linearly increasing significant infragravity swash, see figure 5.11. The incoming infragravity wave height thus is the main driver of the infragravity swash. Infragravity swash is also generated when no infragravity waves are present. In some way incident waves or the interaction between them create infragravity swash. A possible explanation for this is bore merging: incident bores merge together and form infra-

gravity bores within the swash zone (Mase, 1989).

As mentioned above the boundary conditions for the isolated swash zone model were generated with a 1D XBeach Non-hydrostatic and XBeach Surfbeat model of the full cross shore. These full 1D models were forced with the measured frequency-directional spectrum of October 18 19.00. The infragravity swash predicted by these models is also depicted in figure 5.11. The infragravity swash predicted by the isolated and the full XBeach Non-hydrostatic model, where incoming infragravity wave height is the same at the swash zone border, is almost the same. This indicates that the isolation and forcing of the swash zone model goes well and yields the same results as the full model. The full XBeach Surfbeat model predicts a lower infragravity swash than the isolated XBeach Non-hydrostatic model, while the incoming infragravity wave height at the swash zone border is identical. Even when the two XBeach models are forced with an identical incoming infragravity wave height differences develop within the swash zone, which lead to a difference in infragravity swash prediction. Again a possible cause is bore merging: XBeach Surfbeat is not able to predict this while XBeach Non-hydrostatic is.

The difference in infragravity swash prediction between the full 1D XBeach Non-hydrostatic and XBeach Surfbeat model is approximately 1.5 m (difference between red and green point). Of this difference approximately 0.5 m originates within the swash zone: this is the difference in infragravity swash between the two XBeach models when the incoming infragravity wave height at the swash zone border is identical. 1 m difference then originates from outside the swash zone. For this specific case one third of the difference in infragravity swash thus originates from within the swash zone and two third outside of it. However, this ratio is very case dependent: for the isolated swash zone model at the same day but a different time the ratio is the other way around. An exact ratio thus cannot be given but the difference in infragravity swash originating from the swash zone is significant.

The 2D XBeach Non-hydrostatic model of October 18 19.00 as used in the validation predicts an infragravity swash of 1.18 m, the 2D XBeach Surfbeat model 0.32 m. This is a factor 2-3 lower than the infragravity swash predicted by the full 1D models, due to the fact that wave heights and thus swash are higher in 1D than 2D.
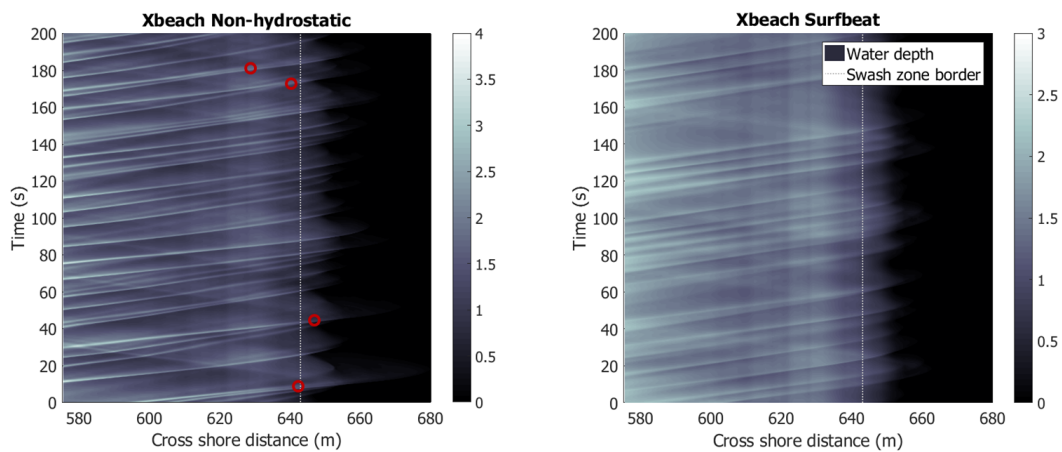
Figure 5.12: x-t plots of the water depth for both XBeach models for October 18 19.00. The plots start at x = 575 m, generally the point of incident wave breaking. The swash zone border is indicated and occurence of bore merging is indicated with red dots.

Bore merging was mentioned as a possible cause for an higher infragravity swash prediction by XBeach Non-hydrostatic. For the specific case of October 18 the occurence of bore merging in the swash zone was investigated. In figure 5.12 a x-t plot of the water depth can be seen for both XBeach models. Locations where bores merge are indicated with red dots. For XBeach Surfbeat the bores all propagate with the same speed and never overtake each other (lines are parallel). For XBeach Non-hydrostatic bores overtake each other multiple times, of which two times outside the swash zone and two times

within the swash zone or on the swash zone border. Whether these merges actually lead to more infragravity swash is not known. Other possible reasons for a higher infragravity swash are generation of extra infragravity waves by the model or a difference in incoming incident wave height. However, the difference in incoming incident wave height between the full 1D XBeach models is much smaller than the difference in incoming infragravity wave height. Its influence is therefore assumed to be smaller.

Swash zone model of October 4 and 27: low and medium offshore wave heights   Besides the case described above an isolated swash zone model was made for two other cases, representing low and intermediate offshore energetic conditions (October 4 and October 27 respectively). The relation between incoming infragravity wave height at the swash zone border and infragravity swash is shown in figure 5.13. Positive relations between the incoming infragravity wave height and infragravity swash were found but less strong than for the October 18 case.
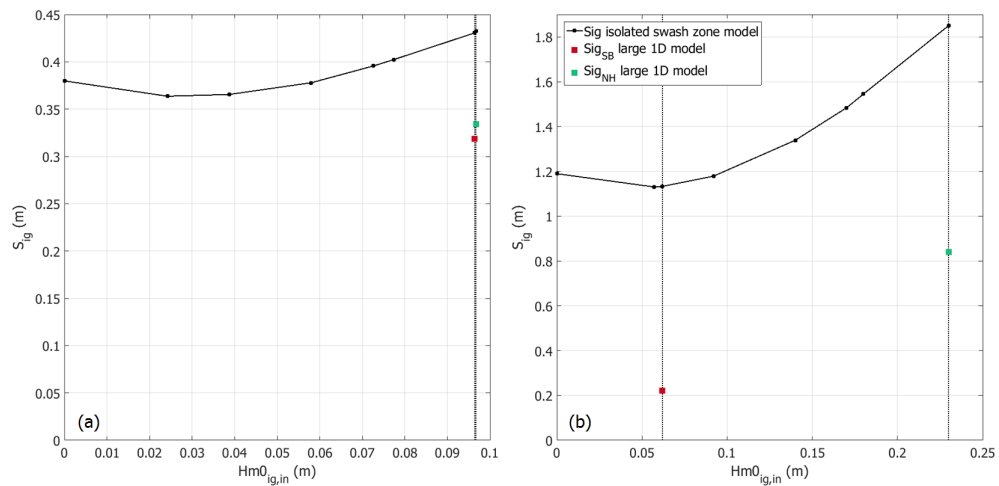
Figure 5.13: Relationship between the infragravity wave height at the border of the isolated models of the swash zone of October 4 and 27 and the significant infragravity swash. (a) October 4. (b) October 27.

In figure 5.13 a the relation between the incoming infragravity wave height and the infragravity swash can be seen for the October 4 case, where offshore energetic conditions were mild. For increasing infragravity wave height infragravity swash increases but the growth is mild. In figure 5.13 b the relation between the incoming infragravity wave height and the infragravity swash can be seen for the October 27 case, where offshore energetic conditions were intermediate. A positive relation is found, stronger than for the October 4 case. The increase in infragravity swash per unit increase in incoming infragravity wave height is 0.5 m for the October 4 case, while this is 2.6 for the October 18 case and 2.8 for the October 27 case. The strongest relation is thus found for the case with intermediate offshore energetic conditions.

For the October 18 case the full and the isolated 1D XBeach Non-hydrostatic model predict a similar infragravity swash. This is not the case for the two cases shown here. The infragravity swash predicted by the full 1D model is lower than the one predicted by the isolated model. The difference between the isolated and full 1D XBeach Non-hydrostatic model (with identical incoming infragravity wave height at the swash zone border) and the difference between the isolated XBeach Non-hydrostatic and full XBeach Surfbeat model (again with identical incoming infragravity wave height at the swash zone border) are of similar magnitude. Even when there are no infragravity waves present the infragravity swash predicted by the isolated model is larger than that predicted by the full 1D XBeach Non-hydrostatic model. This indicates that for isolation cases with lower energetic conditions incident waves play a role for the infragravity swash. However, the incident waves of the isolated and the full XBeach Non-hydrostatic model are also identical. Clearly something goes wrong in how the incident waves are enforced on the isolated model: for lower energetic conditions a beach is more reflective,

incident waves play a larger role and a mistake in enforcing incident waves has a larger effect. This can also be seen from figure 5.14. The water movements in the swash zone can be seen at different moments in time for the October 4 case. The peaks of the waves are predicted slightly higher by the isolated model and a larger runup height is predicted. From an animation of the water level it can be seen that for the October 4 case the water motions close to shore are of higher frequency: the runup is not driven by infragravity waves but by incident waves. The swash is also much more high frequent than the swash of October 18. The relatively high infragravity swash found in the October 4 case (for very low infragravity wave heights) is the results of high peaks of the high frequent swash and as they do not occur often they are marked as infragravity swash.
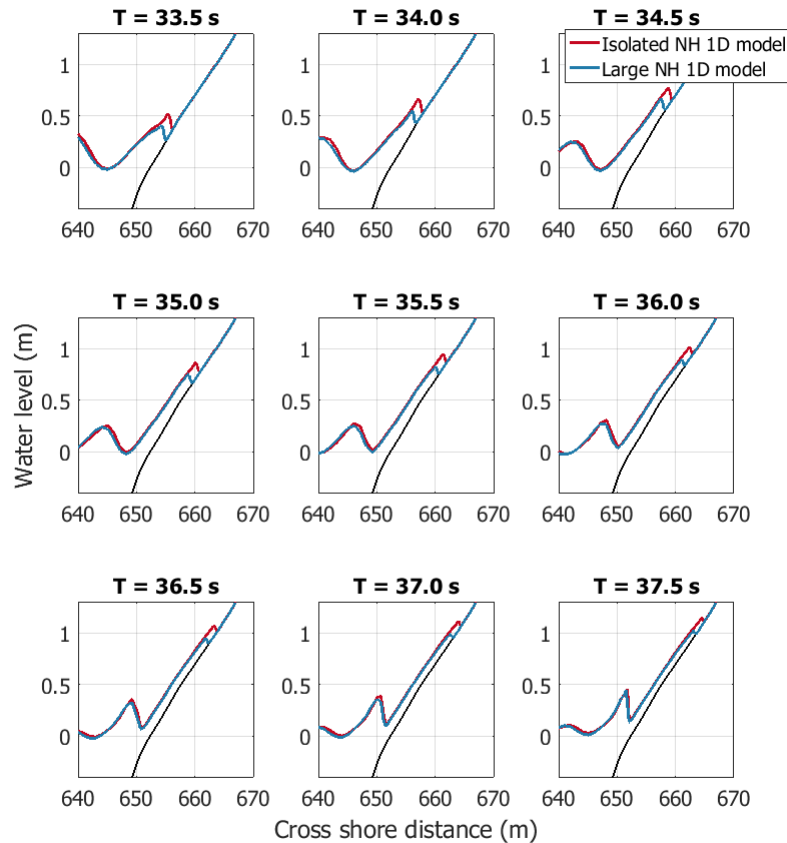
Figure 5.14: Water level in the swash zone for the full 1D and isolated swash zone XBeach Non-hydrostatic model for October 4. The situation at different moments in time is shown.

Occurence of bore merging is investigated for the October 4 and 27 case but bore merging is identified less often, see figures 5.15. Only one location of bore merging was found for the October 27 case.
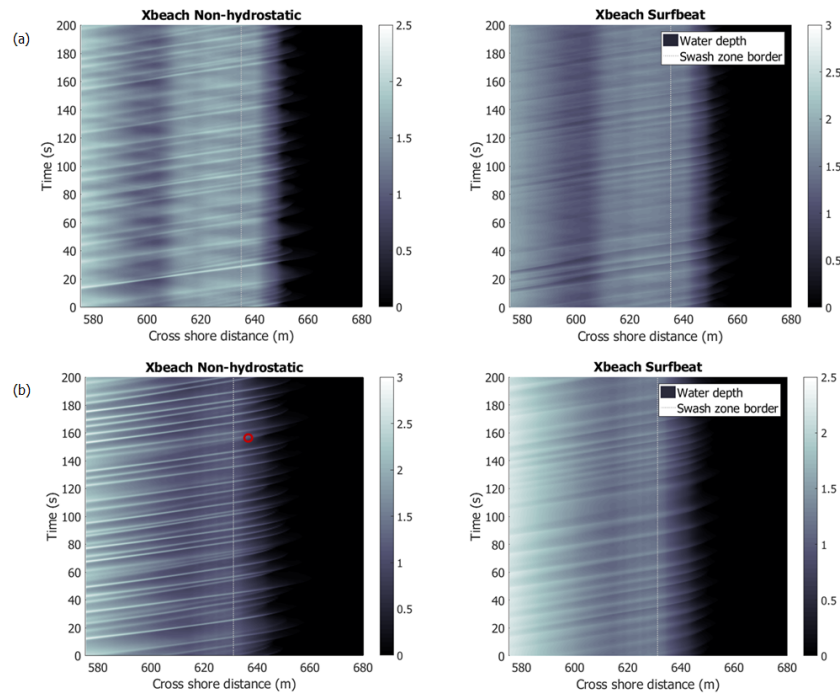
Figure 5.15: x-t plots of the water depth for both XBeach models for October 4 12.00 and October 27 20.00. The plots start at x = 575 m, generally the point of incident wave breaking. The swash zone border is indicated and occurence of bore merging is indicated with red dots.

5.5.2. Forcing the swash zone with incident wave height

The fact that the incident swash is not influenced by the incoming incident wave height but by aspects of resolving the incident waves is proven by forcing the swash zone border of the isolated swash zone model for the October 18 case with different incoming incident wave heights. The incoming incident wave height at the swash zone border predicted by the full 1D XBeach Surfbeat model is 0.73 m. When forcing the isolated 1D XBeach Non-hydrostatic swash zone model with the same incident wave height a higher incident swash results, see table 5.1.

Table 5.1: Incoming incident wave height at the swash zone border and the resulting incident swash for the full 1D XBeach Surfbeat model and the isolated XBeach Non-hydrostatic model.

Model	$H_{m0,in,inc}$ (m)	S_{inc} (m)
Full 1D XBeach SB	0.73	0.65
Isolated 1D XBeach NH	0.73	1.33

5.6. Conclusion & Discussion

XBeach Non-hydrostatic and XBeach Surfbeat predict a similar setup, but XBeach Non-hydrostatic is a better predictor of incident and infragravity swash. XBeach Surfbeat does not resolve incident waves and swash, which probably is the reason behind the better prediction of incident swash. This is supported by the fact that while having the same incoming incident wave height at the swash zone border XBeach Non-hydrostatic predicts a larger incident swash. The difference in significant incident swash thus already originates at the boundary.

The difference in significant infragravity swash is strongly correlated with the difference in incoming infragravity wave height, which generally is in the favour of XBeach Non-hydrostatic. This difference is already present near the offshore boundary and relevant for the infragravity swash difference there.

Over the cross shore it becomes more relevant, indicating that there are also differences in incoming infragravity wave height developing within the domain. Between the location of most nearshore pressure gauges and the swash zone border the correlation between infragravity wave height and swash hardly increases anymore, possibly but not necessarily indicating that hydrodynamic differences mainly develop offshore of the most nearshore pressure gauge location. Finally, hydrodynamic differences are developing within the swash zone, as XBeach Non-hydrostatic predicts a larger infragravity swash when the infragravity wave height at the swash zone border is the same as for XBeach Surfbeat. The contribution of each part of the cross shore to the infragravity swash difference should be investigated further, but it can be said that differences originating in the swash zone can be significant.

The relevance of infragravity waves for infragravity swash increases with offshore energetic conditions: for higher offshore energetic conditions and thus a more dissipative beach infragravity waves are the main driver of infragravity swash. This is consistent with Ruessink et al. (1998), who states that infragravity motions become more important on a more dissipative beach. Even without the presence of infragravity waves infragravity swash is generated, as also seen by Mase (1989) and Carlson and Asce (1984): due to the interaction of bores infragravity swash is generated. This also explains why XBeach Non-hydrostatic predicts a larger infragravity swash while having the same infragravity wave height as XBeach Surfbeat at the swash zone border, as XBeach Surfbeat is not able to capture incident bore merging. Evidence of bore merging was found for high offshore energetic conditions but less for lower energetic conditions: Tissier et al. (2017) and Tissier et al. (2015) report that bore merging occurs where infragravity waves dominate (the variability in wave celerity is related to the ratio of infragravity wave height to water depth, which is maximum in the inner surf zone). However, Tissier et al. (2017) found no proof that bore merging leads to generation of infragravity energy and this should be investigated further for this case. Infragravity swash predicted by the 1D models used to generate boundary conditions for the swash zone models is a factor 2-3 higher than for the 2D simulations used in the validation. The same order of magnitude factor was found by Stockdon et al. (2014) between a 1D and 2D XBeach Surfbeat model and a factor 1.5 was found between a 1D and 2D SWASH model by Lerma et al. (2017).

The above was shown using a 1D XBeach Non-hydrostatic model of the isolated swash zone. The assumption that everything is cross shore dominated at the swash zone border and that therefore a 1D model is sufficient, was also made by van Rooijen et al. (2012). Difficulties arose with enforcing boundary conditions on the swash zone border for lower energetic conditions. In previous research by van Rooijen et al. (2012) and Reniers et al. (2013) where a XBeach model of only the swash zone was used no such difficulties were reported.

No significant correlation was found between the groupiness of the incident waves and runup or between $\rho_{lf,hf}$ and runup, indicating these parameters are not the primary cause for a difference in runup. However, they can still be a secondary cause by leading to a difference in infragravity wave height. The transformation of both the groupiness factor GF and $\rho_{lf,hf}$ are not entirely as expected. According to List (1990) and Medina (1992) the offshore value of GF at 8 m depth should be 0.74, which is approximately the case for XBeach Surfbeat but the value for XBeach Non-hydrostatic is lower. This is due to use of the Hilbert-Huang transformation, as offshore it predicts a lower value of GF than the Hilbert transformation, see appendix F. Close to shore its performance is better but further offshore the choice for the Hilbert transformation would have been better. However, the choice was made to use one method for the entire cross shore and conclusions regarding the groupiness or the phase difference do not change when using the Hilbert transformation in the offshore region instead. According to van Thiel de Vries (2009) $\rho_{lf,hf}$ should be close to -1 offshore, stay constant and increase at the point of short wave breaking. Tissier et al. (2017) reports that the offshore value can be closer to -0.5 for irregular wave cases. However, for both XBeach models it is close to 0. A simple 1D case reflects the transformation reported by van Thiel de Vries (2009) just as the 1D XBeach Surfbeat model used by van Thiel de Vries (2009), suggesting that directional spreading reduces the capability of reproducing $\rho_{lf,hf}$ well.

Splitting incoming and reflected waves with the Guza method does not have a significant effect on the trends described above. This suggests that the Guza method is not the cause for strange model results

or that there is little reflection. However, on a intermediate reflective beach such as Duck significant reflection is expected, as reflection coefficients were seen to be influenced by the beach steepness by van Dongeren et al. (2007). The Guza method should be compared to the Maximum Entropy Method (Lygre and Krogstad, 1986), a method for splitting incoming and reflected waves suitable for a 2D wave field. In this way errors from the Guza method can be estimated better.

<div style="text-align: right; font-size: 3em;">6</div>

Boundary related infragravity wave differences between the XBeach models

6.1. Introduction

A difference in significant infragravity swash prediction between XBeach Non-hydrostatic and XBeach Surfbeat was seen, which has been linked to a difference in incoming infragravity wave height at the swash zone border in chapter 5. This difference in infragravity wave height has its origin partly at the offshore boundary and partly in the transformation over the surfzone. This chapter describes the differences in infragravity wave height at or near the boundary. In section 6.2 the differences in infragravity wave height very close to the boundary (at the second grid cell, as on the first grid cell velocities have not yet been enforced) are investigated for simple test cases. In section 6.3 the difference in infragravity waves is not approached spectrally but in the time domain: infragravity water levels close to the boundary are compared. Finally in section 6.4 the generation of wave boundary conditions for both XBeach models is considered and how the boundary conditions are transferred from the boundary to the first grid cells within the domain. It should be noted that for all simulations in this chapter random generation of the boundary conditions was turned off, indicating that exactly the same wave components are drawn from the input spectrum.
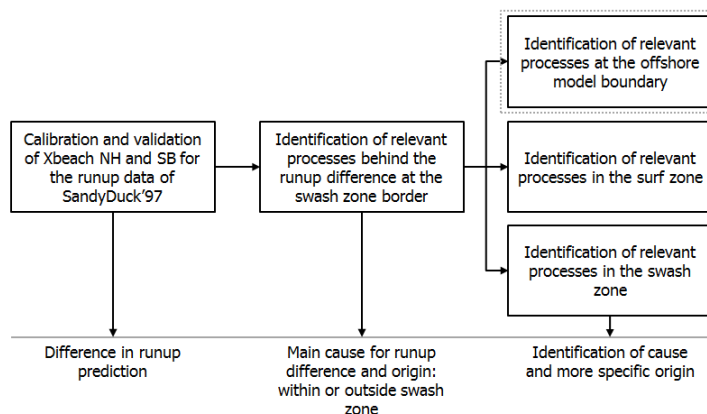
6.2. Infragravity wave height for simple test cases

6.2.1. Testcases using the bathymetry of Duck

By using simple 1- and 2-dimensional testcases the presence of a difference in infragravity wave height very close to the boundary (at the second grid cell) was determined and mechanisms influencing these differences, such as directional spreading and offshore significant wave height, were investigated. From these test cases it was seen that a very small difference in infragravity wave height is present in 1D

which increases for 2D simulations with increasing directional spreading.
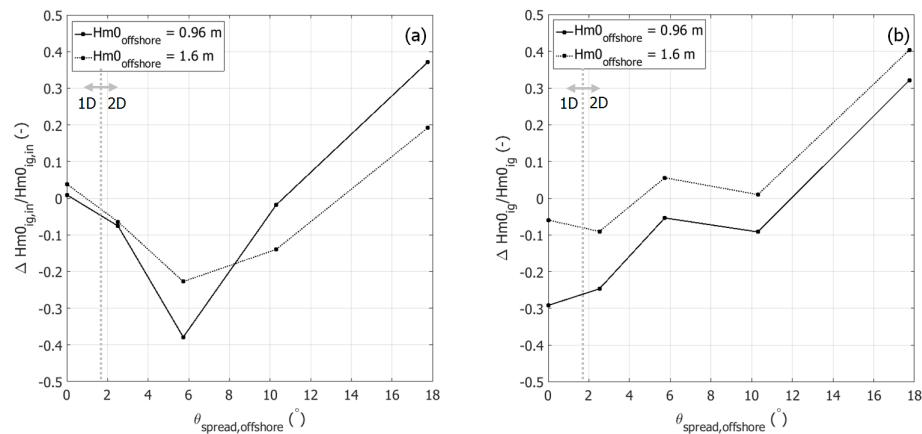
Figure 6.1: Difference in incoming and total infragravity wave height between XBeach Non-hydrostatic and XBeach Surfbeat at the second grid cell of the domain, for 1D and 2D testcases with different degrees of directional spreading and two offshore significant wave heights.

To show this multiple test cases were used (for a full list see appendix L). From the measured bathymetry at Duck a 1D grid and a 2D alongshore uniform grid were constructed. The 1D cases were forced with a narrow JONSWAP spectrum without directional spreading, while the 2D cases were forced with the same narrow JONSWAP spectrum but with increasing directional spreading. Besides the directional spreading two significant wave heights of the JONSWAP spectrum were used. In figure 6.1 the differences in infragravity wave height between XBeach Non-hydrostatic and XBeach Surfbeat on the second grid cell are shown. A positive difference indicates XBeach Non-hydrostatic predicts a higher infragravity wave height and the differences are relative. Figure 6.1 a gives the results for the incoming infragravity wave height, while b shows the total infragravity wave height.

For the 1D case there is a positive difference of 1% in $H_{m0,ig,in}$ for a offshore wave height of 0.96 m and a difference of 4% for a offshore wave height of 1.6 m: XBeach Non-hydrostatic predicts a higher incoming infragravity wave height at the second grid cell and the difference increases for a higher offshore significant wave height. However, the increase is small. It should be noted that only two offshore significant wave heights were tested and to see proper trends at least 3 should be used. For a 2D case with a directional spread of 2.52 °, which is very similar to the 1D case (see figure 6.2 a and b), the difference in incoming infragravity wave height is negative and the same for both offshore significant wave heights. For increasing directional spread first the difference in incoming infragravity wave heights increases in magnitude in negative direction, up to differences of 40%. Between $\theta_{spread,offshore}$ of 5.73 and 10.31 ° a transition point can be identified: from that point onward the difference in incoming infragravity wave height becomes positive again (XBeach Non-hydrostatic predicts a larger wave height) and increases in magnitude in positive direction, up to differences of 37%. From $\theta_{spread,offshore} = 5.73°$ onwards a higher offshore significant offshore wave height results in a smaller difference in incoming infragravity wave height and the difference between the low and high offshore significant wave height remains constant. Generally a higher offshore significant wave height gives the same trends but the absolute value of the difference in incoming infragravity wave height is smaller.

The 1D case results in larger and negative differences for the total infragravity wave height, with differences of 29% for an offshore wave height of 0.96 m and 6% for an offshore wave height of 1.6 m. The larger differences for total infragravity wave height are due to a difference in propagation in the domain, visible in figure 6.2 a. For the 1D case a much stronger growth in incoming infragravity wave height is present for XBeach Surfbeat. For increasing directional spread the difference in total infragravity wave height increases, becomes positive again between $\theta_{spread,offshore}$ of 5.73 and 10.31 ° and increases in magnitude, up to differences of 31%. A larger offshore significant wave height results

in a smaller difference when XBeach Surfbeat dominates at the boundary but in a larger difference when XBeach Non-hydrostatic dominates (up to 41%). This suggests that the total infragravity wave height predicted by XBeach Non-hydrostatic increases for increasing offshore significant wave height, while this happens for XBeach Surfbeat to a smaller degree.

The directional spread imposed on the boundary determines both the magnitude of the difference in infragravity wave height and the sign, or in other words which XBeach model predicts a larger infragravity wave height at the second grid cell. Offshore significant wave height influences the difference in incoming and total infragravity wave height in opposing directions: a higher offshore wave height leads to a smaller difference in incoming infragravity wave height but to a larger difference in total infragravity wave height (only for $\theta_{spread,offshore} > 5.73°$).
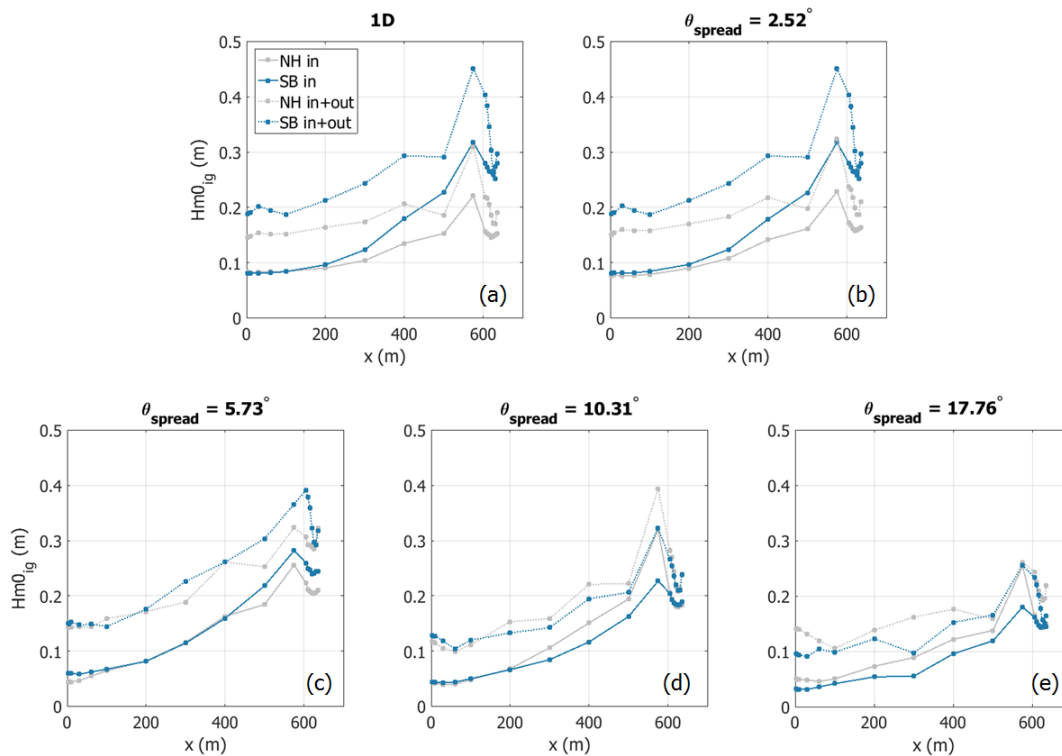
Figure 6.2: Transformation of incoming and total infragravity wave height over the cross shore for the 1D and 2D testcases with different degrees of directional spreading and for both XBeach models.

In figure 6.2 and 6.3 the transformation of infragravity wave height and the transformation in the difference in infragravity wave height over the cross shore for both XBeach models and for the incoming and total infragravity wave height can be seen. For a 1D case the incoming infragravity wave height predicted by XBeach Surfbeat grows much stronger than for XBeach Non-hydrostatic. The difference in incoming infragravity wave height thus becomes more negative as going towards shore. The same trend can be seen for a 2D case with $\theta_{spread,offshore} = 2.52°$. For increasing directional spread the difference in incoming infragravity wave height between the XBeach models becomes smaller until the difference becomes positive for $\theta_{spread,offshore} = 10.31°$. This is consistent with the fact that for the 2D simulations of Duck XBeach Non-hydrostatic predicts higher incoming infragravity wave heights over the entire cross shore.

For a 1D case the same behaviour for total as for incoming infragravity wave height can be seen: XBeach Surfbeat predicts a stronger growth. For increasing directional spread again XBeach Non-hydrostatic starts predicting higher total infragravity wave heights but the difference lines show wiggles. This can also be seen in figure 6.2 c and e: the transformation of total infragravity wave height is not increasing continuously but experiences some dips. If this only occurs for either XBeach Non-hydrostatic or
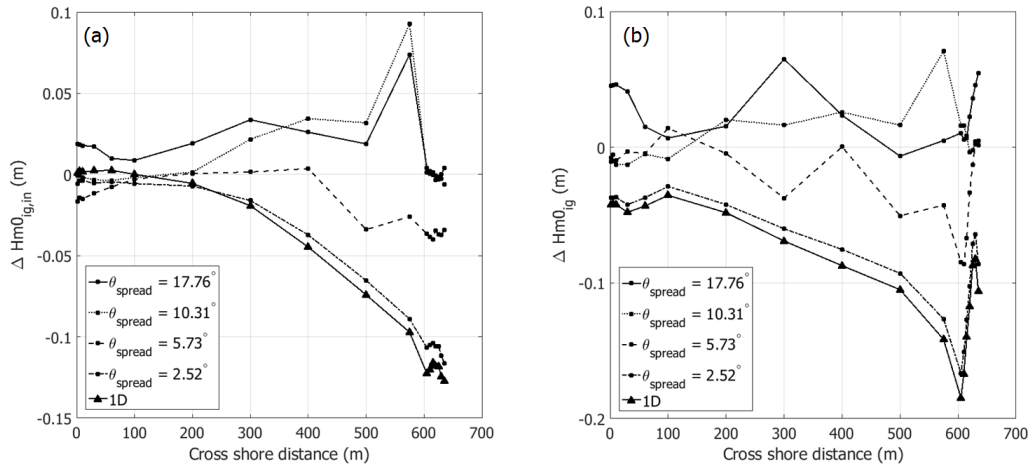
Figure 6.3: Transformation of the difference in infragravity wave height between XBeach Non-hydrostatic and XBeach Surfbeat over the cross shore for a 1D test case and 2D testcases with different degrees of directional spreading (increasing from $\theta_{spread} = 2.52°$ to $17.76°$).

XBeach Surfbeat a wiggle in the difference line can be seen.

To estimate which difference in incoming infragravity wave height is more relevant, the one on the second grid cell or the ones in the domain, the spread in relative differences in absolute sense is determined for the four 2D testcases in figure 6.2: no attention is paid to which model predicts a larger incoming infragravity wave height but only the magnitude of the relative difference is considered. This can be seen in table 6.1. When going from the second grid cell to shore the difference first decreases as in some cases the difference in incoming infragravity wave height changes sign here. It then increases towards shore and the differences there are larger than at the second grid cell. The differences developing within the domain are thus more important than the differences at the boundary, which can also be seen from figure 6.2.

Table 6.1: Spread in the relative difference in incoming infragravity wave height between the XBeach models in absolute sense at different locations in the cross shore. x = 2 m is the second grid cell.

X-coordinate (m)	Spread in $\left\|\frac{\Delta H_{mo,ig,in}}{H_{mo,ig,in}}\right\|$ (%)	X-coordinate (m)	Spread in $\left\|\frac{\Delta H_{mo,ig,in}}{H_{mo,ig,in}}\right\|$ (%)
2	2-37	400	2-26
30	7-36	500	14-41
100	4-17	575	10-39
200	1-26	605	1-62
300	1-38		

6.2.2. Test cases on a horizontal bottom

To further isolate what happens at the boundary two other type of test cases were used: one where only infragravity waves and one where only incident waves are enforced on the domain (with the random phase model only waves are generated from either the infragravity or incident part of the spectrum). A grid with a horizontal bottom and an absorbing boundary at the other side of the domain are used to exclude reflected waves. Even in these very simple cases there is a difference in infragravity wave height at the second grid cell.

Simulating only infragravity waves In table 6.2 the relative difference in incoming infragravity wave height at the second grid cell can be found for different degrees of directional spreading when only infragravity waves have been enforced on the model. A difference in infragravity wave height between 5 and 10% was found. The difference is negative: XBeach Surfbeat predicts a larger infragravity wave height for all cases, which is different for the 2D testcases on an alongshore uniform Duck bathymetry. For increasing directional spread the difference first decreases and then increases again, so no clear relation between the directional spread and the difference in infragravity wave height can be seen here. From this test case it can be concluded that there either is a difference in the way the infragravity wave boundary conditions are generated or in how they are enforced on the domain.

Simulating only incident waves In table 6.2 the relative difference in incoming infragravity wave height between XBeach Non-hydrostatic and XBeach Surfbeat is given for four 2D cases with different degrees of directional spreading, when only enforcing incident waves on the model. XBeach Surfbeat predicts a much higher infragravity wave height with differences close to 100%. However, the infragravity water level amplitude predicted by XBeach Surfbeat is still very small (order of 1 cm). Apparantly when only enforcing incident waves XBeach Surfbeat generates very small waves in the infragravity frequency band in the first two grid cells while XBeach Non-hydrostatic hardly does. The difference in infragravity wave height decreases for increasing directional spread. The fact that a different infragravity water level is created for XBeach Non-hydrostatic and XBeach Surfbeat when only incident waves are enforced indicates that not only infragravity wave boundary generation and enforcement differs between the models but also incident wave boundary generation and enforcement. However, in all four cases here XBeach Surfbeat predicts a higher infragravity wave height, while when forcing with the full spectrum on the grid of Duck XBeach Non-hydrostatic predicts a higher infragravity wave height for 2D simulations with directional spread.

Table 6.2: Difference in infragravity wave height between the XBeach models at the second grid cell of the domain for a testcase with a horizontal bottom and when only forcing incident or infragravity waves on the model. The difference is given in percentages for different degrees of directional spreading (a positive difference indicates that XBeach Non-hydrostatic predicts a larger value).

Test case	$\Delta H_{m0,ig,in}$ (%)			
	$\theta_{spread} = 2.52°$	$\theta_{spread} = 5.73°$	$\theta_{spread} = 10.31°$	$\theta_{spread} = 17.76°$
Infragravity waves only	-9.72	-6.66	-5.26	-7.07
Incident waves only	-97.9	-97.8	-97.7	-94.1

6.3. Comparison of infragravity water level timeseries

The difference in incoming infragravity wave height at the second grid cell as discussed in section 6.2 could be the result of splitting incoming and reflected waves with the Guza method. Therefore a comparison was also made between the total infragravity water level timeseries of XBeach Non-hydrostatic and XBeach Surfbeat at the second grid cell. Only the first 50 seconds are considered, in that way excluding reflected waves. Also in this analysis differences in infragravity band energy are present between the XBeach models, with more infragravity energy for XBeach Non-hydrostatic.

In figure 6.4 the infragravity water level timeseries of both XBeach models are compared for three 2D cases of Duck (the same as were used in chapter 5: low offshore wave height at October 4, high at October 18 and medium at October 27). It is clear that the amplitude of the water level is larger for XBeach Non-hydrostatic with an increasing difference for increasing offshore wave height, resulting in an higher incoming infragravity wave height. For the 2D testcases with different degrees of directional spreading on an alongshore uniform grid of Duck the same analysis was done of which the results are shown in figure 6.5. The difference in amplitude between XBeach Non-hydrostatic and XBeach Surfbeat is less distinctive, but the amplitude is again larger for XBeach Non-hydrostatic. This can be
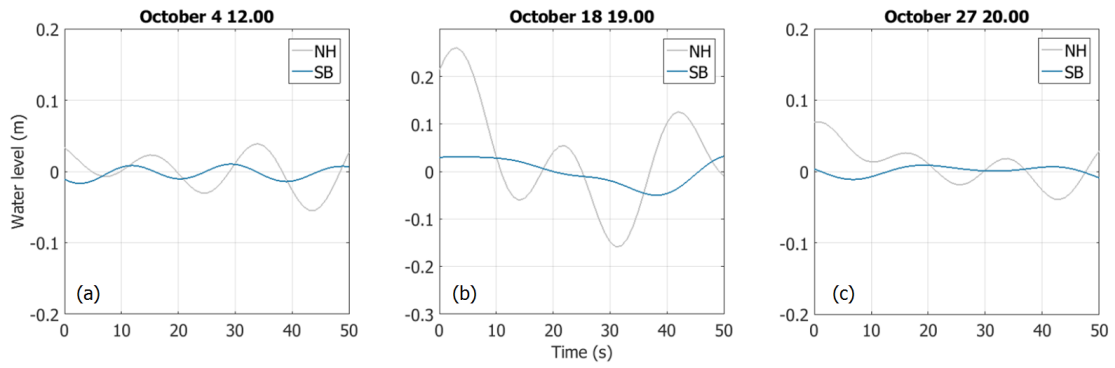
Figure 6.4: Comparison of infragravity water levels for XBeach Non-hydrostatic and XBeach Surfbeat on the second grid cell and for the first timesteps (no reflected waves yet), for three specific cases (low offshore wave height at October 4, high offshore wave height at October 18 and intermediate offshore wave height at October 27).

seen more clearly from the difference in variance $\Delta\sigma^2$ of the timeseries in the first 50 seconds: this is negative only for $\theta_{spread} = 2.52°$ and positive for the other values of θ_{spread}. Besides that no clear relation can be seen between the directional spread and the difference in variance.
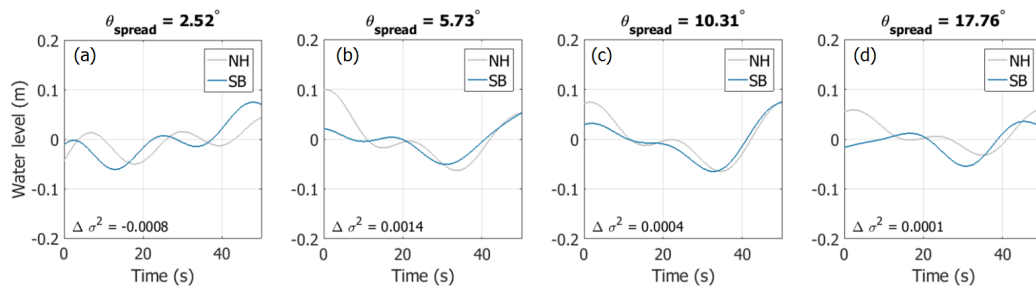
Figure 6.5: Comparison of infragravity water levels for XBeach Non-hydrostatic and XBeach Surfbeat on the second grid cell and for the first timesteps (no reflected waves yet), for the 2D test cases. For each plot the difference in variance of the timeseries is indicated with $\Delta\sigma^2$ (a positive difference indicates XBeach Non-hydrostatic predicts a larger value).

6.4. Generation of boundary conditions

In the previous sections it was shown that when forcing the models with the same spectrum XBeach Non-hydrostatic predicts a different infragravity wave height at the second grid cell than XBeach Surfbeat. This means that there either is a difference in wave boundary generation between XBeach Non-hydrostatic and XBeach Surfbeat or in the way the boundary conditions are enforced on the model. In this section both elements are discussed for a simple 1D test case with a narrow JONSWAP spectrum without directional spreading. From the wave boundary generation the same boundary conditions result but a different spectrum results at the second grid cell.

As described in section 2.5.2 both XBeach models generate a high frequency water level timeseries from the input spectrum with a random phase model. With the transformation function of Herbers et al. (1994) the low frequency water level timeseries is generated. Above steps are identical for the two models. From the high frequency water level timeseries XBeach Surfbeat takes the envelope and enforces this on the model along with the low frequency water level timeseries. XBeach Non-hydrostatic adds high and low frequency water level timeseries together and enforces this on the model. The spectrum of the low and high frequency water level timeseries are compared for both models in figure
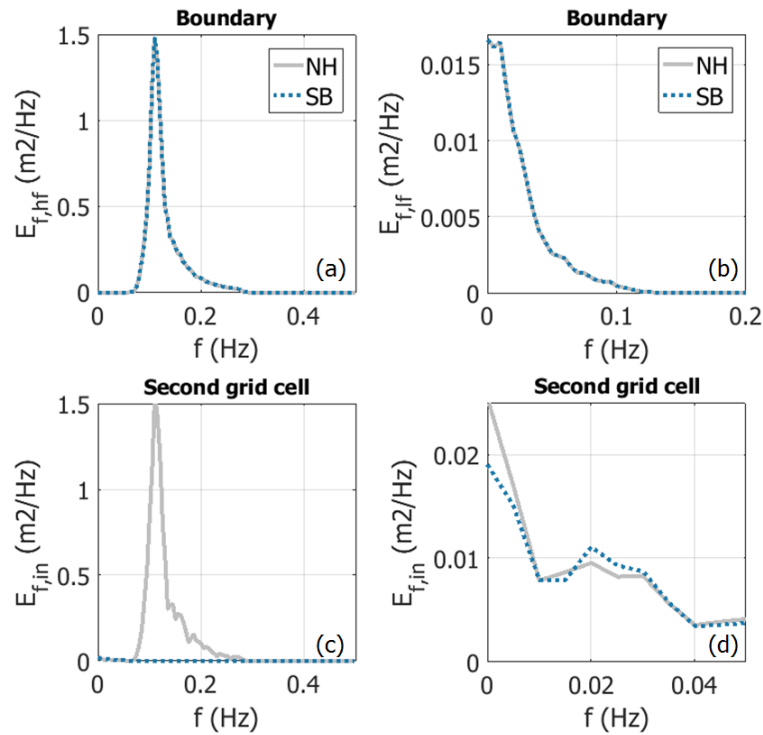
Figure 6.6: Comparison of the boundary conditions generated by XBeach Non-hydrostatic and XBeach Surfbeat. (a) Spectrum of the high frequency waves for both XBeach Non-hydrostatic and XBeach Surfbeat. (b) Spectrum of the low frequency waves for both XBeach Non-hydrostatic and XBeach Surfbeat. (c) Resulting spectrum on the second grid cell. (d) Infragravity part of the spectrum in (c).

6.6 a and b. They are indeed identical. In figure 6.6 c the spectrum of the incoming total water level timeseries at the second grid cell in the domain is shown, with the infragravity part of that spectrum shown in figure 6.6 d. The variance m_0 for the low and high frequency spectrum and for the spectrum predicted by XBeach Non-hydrostatic and XBeach Surfbeat at the second grid cell is given in table 6.3.

Table 6.3: Variance of the high, low and total frequency spectrum generated at the boundary and of the spectrum at the second grid cell within the domain for both XBeach models.

Location	Model	$m_0 (m^2)$		
		Low frequency	High frequency	Total
Boundary	NH/SB	0.000556	0.0576	0.0582
Domain	NH	0.000438	0.0616	0.0620
	SB	0.000422	0.000067	0.000489

From the m_0-values in the table it can be seen that both XBeach models lose infragravity energy between the boundary and the second grid cell. XBeach Surfbeat thus does not create extra infragravity energy in this case. Even though losing infragravity energy XBeach Non-hydrostatic still contains more than XBeach Surfbeat. Considering total variance XBeach Non-hydrostatic gains some energy between the boundary and the first grid cell, which ends up in the high frequency band. Why XBeach Non-hydrostatic gains energy is not known. Concluding, boundary conditions generated from the input spectrum are identical for XBeach Non-hydrostatic and XBeach Surfbeat. Either in the way they are enforced on the domain or in processes in the first grid cell must be a difference.

6.5. Conclusion & Discussion

Differences in incoming infragravity wave height lead to a different prediction of infragravity swash by XBeach Non-hydrostatic and XBeach Surfbeat. The difference in incoming infragravity wave height is already present at the second grid cell of the domain and can be significant. This was shown in the chapter above for multiple test cases.

For a 1D case there is a small difference in incoming infragravity wave height at the second grid cell, which increases for 2D cases with increasing directional spread. For a 2D case with a large directional spread XBeach Non-hydrostatic predicts larger incoming infragravity wave heights. This is consistent with 2D validation simulations of Duck where the directional spread was 49.25 °: for a directional spread wave field XBeach Non-hydrostatic predicts larger incoming infragravity wave heights. Differences go up to 37%. Higher energetic conditions offshore result in smaller differences in incoming infragravity wave height, but this is based on only two offshore wave heights. To distinguish a clear trend more offshore wave heights should be investigated. Differences in incoming infragravity wave height not only become clear from the spectral domain, but also from the time domain: infragravity water levels from XBeach Non-hydrostatic clearly have a larger amplitude than the ones predicted by XBeach Surfbeat. Besides a difference in incoming infragravity wave height close to the boundary there also is a difference in propagation, even when boundary differences are very small. The differences originating within the domain are thus just as or more relevant than the differences at the boundary. Possible causes for differences originating within the domain are discussed in chapter 7.

Differences in incoming infragravity wave height are not caused by a difference in boundary generation, as this yields identical boundary conditions, or boundary condition enforcement. When enforcing either only infragravity or incident waves XBeach Surfbeat predicts a larger incoming infragravity wave height, but when forcing with a full spectrum XBeach Non-hydrostatic predicts a larger wave height. This indicates that there must be an interaction between the imposed infragravity and incident wave boundary conditions in the first grid cell. The mechanism through which this happens is not clear yet and should be investigated further.

Concluding, forcing XBeach Non-hydrostatic and XBeach Surfbeat with the same spectrum results in differences near the boundary within the domain, where XBeach Non-hydrostatic generally predicts larger infragravity waves for cases with directional spreading. An attempt was made to find the causes both for differences between the XBeach models and between boundary conditions and hydrodynamics at the second grid cell. This proved to be difficult. Also, no mention was made of similar problems in literature, either for XBeach or other models such as SWASH. For most models no comparison can be made between a phase-averaged and a phase-resolving mode. A relation between directional spread and infragravity motions was found by Guza and Feddersen (2012), but this was for infragravity swash and did not specifically consider boundary conditions.

Differences in propagation of infragravity waves

7.1. Introduction

In chapter 5 it was concluded that the difference between XBeach Non-hydrostatic and XBeach Surfbeat in infragravity wave height responsible for a different prediction of infragravity swash partly originates at the offshore boundary of the model and partly in the domain: there also is a difference in propagation of the infragravity waves. The difference in infragravity wave height at the boundary was treated in chapter 6, the difference in propagation is treated in this chapter. Possible causes for a difference in infragravity wave height transformation, such as features of the offshore wave spectra used to force the model with, groupiness of the incident waves, the phase difference between incident and infragravity waves and shoaling of the infragravity waves, are investigated in the following sections.
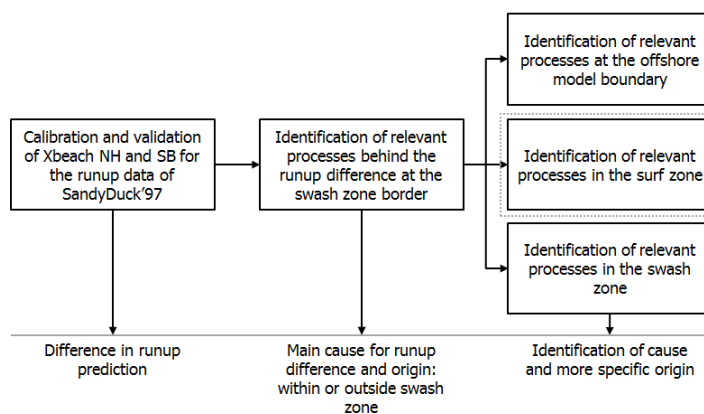
7.2. Offshore parameters

The correlation between features of the offshore wave spectra, such as the significant wave height, wave period, wave steepness, directional spreading and frequency spreading, and the difference in incoming infragravity wave height is shown in figure 7.1. Both the absolute and relative difference in incoming infragravity wave height are considered.

In section 5.2.1 it was hypothesized that a higher offshore wave height leads to a larger difference in incoming infragravity wave height between the XBeach models. This is confirmed by figure 7.1 a which shows a high positive correlation between offshore significant wave height and absolute difference in incoming infragravity wave height between XBeach Non-hydrostatic and XBeach Surfbeat. This indicates that for higher offshore energetic conditions the two XBeach models deviate more in absolute sense.
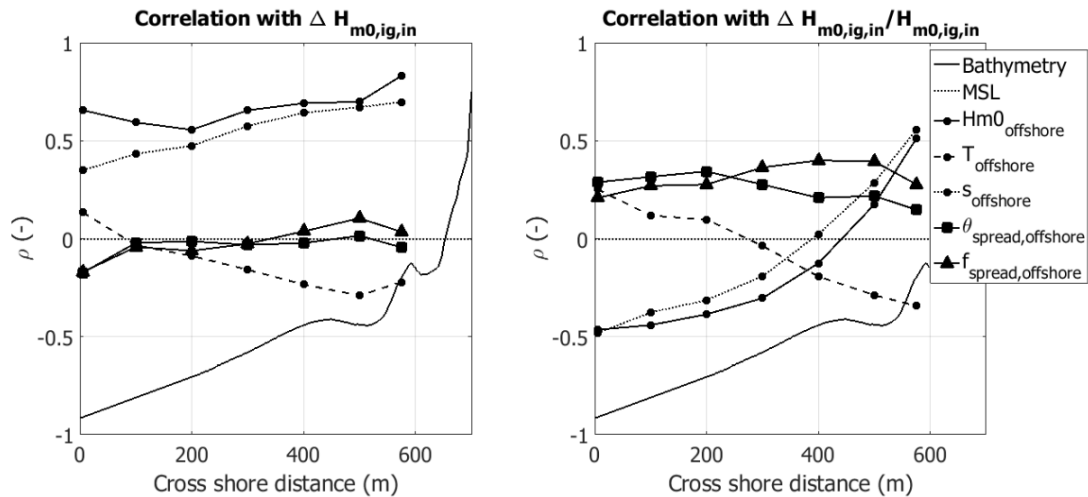
Figure 7.1: Correlation at different points in the cross shore between features of the offshore wave spectra and the difference in incoming infragravity wave height between the XBeach models. The offshore significant wave height, wave period, wave steepness and directional and frequency spreading are considered. (a) Absolute difference in incoming infragravity wave height. (b) Relative difference in incoming infragravity wave height.

The same can be said for offshore wave steepness. A correlation of 0.83 is found between offshore wave height and wave steepness, indicating that usually a high offshore wave height and steepness coincide. However, for higher offshore waves infragravity waves are larger and thus the absolute difference can be larger automatically. Therefore the relative difference in incoming infragravity wave height is considered in figure 7.1 b: offshore a negative correlation is found between offshore wave height and steepness and the relative difference in incoming infragravity wave height, which becomes positive near shore. This is consistent with findings in chapter 6 for differences near the boundary. A small negative correlation is found between offshore wave period and the absolute difference in incoming infragravity wave height, indicating that for larger wave periods the models behave more similar. When considering relative differences a positive correlation is found offshore which becomes negative closer to shore. From the above it can be concluded that in mild conditions the XBeach models behave more similar in absolute sense than in storm conditions, where higher, steeper and shorter waves occur. In relative sense the XBeach models behave more similar for higher energetic conditions in the offshore region, while behaving more similar for lower energetic conditions in the nearshore region.

For both the directional and frequency spreading a small and insignificant correlation is found between the offshore spreading and the absolute difference in infragravity wave height, but a positive correlation with the relative difference: larger directional or frequency spread of the offshore spectrum leads to larger relative differences in incoming infragravity wave height.

7.3. Groupiness

From section 5.3.1 it was concluded that there is a difference in groupiness factor prediction between XBeach Non-hydrostatic and XBeach Surfbeat. This could cause the difference in incoming infragravity wave height, as a larger groupiness of incident waves results in stronger forcing of the infragravity waves. The relation between the groupiness factor and the incoming infragravity wave height was investigated. An intermediate correlation was found between groupiness factor and incoming infragravity wave height, same order of magnitude as between groupiness factor and significant infragravity swash in chapter 5.

This can be seen from figure 7.2. In a an example of the transformation of the groupiness factor GF over the cross shore is given for both XBeach models. In b the correlation between the difference in
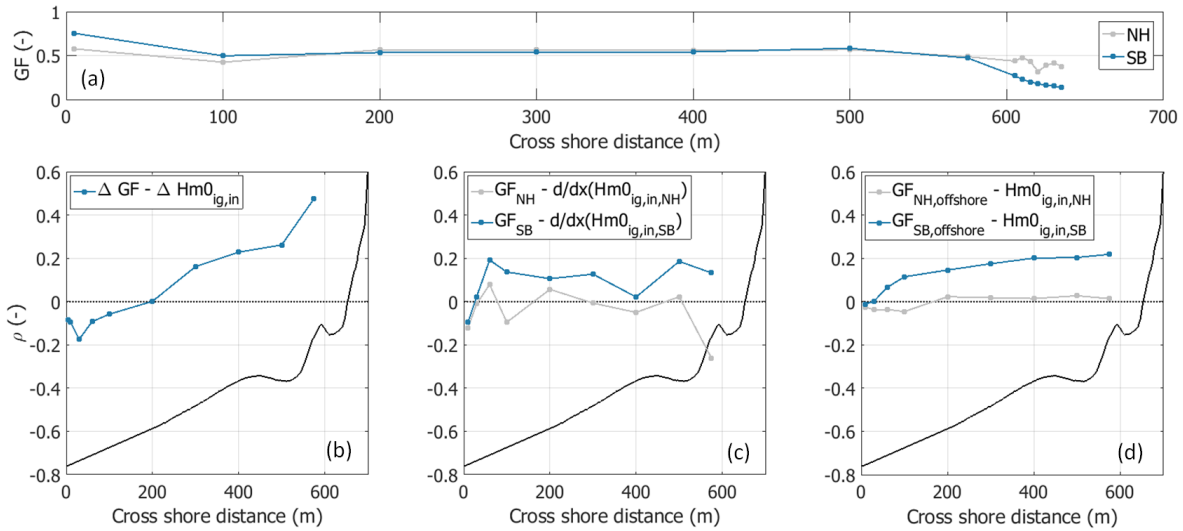
Figure 7.2: Relationship between the groupiness factor GF and the incoming infragravity wave height. (a) Example of transformation of the groupiness factor over the cross shore for both XBeach models. (b) Correlation between ΔGF and $\Delta H_{m0,ig,in}$. (c) Correlation between GF and the local growth of $H_{m0,ig,in}$. (d) Correlation between GF offshore and $H_{m0,ig,in}$ at different points in the cross shore.

groupiness factor and the difference in incoming infragravity wave height is shown, which is negative offshore but becomes positive and increases towards shore. The magnitude of the positive correlation is intermediate, indicating that the difference in groupiness factor has something to do with the difference in infragravity wave height close to shore, where also the deviation in groupiness factor prediction between XBeach Non-hydrostatic and XBeach Surfbeat becomes larger, see section 5.3.1 and figure 7.2 a. In this part of the cross shore XBeach Non-hydrostatic predicts a larger groupiness factor, which leads to extra forcing of the infragravity waves. In d the correlation between the groupiness factor close to the boundary and the incoming infragravity wave height at different locations in the cross shore is shown. A positive correlation is found for XBeach Surfbeat and a zero correlation for XBeach Non-hydrostatic. The groupiness is generally larger for XBeach Surfbeat and should thus theoretically lead to a higher infragravity wave height. The fact that it does not indicates that the difference in groupiness factor is not the cause of the difference in incoming infragravity wave height. In c the correlation between the groupiness at different locations in the cross shore and the local growth of incoming infragravity wave height at that location is shown. This correlation is mostly positive for XBeach Surfbeat while it is alternating positive and negative but close to zero for XBeach Non-hydrostatic. This again indicates that the groupiness is not the cause for the infragravity wave height difference: if it would have been the positive correlation for XBeach Surfbeat combined with a larger groupiness factor should have led to a higher incoming infragravity wave height for XBeach Surfbeat.

7.4. Phase difference

From section 5.4.1 it was concluded that there is a small difference in the correlation between the incident wave group and the infragravity water level $\rho_{lf,hf}$, which is an indicator of the phase difference between them, between the two XBeach models. It could still be a reason for the difference in incoming infragravity wave height but it is shown below that, from examining the relationship between $\rho_{lf,hf}$ and the infragravity wave height, $\rho_{lf,hf}$ is not the cause for the difference in incoming infragravity wave height.

This can be seen in figure 7.3. In a an example of the transformation of $\rho_{lf,hf}$ over the cross shore is given for both XBeach models. The analysis is only done uptil x = 575 m as over that part of the cross shore $\rho_{lf,hf}$ is negative and can be related to R, the energy transfer into the infragravity waves. The same analyses could be done from x = 575 m onwards but has not been done here. In b the correlation between the difference in $\rho_{lf,hf}$ and the difference in incoming infragravity wave height is shown. The
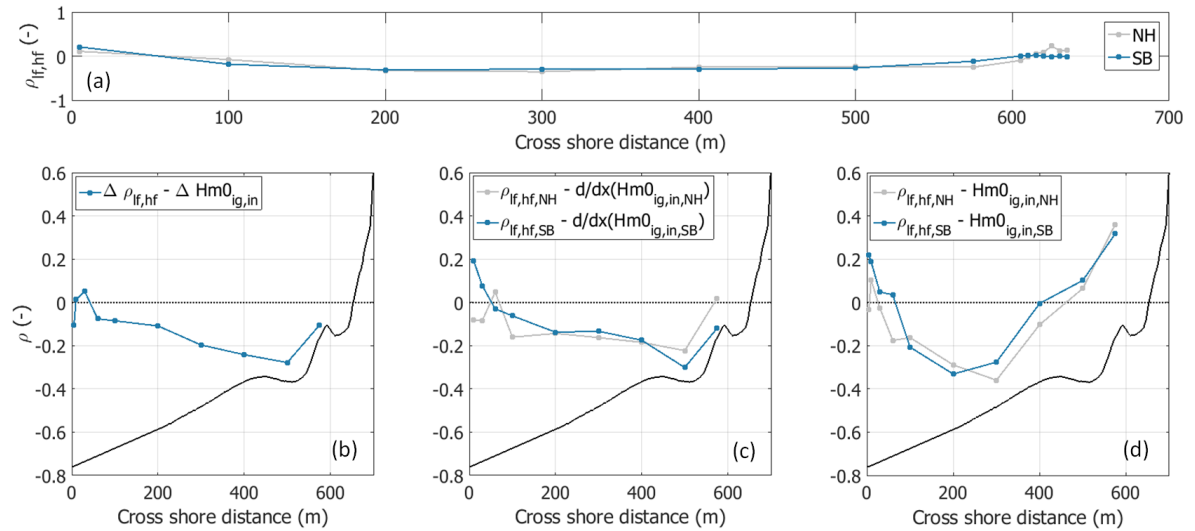
Figure 7.3: Relationship between $\rho_{lf,hf}$ and the incoming infragravity wave height. (a) Example of transformation of $\rho_{lf,hf}$ over the cross shore for both XBeach models. (b) Correlation between $\Delta\rho_{lf,hf}$ and $\Delta H_{mo,ig,in}$. (c) Correlation between $\rho_{lf,hf}$ and the local growth of $H_{mo,ig,in}$. (d) Correlation between $\rho_{lf,hf}$ and $H_{mo,ig,in}$ at different points in the cross shore.

correlation is negative, indicating that a larger difference in $\rho_{lf,hf}$ leads to a smaller difference in incoming infragravity wave height, but is small. In c the correlation between $\rho_{lf,hf}$ at a certain location in the cross shore and the local infragravity wave height growth is shown. It is negative for both models, so a larger $\rho_{lf,hf}$ results in smaller infragravity wave height growth, and comparable in magnitude. This is contrary to what Battjes et al. (2004) suggests: a parabolic relation between $\rho_{lf,hf}$ and R with its peak at $\rho_{lf,hf} = 0$, which should lead to a positive correlation between $\rho_{lf,hf}$ and the infragravity wave height growth for the part of the curve between $\rho_{lf,hf}$ of -1 and 0. It is obvious that this does not hold for the 2D simulations of Duck, but for the 1D testcase with a narrow JONSWAP spectrum and no directional spreading a positive correlation is found for both XBeach models (0.69 for XBeach Non-hydrostatic and 0.96 for XBeach Surfbeat). The theoretical relation between $\rho_{lf,hf}$ and R thus holds, but only for a simple 1D case. In d the correlation between $\rho_{lf,hf}$ and the incoming infragravity wave height at a certain location in the cross shore is shown. Again the trend is similar for both models, just as the magnitude. Combining above three findings leads to the conclusion that $\rho_{lf,hf}$ is not the cause for the difference in incoming infragravity wave height, at least not for the 2D simulations of Duck.

7.5. Directional spreading

Not only the phase difference $\rho_{lf,hf}$ between the wave group and the infragravity wave influences the degree of energy transfers between them but also the directional spread. In section 7.2 it was shown that there is a positive correlation between the offshore directional spread in the incident band and the relative difference in incoming infragravity wave height between the XBeach models. Here it is shown that the XBeach models respond differently to directional spreading, which can explain part of the difference in incoming infragravity wave height.

This can be seen in figure 7.4. For both XBeach models a negative correlation is found between offshore directional spread in the incident band and the incoming infragravity wave height, indicating that larger directional spread leads to lower incoming infragravity wave heights. This is expected as a larger directional spread in the incident band decreases forcing of infragravity waves (van Dongeren et al., 2003). A similar transformation over the cross shore can be seen, but the response to directional spread is stronger for XBeach Surfbeat. For the same offshore directional spread the incoming infragravity wave height as predicted by XBeach Non-hydrostatic is larger than the one predicted by XBeach Surfbeat, which can explain part of the incoming infragravity wave height difference.
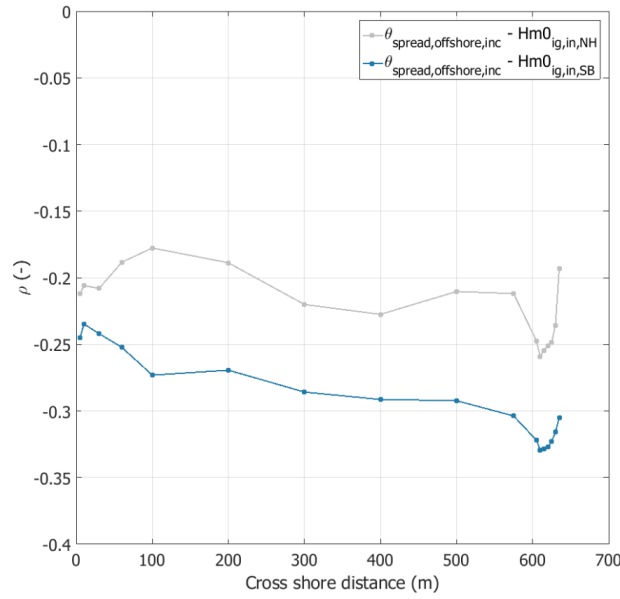
Figure 7.4: Correlation between the offshore directional spread in the incident band and the incoming infragravity wave height for both XBeach models.

7.6. Shoaling

In section 5.2.1 it was noted that already early in the cross shore a strong growth of the incoming infragravity wave height predicted by XBeach Non-hydrostatic occurs, which is not visible for XBeach Surfbeat. As the infragravity wave height predicted by XBeach Non-hydrostatic is already larger at the boundary these waves should also shoal earlier. The mean infragravity wave period $T_{m01,ig}$ was compared for the two XBeach models, indicating that shoaling can be a possible explanation of the stronger infragravity wave growth predicted by XBeach Non-hydrostatic.

The shoaling rate of bound infragravity waves is determined by the normalized bed slope β (Battjes et al., 2004; van Dongeren et al., 2007):

$$\beta = \frac{h_x}{\omega} \sqrt{\frac{g}{h}} \tag{7.1}$$

h_x is the bed slope and ω the radial frequency of the bound infragravity wave. ω is larger for shorter waves, decreasing β. The amplitude variation of the shoaling infragravity waves can be written as follows:

$$\hat{\zeta} \sim h^{-\alpha} \tag{7.2}$$

The value of α decreases for increasing β: shorter infragravity waves, thus with a smaller mean infragravity wave period, shoal stronger. In figure 7.5 the transformation of the mean, minimum and maximum difference in mean infragravity wave period between XBeach Non-hydrostatic and XBeach Surfbeat over the cross shore is shown. In figure 7.6 the transformation of $T_{m01,ig}$ over the cross shore is shown for three specific cases, representing low, high and intermediate offshore energetic conditions. Between x = 0 and x = 100 very strange behaviour for XBeach Surfbeat can be seen, the reason for this is not well known. However, at x = 100 the behaviour has normalised. From x = 100 to the shoreline the mean difference in $T_{m01,ig}$ is negative, indicating XBeach Surfbeat predicts a larger $T_{m01,ig}$. The difference is only a few seconds and decreases close to shore. The shoaling rate of the infragravity waves in XBeach Surfbeat is thus smaller and shoaling could explain the stronger growth in infragravity wave height for XBeach Non-hydrostatic.
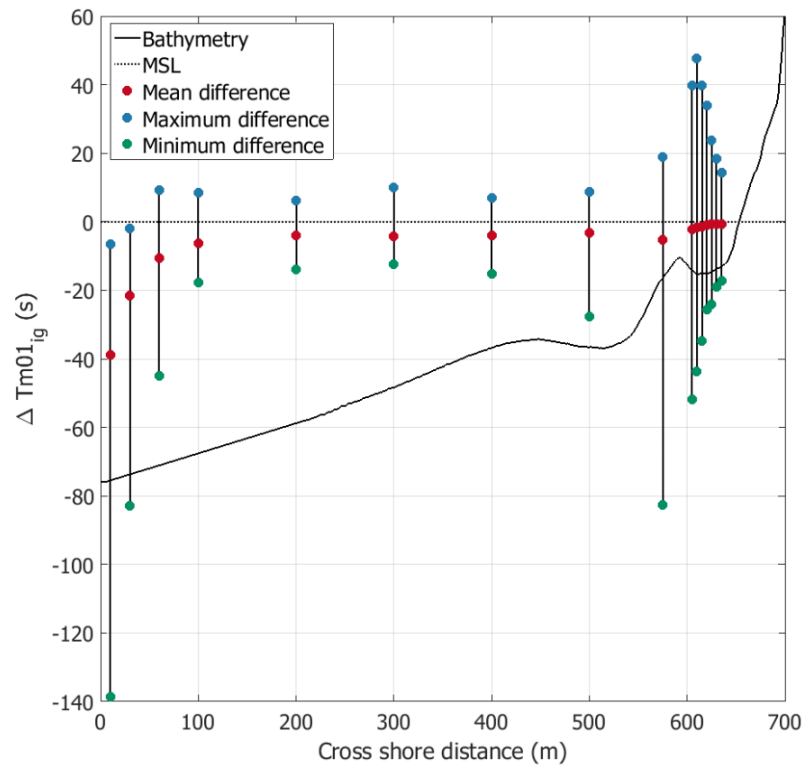
Figure 7.5: Difference in mean infragravity wave period $T_{m01,ig}$ between XBeach Non-hydrostatic and XBeach Surfbeat over the cross shore. The change of the minimum, mean and maximum difference over the cross shore is shown. A positive difference indicates that XBeach Non-hydrostatic predicts a larger value.
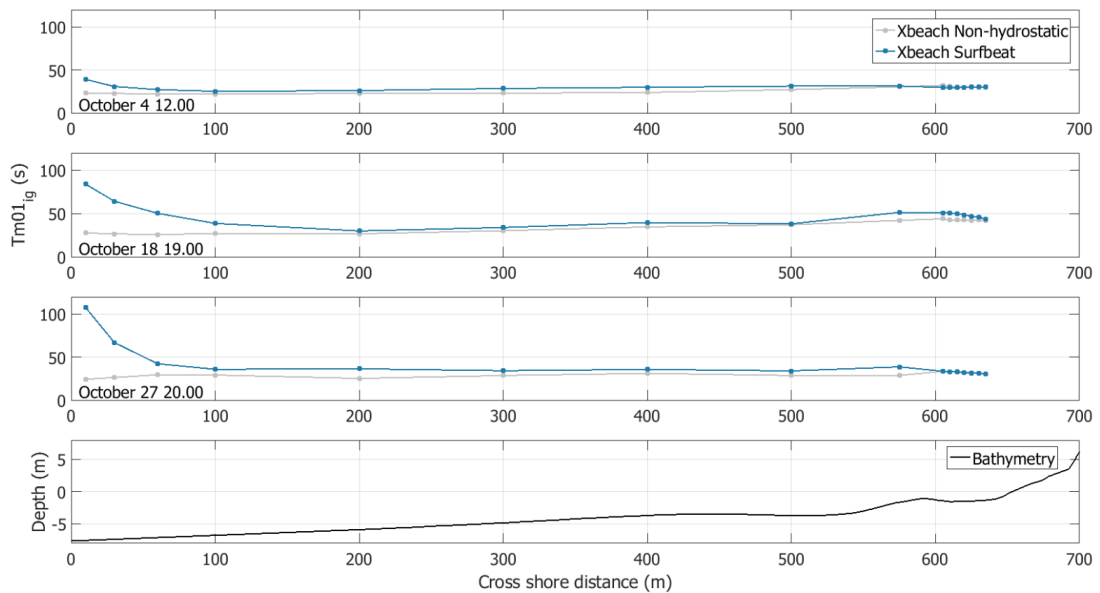
Figure 7.6: Transformation of the mean infragravity wave period $T_{m01,ig}$ for XBeach Non-hydrostatic and XBeach Surfbeat over the cross shore for three wave conditions (low offshore wave height on October 4 12.00, high offshore wave height on October 18 19.00, intermediate offshore wave height on October 27 20.00).

7.7. Conclusion & Discussion

In this chapter possible causes for a difference in infragravity wave propagation between XBeach Non-hydrostatic and XBeach Surfbeat were investigated and a few possible cause were identified. Also, general conditions under which the XBeach models behave more similar or deviate more were found. Propagation of infragravity waves in the offshore region is more similar in case of high offshore energetic conditions, while in the nearshore region it is more similar for low offshore energetic conditions. The reason for this transition is not known. Inch et al. (2017) noted that the degree of nonlinear interactions increases for higher offshore energetic conditions. This could explain why XBeach Non-hydrostatic predicts a higher infragravity wave height than XBeach Surfbeat for high offshore energetic conditions.

One of the possible drivers behind a difference in infragravity wave propagation investigated is the groupiness of the incident waves: a larger groupiness increases forcing of the infragravity waves. However, no convincing indication that the groupiness is the cause of the difference was found. Only close to shore it is relevant and can it explain the higher infragravity wave heights predicted there by XBeach Non-hydrostatic. As already noted in section 5.6 the Hilbert-Huang transformation predicts lower groupiness factors offshore than the Hilbert transformation. However, applying the Hilbert transformation instead of the Hilbert-Huang transformation until the point of incident wave breaking does not change the trends shown in figure 7.2, or the conclusions drawn in this chapter.

Also the phase difference between the incident wave groups and the infragravity waves was considered, which can theoretically be linked to the energy transfer into the infragravity waves (Battjes et al., 2004). However, Battjes et al. (2004) developed this method for a 1D wave field. For a 2D wave field such as at Duck the theoretical relation does not hold. Besides, the difference in phase difference between the XBeach models is not relevant for the difference in infragravity wave propagation. For a 2D wave field such as Duck not only the phase difference but also the directional difference between the wave components plays a role in the energy transfers, which should be included in the analysis. Difference interactions are responsible for transferring energy to infragravity frequencies. The difference-interaction coefficient D determines the bound infragravity energy density and this interaction coefficient is dependent on the directional spread between the two interacting components (Herbers et al., 1994; Reniers et al., 2002). D is significantly reduced by directional spreading.

A positive correlation was found between offshore directional spread in the incident frequency band and the difference in infragravity wave propagation. XBeach Surfbeat has a stronger response to the directional spread than XBeach Non-hydrostatic, which can explain part of the phenomenon that XBeach Surfbeat generally predicts a lower incoming infragravity wave height. The fact that infragravity wave heights are smaller for a larger directional spread was also seen by Guza and Feddersen (2012), only for infragravity swash instead of infragravity wave height. An equally positive correlation was found between offshore frequency spread in the incident band and the difference in incoming infragravity wave height. Guza and Feddersen (2012) found that the infragravity swash increases for increasing frequency spread. As XBeach Surfbeat predicts lower infragravity wave heights it probably has a weaker response to frequency spread than XBeach Non-hydrostatic.

Here only the directional spread of the offshore frequency-directional spectra has been considered. The directional spread of waves in the infragravity band within the domain can be determined with the help of the Maximum Entropy Method (Lygre and Krogstad, 1986), which computes the frequency-directional spectrum from an array of water level output. In this way the behaviour for XBeach Non-hydrostatic and XBeach Surfbeat can be compared. In this study a very simple definition of directional spread was adopted but when looking more closely at the transformation of directional spread over the cross shore also this definition should be compared to other measures of directional spread, such as the one defined by Kuik et al. (1988).

Shoaling of the infragravity waves can possibly be marked as the reason why a stronger growth of the incoming infragravity waves is predicted early in the cross shore by XBeach Non-hydrostatic. However, shoaling has only been considered superficially. Only the difference in mean infragravity wave period was investigated. To give more conclusive answers about shoaling of the infragravity waves it should

be considered in more depth, for example by comparing shoaling rates of the infragravity waves for both XBeach models with Green's law and the shallow water equilibrium solution of Longuet-Higgins and Stewart (1962). Battjes et al. (2004) and van Dongeren et al. (2007) found that the shoaling rate of low frequency infragravity waves nearly equals Green's law ($h^{-1/4}$) while for higher frequency infragravity waves it nears the equilibrium solution ($h^{-5/2}$). Also, the mean infragravity wave period of the incoming infragravity waves is strange for XBeach Surfbeat in the first 100 meters of the cross shore. This behaviour has disappeared when considering the mean infragravity wave period of the total infragravity wave field. It is therefore probably caused by splitting the incoming and reflected waves with the Guza method, in what way is not known. This should further be looked into. Also an infragravity energy balance following Henderson and Bowen (2002) should be carried out, to identify differences in forcing and dissipation of the infragravity waves between XBeach Non-hydrostatic and XBeach Surfbeat over the cross shore.

<div style="text-align: right; font-size: 3em;">8</div>
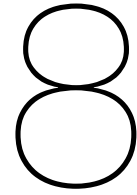
Conclusions & recommendations

8.1. Introduction

In this thesis report the influence of simulating runup with a phase-resolving model (XBeach Non-hydrostatic) instead of a phase-averaged model (XBeach Surfbeat), and therefore the influence of incident waves on runup, is investigated. Both XBeach models were validated for wave height and runup data of the field experiment SandyDuck'97 at Duck, North Carolina, an intermediate reflective beach with mild to intermediate energetic conditions. A difference was found in runup predictions between XBeach Non-hydrostatic and XBeach Surfbeat and different, hydrodynamically related, causes were investigated: what is the dominant process leading to the difference in runup prediction and where in the cross shore does this originate. In this chapter first the conclusions to the subquestions as defined in chapter 1 are given in section 8.2, followed by the conclusion to the research question. From the conclusions recommendations follow, which are given in section 8.3.

8.2. Conclusions

Is XBeach Non-hydrostatic capable of reproducing runup data, specifically setup and infragravity swash, from an intermediate reflective beach better than XBeach Surfbeat?

For the intermediate reflective beach of Duck, North Carolina, XBeach Non-hydrostatic is a better predictor of runup than XBeach Surfbeat. Significant incident and infragravity swash are predicted better, while the performance for setup is similar for both models. The improvement for significant incident swash was expected as XBeach Non-hydrostatic resolves incident waves and swash while XBeach Surfbeat only resolves incident wave groups. The 2% runup level is also predicted better by XBeach Non-hydrostatic, indicating that for XBeach Surfbeat the different runup components (setup, significant incident and infragravity swash) do not compensate for each other to predict an accurate total runup level. The main forcing of runup is the incident and infragravity wave height of which the former is predicted similarly for both XBeach models and the latter is predicted better by XBeach Non-hydrostatic. When predicting runup on an intermediate reflective beach under relatively mild conditions it is therefore better to use XBeach Non-hydrostatic instead of XBeach Surfbeat.

What are the dominant processes leading to a difference in runup predictions and does the difference in runup (mainly) originate from differences in the hydrodynamics of the surf zone, the swash zone or the offshore boundary?

The difference in infragravity swash prediction is mainly driven by a difference in infragravity wave height transformation between the two XBeach models. A part of the difference in infragravity wave height is already present close to the offshore boundary but also between the offshore boundary and the swash zone border differences develop relevant for the infragravity swash prediction. Besides differences in infragravity wave height transformation hydrodynamic differences relevant for the infragravity swash prediction develop within the swash zone. The exact contribution of each part of the

cross shore is not known but developments within the domain are more relevant than at the boundary and differences originating from the swash zone can be significant. Forcing both XBeach models with the same spectrum at the boundary results in different infragravity waves at the start of the domain, where the directional spread of the offshore spectrum is the parameter mainly influencing the difference. Differences in the surf zone are most likely caused by a different response to directional spreading and different shoaling rates, while differences developing within the swash zone can be due to incident bore merging. Incident swash is predicted better by XBeach Non-hydrostatic most likely due to resolving of incident waves. The difference therefore originates at the boundary.

Does phase-resolved modelling of incident waves with XBeach increase the predictive skill for wave runup and why (not)?

Using a phase-resolving XBeach model on an intermediate reflective beach increases the predictive skill for wave runup significantly. Especially the runup components incident and infragravity swash are beneficially influenced, while the predictive skill for setup remains similar. This indicates that time-averaged radiation stress gradients, the main driver of setup, are similar for a phase-averaged and a phase-resolving XBeach model. A phase-resolving XBeach model is a better predictor of infragravity wave height transformation, the main driver of a better prediction in infragravity swash. However, this is only partly due to the phase-resolving nature of the model: a small part of the difference in infragravity wave height originates from the boundary. The majority of the difference originates from the domain and thus is the result of resolving incident waves. On an intermediate reflective beach with relatively mild energetic conditions, where both incident and infragravity waves play a role, resolving of incident waves and swash thus is a necessity to accurately predict runup and the phase-resolving XBeach Non-hydrostatic should be used instead of the phase-averaged XBeach Surfbeat model.

8.3. Recommendations

The performance of the phase-averaged XBeach Surfbeat and the phase-resolving XBeach Non-hydrostatic for predicting runup was investigated in this thesis. However, some questions remain unanswered and to help future research, recommendations are given.

Boundary conditions   The infragravity wave height at the boundary is not the same for the two XBeach models, making it difficult to give exclusive answers about the transformation of the infragravity waves in the domain. Further effort should be put into investigating interaction processes of the high and low frequency wave boundary conditions in the first grid cell and how exactly the same infragravity waves can be generated in the domain for XBeach Non-hydrostatic and XBeach Surfbeat. Also, more attention has to be paid to differences between the XBeach models in transformation of the infragravity waves, such as shoaling, forcing and dissipation. The latter can be done by carrying out an infragravity energy balance following Henderson and Bowen (2002). Also hydrodynamic differences between the XBeach models within the swash zone, such as the occurrence of bore merging, should be examined further.

The XBeach models under more extreme conditions   The ultimate goal of Stockdon et al. (2014) was to generate runup under storm conditions with XBeach Surfbeat to validate the empirical parameterization of Stockdon et al. (2005) for more extreme conditions, as runup data under extreme conditions hardly are available. As XBeach Surfbeat underestimates swash significantly this was not accomplished. XBeach Non-hydrostatic however performs much better, but has in this thesis only been validated for low to intermediate energetic conditions. Its behaviour under storm conditions should be tested and compared to that of XBeach Surfbeat. To determine which one actually performs better they should be compared to runup data under storm conditions, which are not available for Duck. The validation of XBeach Surfbeat by Palmsten and Splinter (2016) for a flume experiment with storm condition forcing can be repeated with XBeach Non-hydrostatic or field data of other beaches than Duck can be used: runup data under storm conditions are available for Narrabeen beach, Australia, but no wave height data is available there. Runup data under storm conditions is also available for Truc Vert, France (Senechal et al., 2011). If the above data sets are not sufficient extra data can be collected by setting up a flume experiment. It is expected that under storm conditions a smaller difference be-

tween XBeach Non-hydrostatic and XBeach Surfbeat is present, as a beach becomes more dissipative and incident waves break farther offshore.

Comparison between XBeach Non-hydrostatic and XBeach for other types of beaches   In this thesis it was shown that on an intermediate reflective beach such as Duck XBeach Non-hydrostatic is a better predictor of runup. However, this is only one case. Similar validations need to be done for other types of beaches to be able to advise which XBeach model should be used in which situation, starting with the two extreme cases: a dissipative and a reflective beach. As the role of incident waves close to shore becomes smaller for more dissipative beaches it is expected that for dissipative beaches the difference in runup predictions between XBeach Non-hydrostatic and XBeach Surfbeat becomes smaller, while becoming larger for a reflective beach. Storm conditions should also be simulated on more types of beaches, which will help to validate the empirical parameterization of Stockdon et al. (2005), developed for a range of beach types, under storm conditions.

Bibliography

Ahrens, J. and Seelig, W. (2001). Wave runup on beaches. Coastal Engineering Proceedings, 1(25).

Baldock, T. E., Holmes, P., and Horn, D. P. (1997). Low frequency swash motion induced by wave grouping. Coastal Engineering, 32:197–222.

Battjes, J. A. (1974). Surf similarity. Coastal Engineering Proceedings, 1(14):467–479.

Battjes, J. A., Bakkenes, H. J., Janssen, T. T., and van Dongeren, A. R. (2004). Shoaling of subharmonic gravity waves. Journal of Geophysical Research, 109(C02009).

Bosboom, J. and Stive, M. J. F. (2015). Coastal Dynamics I: lecture notes CIE4305. VSSD.

Brocchini, M. and Baldock, T. E. (2008). Recent advances in modeling swash zone dynamics: influence of surf-swash interaction on nearshore hydrodynamics and morphodynamics. Reviews of Geophysics, 46(RG3003).

Carlson, C. T. and Asce, A. M. (1984). Field studies of run-up on dissipative beaches. Coastal Engineering Proceedings, 1(19):399–414.

Casella, E., Rovere, A., Pedroncini, A., Mucerino, L., Casella, M., Cusati, L. A., Vacchi, M., Ferrari, M., and Firpo, M. (2014). Study of wave runup using numerical models and low-altitude aerial photogrammetry: A tool for coastal management. Estuarine, Coastal and Shelf Science, 149:160–167.

de Bakker, A. T. M., Herbers, T. H. C., Smit, P. B., Tissier, M. F. S., and Ruessink, B. G. (2015). Nonlinear infragravity-wave interactions on a gently sloping laboratory beach. Journal of Physical Oceanography, 45:589–605.

de Bakker, A. T. M., Tissier, M. F. S., and Ruessink, B. G. (2016). Beach steepness effects on nonlinear infragravity-wave interactions: a numerical study. Journal of Geophysical Research, 121:554–570.

FRF (2004). Sandyduck '97 coastal field experiment. http://www.frf.usace.army.mil/SandyDuck/Sandy Duck.st.

Guedes, R. M. C., Bryan, K. R., and Coco, G. (2013). Observations of wave energy fluxes and swash motions on a low-sloping, dissipative beach. Journal of Geophysical Research: Oceans, 118:3651–3669.

Guza, R. T. and Feddersen, F. (2012). Effect of wave frequency and directional spread on shoreline runup. Geophysical Research Letters, 39(L11607).

Guza, R. T., Thornton, E. B., and Holman, R. A. (1984). Swash on steep and shallow beaches. Coastal Engineering Proceedings, 1(19):708–722.

Henderson, S. M. and Bowen, A. J. (2002). Observations of surf beat forcing and dissipation. Journal of Geophysical Research, 107(C11):3193.

Henderson, S. M., Guza, R. T., Elgar, S., Herbers, T. H. C., and Bowen, A. J. (2006). Nonlinear generation and loss of infragravity wave energy. Journal of Geophysical Research, 111(C12007).

Herbers, T. H. C., Elgar, S., and Guza, R. T. (1994). Infragravity-frequency (0.005-0.05 hz) motions on the shelf. part 1: forced waves. Journal of Physical Oceanography, 24:917–927.

Holthuijsen, L. H. (2007). Waves in oceanic and coastal waters. Cambridge University Press.

Huang, N. E. and Chen, S. S. P. (2005). Hilbert-Huang Transform and its Applications. World Scientific Publishing Company.

Inch, K., Davidson, M., Masselink, G., and Russell, P. (2017). Observations of nearshore infragravity wave dynamics under high energy swell and wind-wave conditions. Continental Shelf Research, 138:19–31.

Kuik, A. J., van Vledder, G. P., and Holthuijsen, L. H. (1988). A method for routine analysis of pitch-and-roll buoy data. Journal of Physical Oceanography, 18:1020–1043.

Lerma, A. N., Pedreros, R., Robinet, A., and Senechal, N. (2017). Simulating wave setup and runup during storm conditions on a complex barred beach. Coastal Engineering, 123:29–41.

List, J. H. (1990). Wave groupiness variations in the nearshore. Coastal Engineering, 15:475–496.

Long, J. W. (2017). Definition of directional spreading.

Longuet-Higgins, M. S. and Stewart, R. W. (1962). Radiation stress and mass transport in gravity waves, with application to 'surf beats'. Journal of Fluid Mechanics, 13:481–504.

Lygre, A. and Krogstad, H. E. (1986). Maximum entropy estimation of the directional distribution in ocean wave spectra. Journal of Physical Oceanography, 16:2052–2060.

Mase, H. (1989). Spectral characteristics of random wave runup-up. Coastal Engineering, 12:175–189.

Medina, J. R. (1992). Wave groupiness variations in the nearshore, by j. h. list*: comments. Coastal Engineering, 18:353–362.

Palmsten, M. L. and Splinter, K. D. (2016). Observations and simulations of wave runup during a laboratory dune erosion experiment. Coastal Engineering, 115:58–66.

Puleo, J. A. and Butt, T. (2006). The first international workshop on swash-zone processes. Continental Shelf Research, 26:556–560.

Raubenheimer, B., Guza, R. T., Elgar, S., and Kobayashi, N. (1995). Swash on a gently sloping beach. Journal of Geophysical Research, 100:8751–8760.

Reniers, A. J. H. M., Gallagher, E. L., MacMahan, J. H., Brown, J. A., van Rooijen, A. A., van Thiel de Vries, J. S. M., and van Prooijen, B. C. (2013). Observations and modeling of steep-beach grain-size variability. Journal of Geophysical Research: Oceans, 118:577–591.

Reniers, A. J. H. M., van Dongeren, A. R., Battjes, J. A., and Thornton, E. B. (2002). Linear modeling of infragravity waves during delilah. Journal of Geophysical Research, 107(C10):3137.

Roelvink, D., Reniers, A., van Dongeren, A., van Thiel de Vries, J., McCall, R., and Lescinski, J. (2009). Modelling storm impacts on beaches, dunes and barrier islands. Coastal Engineering, 56:1133–1152.

Roelvink, J. A., Reniers, A. J. H. M., van Dongeren, A. R., van Tiel de Vries, A. R., Lescinski, J. S. M., and McCall, R. T. (2010). Xbeach model description and manual. Unesco-IHE Institute for Water Education, Deltares and Delft University of Technology.

Ruessink, B. G., Kleinhans, M. G., and van den Beukel, P. G. L. (1998). Observations of swash under highly dissipative conditions. Journal of Geophysical Research, 103:3111–3118.

Ruggiero, P., Komar, J. J., Marra, W. G., McDougal, W. G., and Beach, R. A. (2001). Wave runup, extreme water levels and the erosion of properties backing beach. Journal of Coastal Research, 17(2):407–419.

Senechal, N., Coco, G., Bryan, K. R., and Holman, R. A. (2011). Wave runup during extreme storm conditions. Journal of Geophysical Research, 116(C07032).

Short, A. D. (1999). Handbook of beach and shoreface morphodynamics. New York: John Wiley.

Smit, P., Zijlema, M., and Stelling, G. (2013). Depth-induced wave breaking in a non-hydrostatic, near-shore wave model. Coastal Engineering, 76:1–16.

Stockdon, H. F., Holman, R. A., Howd, P. A., and Junior, A. H. S. (2005). Empirical parameterization of setup, swash and runup. Coastal Engineering, 53:573–588.

Stockdon, H. F., Thompson, D. M., Plant, N. G., and Long, J. W. (2014). Evaluation of wave runup predictions from numerical and parametric models. Coastal Engineering, 92:1–11.

Thomson, J., Elgar, S., Raubenheimer, B., Herbers, T. H. C., and Guza, R. T. (2006). Tidal modulation of infragravity waves via nonlinear energy losses in the surfzone. Geophysical Research Letters, 33(L05601).

Thornton, E. B. and Guza, R. T. (1982). Energy saturation and phase speeds measured on a natural beach. Journal of Geophysical Research, 87:9499–9508.

Tissier, M., Bonneton, P., Michallet, H., and Ruessink, B. G. (2015). Infragravity-wave modulation of short-wave celerity in the surf zone. Journal of Geophysical Research: Oceans, 120:6799–6814.

Tissier, M., Bonneton, P., and Ruessink, G. (2017). Infragravity waves and bore merging. Proceedings Coastal Dynamics, pages 451–460.

van der Meer, J. W. and Stam, J. C. (1992). Wave runup on smooth and rock slopes of coastal structures. Journal of Waterway, Port, Coastal and Ocean Engineering, 118(5):534–550.

van Dongeren, A., Battjes, J., Janssen, T., van Noorloos, J., Steenhauer, K., Steenbergen, G., and Reniers, A. (2007). Shoaling and shoreline dissipation of low-frequency waves. Journal of Geophysical Research, 112(C02011).

van Dongeren, A., Reniers, A., Battjes, J., and Svendsen, I. (2003). Numerical modeling of infragravity wave response during delilah. Journal of Geophysical Research, 108(C9):3288.

van Rooijen, A., Reniers, A., van Thiel de Vries, J., Blenkinsopp, C., and McCall, R. (2012). Modelling swash zone sediment transport at truc vert beach. Coastal Engineering Proceedings, 1(33):105.

van Rooijen, A. A. (2011). Modelling sediment transport in the swash zone. Master's thesis, TU Delft.

van Thiel de Vries, J. S. M. (2009). Dune erosion during storm surges. PhD thesis, Delft University of Technology.

Veltcheva, A. and Soares, C. G. (2016). Analysis of wave groups by wave envelope-phase and the hilbert-huang transform methods. Applied Ocean Research, 60:176–184.

Wikipedia (2016). Sea level datum of 1929. https://en.wikipedia.org/wiki/Sea Level Datum of 1929.

Wikipedia (2017a). Bias of an estimator. https://en.wikipedia.org/wiki/Bias of an estimator.

Wikipedia (2017b). Coefficient of correlation. https://en.wikipedia.org/wiki/Coefficient of determination.

Wright, L. and Short, A. (1984). Morphodynamic variability of surf zones and beaches: a synthesis. Marine Geology, 56:93–118.

Zijlema, M. (2015). Computational modelling of flow and transport. Technical report, Faculty of Civil Engineering and Geosciences, Delft University of Technology.

A
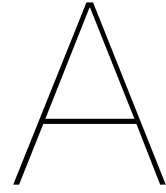
Model setup

Introduction
In this appendix the setup of the XBeach models is described.

Grid & bathymetry
For each day the bathymetry data was complete a bathymetry has been made for XBeach. This could not be done for October 5th, 19th, 20th and 31th, because at those days the bathymetry data were not complete. The x- and y-grid used was the same for all days, to make postprocessing of the data easier.

A XBeach grid needs to have an increasing x-coordinate from offshore to nearshore. As the bathymetry was measured in local coordinates (increasing x-coordinate from the beach to the sea) the data was flipped to generate XBeach x-coordinates (increasing from beach to the shore). The x-resolution differed per measured cross shore transect and per day so the bathymetry was interpolated on a constant x-grid. The maximum measured depth was -5.7 m NGVD so the x-grid was extended offshore until a depth of -7.8 meters, using the slope of the bottom in the last 7 grid cells of the original measured grid. This was done so that the boundary of the XBeach model coincides approximately with the depth at which the offshore frequency-directional spectra were measured and such that the XBeach Non-hydrostatic model was extended until the same depth as the XBeach Surfbeat model in Stockdon et al. (2014). The first three grid cells in the domain have a constant depth.

With an increasing x-coordinate the beach is on the right side of the model, while in reality the beach is on the left side. To be able to match the bathymetry with the right wave boundary conditions also the bathymetry needs to be rotated such that the measured bathymetry line with the highest local y-coordinate has the lowest XBeach y-coordinate, see figure A.1.

All measured bathymetries were interpolated on a x- and y-grid constant for all days. A constant Δy of 5 m was used in combination with a cross shore varying x-grid. The varying x grid was created based on a few requirements:

- The CFL condition: XBeach determines its time step based on the fact that the CFL condition should never be larger than 0.7. For a value of Δt of 1 seconds the grid size in cross shore direction was determined based on the bathymetry. The local waterdepth h was determined assuming a waterlevel of 0 m. Δx was calculated as follows: $\Delta x = \frac{\sqrt{g \cdot h} \cdot \Delta t}{CFL}$
- Numerical diffusion: in order to limit numerical diffusion at least 20 points per wavelength should be used (Zijlema, 2015). For the x-grid 30 points per wavelength were used. The local wavenumber k was calculated from the dispersion relationship with the local depth and the minimum T_{m01} from all measured frequency-directional spectra. The wave length was calculated as $\frac{2\pi}{k}$. $\frac{L}{ppwl}$ gives a Δx_{max}. If $\Delta x > \Delta x_{max}$ the value of Δx_{max} is used.
- A minimum Δx of 0.10 m was used.
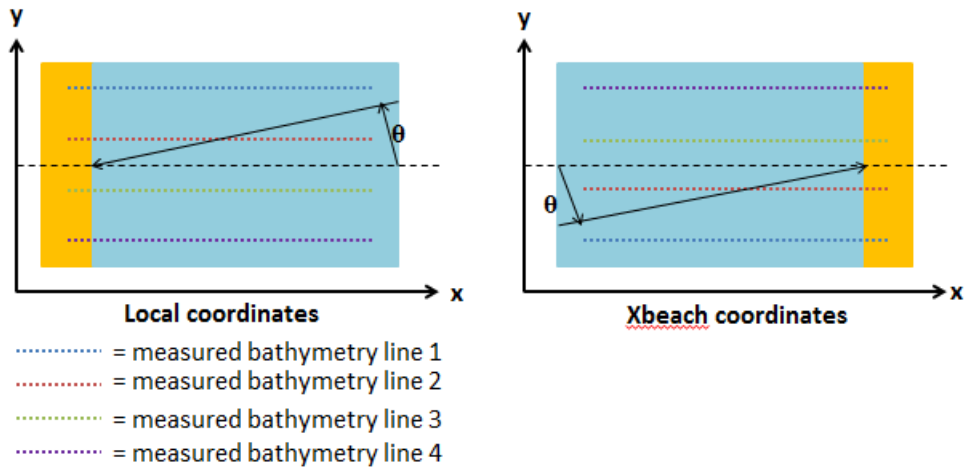
Figure A.1: The conversion from local coordinates to XBeach coordinates. θ gives the angle of incidence of the waves. The whole grid has been rotated over 180 degrees.

Cyclic boundary conditions were used to minimise shadow zones in the model. In order for cyclic boundary conditions to work well the last few alongshore cells at both ends of the grid should be alongshore uniform. To accomplish this the mean was taken of the two cross shore boundaries and was added for 3 alongshore cells at each boundary. A visualisation can be seen in figure A.2.
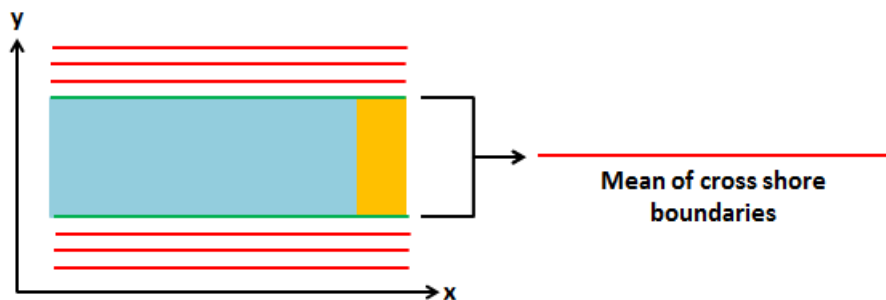
Figure A.2: Making the last 3 grid cells at each cross shore boundary alongshore uniform.

The resulting grid has 76 grid cells in the alongshore direction and 838 in the cross shore direction, with a constant alongshore grid size of 5 m. The cross shore grid size ranged from 1 m offshore to 0.25 m near the waterline.

To test the amount of numerical diffusion the resulting grid generated a simulation was done with a grid twice as fine. Computed wave heights differed with 1-3 cm, which is the same order of magnitude as when running a XBeach simulation with the same boundary conditions twice and in both simulations waves are generated randomly from the offshore wave spectrum.

Interpolation of frequency-directional spectra

The measured frequency-directional spectra at 8 m depth are available daily from 1 AM to 10 PM, with intervals of 3 hours. Because wave height and runup measurements are available at times in between two measured spectra, for example 11 AM and noon, the measured spectra were interpolated linearly such that a spectrum was available for each whole hour from 10 AM to 10 PM. As there are no runup measurements available earlier than 11 AM no interpolated spectra were made between 1 AM and 10 AM. In the measured spectra the spectral density is available for every combination of frequency

and direction, with frequencies ranging from 0.044 to 0.318 Hz with a Δf of 0.01 Hz and directions ranging from -90 to 90 degrees with a Δdir of 2 degrees. The spectra are represented by a matrix of 29 frequencies and 91 directions and their respective spectral density $E_{f,\theta}$ (the spectral density at frequency f and direction θ). The interpolated spectra can then be constructed by linearly interpolating the spectral densities at each frequency and each direction between consecutive measurement times:

$$E_{f,\theta-1100} = E_{f,\theta-1000} + \frac{E_{f,\theta-1300} - E_{f,\theta-1000}}{3} \tag{A.1}$$

$$E_{f,\theta-1100} = E_{f,\theta-1000} + 2 \cdot \frac{E_{f,\theta-1300} - E_{f,\theta-1000}}{3} \tag{A.2}$$

For the 29 days that runup data is available (October 3 - 31) this results in 232 interpolated spectra, as well as 232 original spectra. Whether the interpolation gives good results was checked in two ways:

1. By computing the root mean square error between the significant wave height of the offshore frequency-directional spectrum and the significant wave heights measured at the most offshore pressure gauges: for the original frequency-directional spectra a root mean square error of 0.064 was found, for the interpolated frequency-directional spectra a value of 0.067 m.

2. The statistics as presented in section 3.2.2 for the original frequency-directional spectrum were also computed for the interpolated spectra. The results can be found in table A.1. The difference between the original and interpolated spectra is generally below or only just above 10%.

The differences between the original and interpolated spectra are small and the interpolation thus gives good results.

Table A.1: Comparison of statistics for significant wave height H_{m0}, peak period T_p and peak direction D_p between the original and interpolated frequency-directional spectra

Statistic	H_{m0} (m)			T_p (s)			D_p (degrees)		
	Orig.	Interp.	Δ (%)	Orig.	Interp.	Δ (%)	Orig.	Interp.	Δ (%)
μ	0.96	0.98	2.26	9.74	9.77	0.31	3.83	3.35	12.48
min	0.30	0.31	1.97	4.01	4.17	3.96	-50	-50	0
max	3.46	3.41	-1.50	15.63	15.63	-0.06	56	56	0
σ	0.60	0.64	7.43	2.80	2.72	-2.68	19.19	21.42	11.62

Lastly, the spectra have been rotated such that they match the XBeach grid. In local coordinates a positive angle of incidence indicates waves coming from the North, while in the rotated XBeach grid a positive angle indicates waves coming from the South. Note that the effect is exactly the same, just the grid has been rotated (for a measured spectrum with a negative D_p XBeach gives a $D_p > 270$ degrees North while for a positive measured D_p XBeach gives a $D_p < 270$ degrees North).

Output locations

The output locations in the XBeach models were chosen such that they coincide with the measurement locations as in the experiment. 6 runup gauges were defined and 36 point output locations. Note that the runup gauge and cross shore line of pressure gauges which had the largest y-coordinate in local coordinates has the smallest y-coordinate in XBeach coordinates. Also, the pressure gauge with the smallest x-coordinate in local coordinates has the largest x-coordinate in XBeach coordinates. The coordinates of the output locations are given in table A.2. In this table both the location of the measurement locations of the SandyDuck'97 experiment is given in FRF coordinates (local coordinates) and the location of the output locations in XBeach is given in XBeach coordinates. The distance to the shoreline (at mean sea level) is equal for both coordinate systems, meaning the output locations in XBeach were positioned correctly.

XBeach model settings

The model settings used for the XBeach validation simulations are listed in table A.3.

Table A.2: Location of the measuring locations in X and Y FRF coordinates and the distance of the measuring location to the FRF waterline (at X = 125), as well as the location of the output locations in XBeach and the distance of the output location to the XBeach waterline (at X = 640). It can be seen that the distance to the waterline is equal for the FRF and XBeach coordinates, meaning the output locations have been placed correctly in XBeach.

Output number	X FRF	Y FRF	Distance from waterline (m)	X XB	Y XB	Distance from the waterline (m)
PO1	160	703	35	605	275	35
PO2	160	778	35	605	225	35
PO3	160	815	35	605	198	35
PO4	160	828	35	605	185	35
PO5	160	855	35	605	148	35
PO6	160	905	35	605	73	35
PO7	210	703	85	555	275	85
PO8	210	778	85	555	225	85
PO9	210	815	85	555	198	85
PO10	210	828	85	555	185	85
PO11	210	855	85	555	148	85
PO12	210	905	85	555	73	85
PO13	260	703	145	505	275	145
PO14	260	778	145	505	225	145
PO15	260	815	145	505	198	145
PO16	260	828	145	505	185	145
PO17	260	855	145	505	148	145
PO18	260	905	145	505	73	145
PO19	310	703	185	455	275	185
PO20	310	778	185	455	225	185
PO21	310	815	185	455	198	185
PO22	310	828	185	455	185	185
PO23	310	855	185	455	148	185
PO24	310	905	185	455	73	185
PO25	385	703	260	380	275	260
PO26	385	778	260	380	225	260
PO27	385	815	260	380	198	260
PO28	385	828	260	380	185	260
PO29	385	855	260	380	148	260
PO30	385	905	260	380	73	260
PO31	500	703	375	265	275	375
PO32	500	778	375	265	225	375
PO33	500	815	375	265	198	375
PO34	500	828	375	265	185	375
PO35	500	855	375	265	148	375
PO36	500	905	375	265	73	375
RG1	-	703	0	-	275	-
RG2	-	778	0	-	225	-
RG3	-	815	0	-	198	-
RG4	-	828	0	-	185	-
RG5	-	855	0	-	148	-
RG6	-	905	0	-	73	-

Table A.3: Model settings of the XBeach validation simulations

Input parameter	XBeach Non-hydrostatic	XBeach Surfbeat
cyclic	1	1
nonh	1	0
swave	0	1
swrunup	0	1
sedtrans	0	0
morphology	0	0
posdwn	-1	-1
vardx	1	1
thetamin	-	-90
thetamax	-	90
dtheta	-	-
zs0	tide	tide
sprdthr	0.01	0.01
maxbrsteep	0.4	-
secbrsteep	0.2	-
gamma	-	0.42
bedfriction	Chezy	Chezy
bedfriccoef	57	56
mpiboundary	x	x
rugdepth	0.05	0.05/0.10
single dir	0	1
dheta s	-	5
wavint	-	300
instat	6	6
random	1	1
front	abs 2d	abs 2d
ARC	1	1
order	2	2
tideloc	1	1

B

Calibration of the XBeach Non-hydrostatic model

Introduction

In this appendix the calibration of the XBeach Non-hydrostatic model is described.

Calibration simulations

Three different XBeach simulations were chosen to do the calibration with. The choice was based on wave height and wave period (and thus wave steepness):

- Average wave height with a small wave period (simulation 1): $H_{m0} = 1.19$ m and $T_p = 5.83$ s
- Average wave height with a large wave period (simulation 2): $H_{m0} = 1.16$ m and $T_p = 10.72$ s
- Large wave height (simulation 3): $H_{m0} = 2.11$ m and $T_p = 8.16$ s

Calibration of bottom friction

Three different bottom friction formulations were used in the calibration: Chezy, Manning and White-Colebrook. The formulations are given below:

$$c_{f,Chezy} = \frac{g}{C^2} \tag{B.1}$$

$$c_{f,Manning} = \frac{gn^2}{h^{1/3}} \tag{B.2}$$

$$c_{f,White-Colebrook} = \frac{g}{(18log(\frac{12h}{k_s}))^2} \tag{B.3}$$

For Chezy 11 different values of the C parameter were tested, just as for the Manning parameter n. For the White-Colebrook parameter k_s one value wastested. The values can be found in table B.1. A typical value for sandy beaches for C is 55 $m^{1/2}/s$, for n 0.02 and for k_s 0.01 (Roelvink et al., 2010). The values of n were chosen such that at the offshore boundary, at a depth of approximately 8 m, the resulting c_f values were comparable to the c_f values of the 11 C values, in order to compare the depth dependency and not the amount of friction. Only one value of k_s was used as it turned out this didn't give a significant improvement. Values for maxbrsteep and secbrsteep of 0.6 and 0.3 were used in the calibration simulations, as recommended by Smit et al. (2013).

Calibration of breaker parameters

With the best performing value for the bottom friction different values for maxbrsteep were tested. Consequently different values of secbrsteep were tested using the best perfoming value of maxbrsteep. The values tested can be found in table B.2.

Table B.1: Overview of used values for the bottom friction parameters

Simulation	Chezy: C $(m^{1/2}/s)$	Simulation	Manning: n	White-Colebrook: k_s
C1	55	N1	0.02	0.01
C2	56	N2	0.0196	
C3	57	N3	0.0192	
C4	58	N4	0.0188	
C5	59	N5	0.0184	
C6	60	N6	0.0180	
C7	54	N7	0.0204	
C8	53	N8	0.0208	
C9	52	N9	0.0212	
C10	51	N10	0.0216	
C11	50	N11	0.0220	

Table B.2: Overview of used values for the breaker parameters

Simulation	Maxbrsteep	Secbrsteep
M1	0.7	0.3
M2	0.8	0.3
M3	0.5	0.3
M4	0.4	0.3
M5	0.4	0.2
M6	0.4	0.4

Calibration of the runup gauge depth

With the best performing combination of bottom friction and breaker parameters the value rugdepth, the runup gauge depth, is changed. The values tested can be found in table B.3.

Table B.3: Overview of used values for rugdepth

Simulation	Rugdepth (m)
R1	0
R2	0.05
R3	0.10

Results of the calibration

Results of the bottom friction calibration

In table B.4 and B.5 the results of the bottom friction calibration can be found. The root mean square error (over the 36 wave height measuring locations) is given for each calibration simulation and for each value of C or n. Also the root mean square error for each value of C or n but averaged over the three calibration simulations is given. From this table it can be concluded that when using the Chezy formulation, $C3 = 57m^{1/2}/s$ performs best. Some of the values for the Manning parameter n perform comparable with the Chezy formulation, such as $n = 0.0184$. The root mean square error for the White-Colebrook formulation is not shown in table B.4 or B.5 but is overall 0.1442.

The effect of the different bottom friction formulations on runup was tested, as it was expected that a

Table B.4: Root mean square errors for the three calibration simulations and the different bottom friction parameters and their varying values.

Calibration simulation	C1	C2	C3	C4	C5	C6	C7	C8	C9	C10	C11
1	0.1332	0.1363	0.1323	0.1577	0.1318	0.1512	0.1559	0.1360	0.1484	0.1457	0.1512
2	0.1415	0.1250	0.1078	0.1311	0.1247	0.1264	0.1500	0.1369	0.1168	0.1302	0.1298
3	0.1678	0.1520	0.1501	0.1671	0.1597	0.1359	0.1412	0.1620	0.1642	0.1808	0.1753
Overall	0.1475	0.1377	0.1301	0.1520	0.1387	0.1378	0.1490	0.1459	0.1431	0.1522	0.1521

Table B.5: Root mean square errors for the three calibration simulations and the different bottom friction parameters and their varying values.

Calibration simulation	N1	N2	N3	N4	N5	N6	N7	N8	N9	N10	N11
1	0.1611	0.1458	0.1548	0.1557	0.1488	0.1324	0.1402	0.1393	0.1813	0.1469	0.1638
2	0.1159	0.1274	0.1352	0.1143	0.1116	0.1141	0.1108	0.1130	0.1134	0.1113	0.1286
3	0.1930	0.1818	0.1404	0.1529	0.1311	0.1612	0.1945	0.1538	0.1688	0.1636	0.1640
Overall	0.1567	0.1516	0.1434	0.1409	0.1305	0.1359	0.1485	0.1354	0.1545	0.1406	0.1521

depth dependent bottom friction formulation has a large effect on runup due to increased bottom friction in shallow water. For the three calibration simulations measured runup was compared to modeled runup: model predictions of runup are shown for the three bottom friction formulations and all their tested bottom friction parameter values. The result can be seen in figure B.1 and table B.6. In table B.6 the average runup for all parameter values of one bottom friction formulation were computed just as the spread (maximum runup minus minimum runup). In that way mean and spread can be compared for the different bottom friction formulations. The following things can be said about the results:

- Setup: when setup is already overpredicted, the use of a depth dependent bottom friction formulation results in a larger overprediction. When underpredicted it results in a larger underprediction. However, the effect on setup is smaller than the effect on significant swash. Generally a depth dependent bottom friction formulation predicts a higher value of setup ($\Delta\mu < 0$) with a smaller spread ($\Delta SPR > 0$).

- Significant incident swash: when using a depth dependent bottom friction formulation the significant incident swash is predicted lower than when using a depth independent bottom friction formulation. Generally a depth independent bottom friction formulation predicts a higher value of significant incident swash ($\Delta\mu > 0$) with a similar spread.

- Significant infragravity swash: when using a depth dependent bottom friction formulation the significant infragravity swash is predicted lower than when using a depth independent bottom friction formulation. Generally a depth independent bottom friction formulation predicts a higher value of significant infragravity swash ($\Delta\mu > 0$) with also a slightly larger spread.

A higher predicted value of the setup when using a depth dependent bottom friction formulation can be explained by the fact that water will be pushed up higher due to the increased bottom friction in shallow water. This is also the reason why swash is predicted lower. As significant swash was already underpredicted in Stockdon et al. (2014), while setup was overestimated, it was chosen not to use a depth dependent bottom friction formulation, as this would again lead to an underprediction of swash. Concluding, the Chezy formulation with $C = 57m^{1/2}/s$ has the best performance.

Table B.6: Mean of the 11 Chezy and Manning computations and their spread (max - min) for the setup $\bar{\eta}$, the significant incident swash S_{inc} and the significant infragravity swash S_{ig}. The difference between predicted mean and predicted spread of Chezy/Manning is shown for the three calibration simulations and overall for the runup statistic.

Runup statistic		μ_{Chezy}	$\mu_{Manning}$	$\Delta\mu$	SPR_{Chezy}	$SPR_{Manning}$	ΔSPR
$\bar{\eta}$	1	0.6944	0.7425	-0.0481	0.0357	0.0653	-0.0296
	2	-1.0356	-1.0201	-0.0155	0.1337	0.0930	0.0407
	3	0.9657	0.9934	-0.0277	0.4132	0.1155	0.2977
Mean difference $\bar{\eta}$				**-0.0304**			**0.1029**
S_{inc}	1	0.9218	0.6019	0.3199	0.1343	0.0776	0.0567
	2	0.8443	0.6825	0.1618	0.0971	0.1152	-0.0181
	3	1.286	0.7759	0.5101	0.1647	0.1649	-0.0002
Mean difference S_{inc}				**0.3306**			**0.0128**
S_{ig}	1	1.0216	0.8947	0.1269	0.0853	0.1038	-0.0185
	2	0.5903	0.5772	0.0131	0.2200	0.1287	0.0913
	3	1.2883	1.1391	0.1492	0.3036	0.1544	0.1492
Mean difference S_{ig}				**0.0964**			**0.0740**
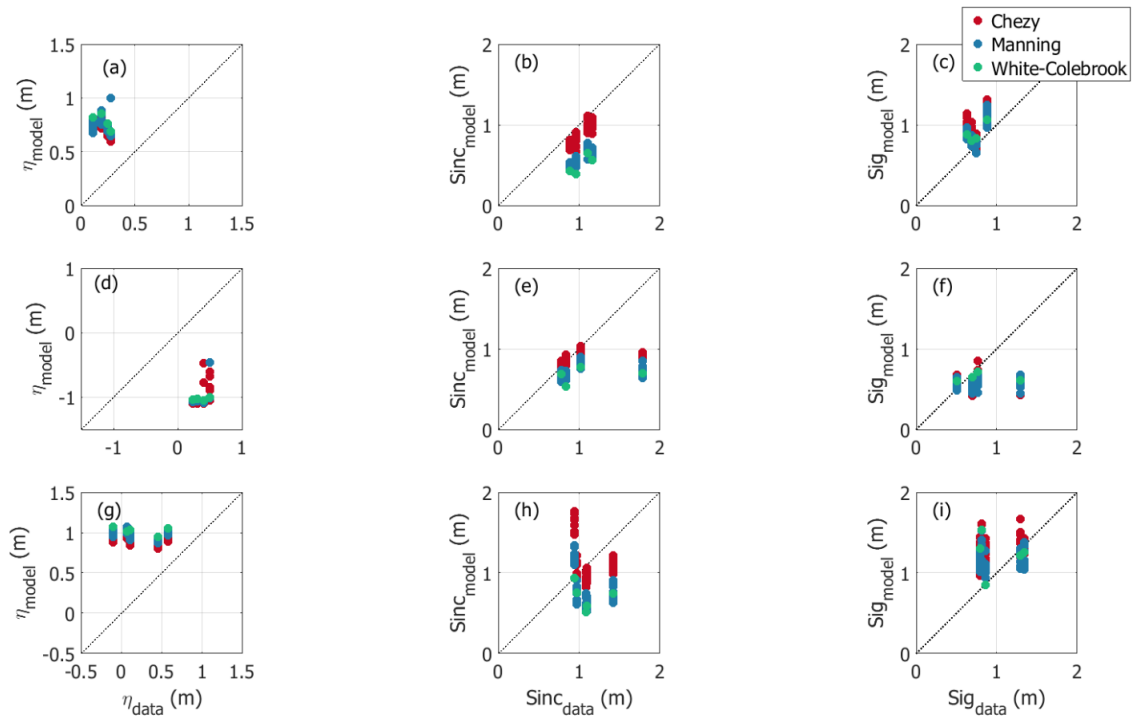
Figure B.1: Measured runup statistics compared to modeled runup statistics for the three bottom friction formulations. In the left column setup, in the middle column significant incident swash and in the right column significant infragravity swash. In the top row the results for simulation 1, in the middle row for 2 and in the bottom row 3.

Results of the breaker parameter calibration

In table B.7 the root mean square errors for the different values of maxbrsteep (for a value of C of 57 $m^{1/2}/s$) can be found. The overall root mean square error (over all 36 output locations) for the calibration simulations seperately and for all three together is given. When looking at the overall root mean square error it can be concluded that C3 with $C = 57$, maxbrsteep = 0.6 and secbrsteep 0.3 still performs the best with a root mean square error of 0.1301 m. However, as in this measure of error all

36 measurement points are included and consequently the points nearest to the shore get a relatively small weight, also the root mean square error for the measuring locations closest to shore are included in table B.7. At this location the waves are always breaking, irrespective of tidal water level and wave height, and therefore the choice for the maximum wave steepness upon breaking will have the largest influence here. When looking at the root mean square error for location 6, M4 performs the best with a root mean square error of 0.0747 m.

Table B.7: Root mean square errors for the three calibration sums and the different values of maxbrsteep. The overall root mean square error for the three simulations together is given just as the root mean square error at the output location 6 which is closest to shore ($x_6 = 605$).

Calibration simulation	M1	M2	M3	M4	C3
1	0.1406	0.1408	0.1545	0.1492	0.1322
2	0.1438	0.1482	0.1508	0.1499	0.1078
3	0.1698	0.1726	0.1574	0.1740	0.1501
Overall	0.1514	0.1539	0.1542	0.1577	0.1301
Location 6	0.0926	0.1202	0.1017	0.0748	0.0955

Finally two other values of secbrsteep, besides the original value of 0.3, were tested. The results can be found in table B.8. The overall root mean square error (over all 36 output locations) for the calibration simulations seperately and for all three together is given. When looking at the overall root mean square error M6 performs best. However, as in this measure of error all 36 measurement points are included and consequently the points nearest to the shore get a relatively small weight, also the root mean square error for the measuring locations closest to shore are also included in table B.8. At this location the waves are always breaking, irrespective of tidal water level and wave height, and therefore the choice for the secundary wave steepness upon breaking will have the largest influence here. When looking at the root mean square error for location 6, M5 performs the best with a root mean square error of 0.0729 m.

Table B.8: Root mean square errors for the three calibration sums and the different values of secbrsteep.

Calibration simulation	M5	M6	M4
1	0.1665	0.1513	0.1492
2	0.1061	0.1152	0.1499
3	0.1610	0.1356	0.1740
Overall	0.1445	0.1340	0.1577
Location 6	0.0729	0.0745	0.0748

Because the best performing values for maxbrsteep and secbrsteep are different values than the ones used in the bottom friction calibration it should be checked whether the best performing bottom friction formulation and parameter value found previously is still the best performing after having calibrated the wave breaker parameters. The results of this second loop of the bottom friction calibration can be found in table B.9 and B.10. From the tables it follows that still C3 is the best perfoming value with a root mean square error of 0.1316 m. The root mean square error for White-Colebrook is not included in the tables but is 0.1493 m overall.

Table B.9: Root mean square errors for the three calibration simulations and the different bottom friction parameters and their varying values.

Calibration simula- tion	C1	C2	C3	C4	C5	C6	C7	C8	C9	C10	C11
1	0.1703	0.1347	0.1499	0.1263	0.1510	0.1276	0.1492	0.1353	0.1452	0.1235	0.1746
2	0.1502	0.1225	0.1093	0.1213	0.1010	0.1251	0.1094	0.1333	0.1418	0.1275	0.1228
3	0.9582	0.1577	0.1356	0.1810	0.1609	0.1632	0.1378	0.1774	0.1515	0.1809	0.1707
Overall	0.4262	0.1383	0.1316	0.1429	0.1376	0.1386	0.1321	0.1487	0.1462	0.1440	0.1561

Table B.10: Root mean square errors for the three calibration simulations and the different bottom friction parameters and their varying values.

Calibration simula- tion	N1	N2	N3	N4	N5	N6	N7	N8	N9	N10	N11
1	0.1257	0.1506	0.1392	0.1364	0.1492	0.1272	0.1235	0.1380	0.1358	0.1551	0.1423
2	0.1134	0.1172	0.1150	0.1251	0.1095	0.1227	0.1433	0.1373	0.1234	0.1252	0.1315
3	0.1615	0.1842	0.1690	0.1628	0.1716	0.1507	0.1567	0.1311	0.1482	0.1645	0.1407
Overall	0.1336	0.1507	0.1411	0.1414	0.1434	0.1335	0.1412	0.1355	0.1358	0.1482	0.1382

Results of the runup gauge depth calibration

Finally the effect of varying value of rugdepth on setup and swash is tested. The results can be found in table B.11. The results are also visualized in figure B.2. The root mean square error of the setup decreases with increasing rugdepth. The root mean square error of the significant incident swash increases with increasing rugdepth. The root mean square error of the significant infragravity swash decreases first and then increases again for increasing rugdepth. The reason for this is not completely clear. The value of 0.05 m performs best overall.
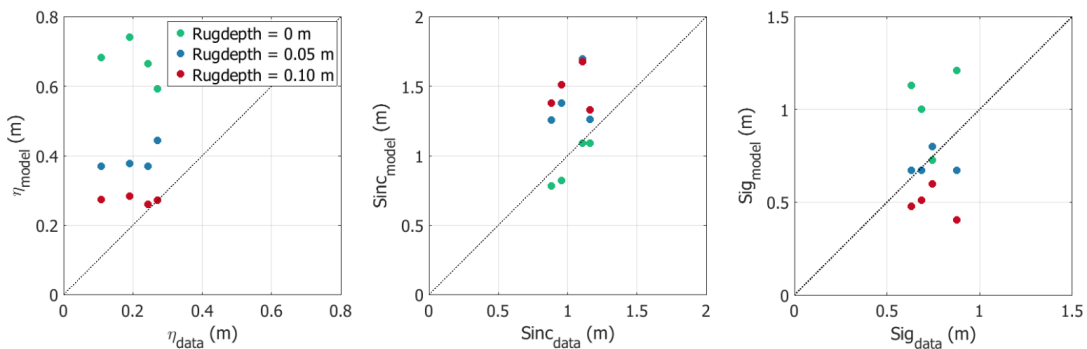
Figure B.2: Measured runup statistics compared to modeled runup statistics for the three different values of rugdepth.

Conclusion

The optimal set of parameter values has been investigated in the calibration. The values which will be used in the validation can be found in table B.12.

Table B.11: Root mean square errors for different values of rugdepth for setup, significant incident swash and significant infragravity swash, for calibration simulation 1. The RMSE per statistic and per rugdepth value is given and the overall RMSE for all statistics and each value of rugdepth is given.

Calibration simulation	Runup statistic	R1	R2	R3
1	$\bar{\eta}$	0.4699	0.1997	0.0873
	S_{inc}	0.1008	0.4012	0.4704
	S_{ig}	0.3777	0.0563	0.2503
	Mean	0.3161	0.2191	0.2694

Table B.12: Values of parameters, resulting from the calibration, which will be used in the validation.

Parameter	Value
C	$57\ m^{1/2}/s$
Maxbrsteep	0.4
Secbrsteep	0.2
Rugdepth	0.05 m

C
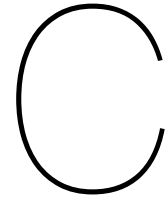
Calibration of the XBeach Surfbeat model

Introduction

In this appendix the calibration of the XBeach Surfbeat is presented. A briefer calibration has been carried out than for the XBeach Non-hydrostatic model as the aim was to keep the XBeach Surfbeat model as comparable as possible to the XBeach Surfbeat model used by Stockdon et al. (2014). Only parameters either not reported by Stockdon et al. (2014) or known to have caused difficulties during their calibration were checked again: the C parameter of the Chezy bottom friction formulation and the breaker parameter γ. The value for the runup gauge depth as used in Stockdon et al. (2014) (0.10 m) is used without checking other values.

Calibration simulations

The same simulations were used as in the calibration of the XBeach Non-hydrostatic model, representing a range in wave steepnesses and wave heights:

- Average wave height with a small wave period (simulation 1): $H_{m0} = 1.19$ m and $T_p = 5.83$ s
- Average wave height with a large wave period (simulation 2): $H_{m0} = 1.16$ m and $T_p = 10.72$ s
- Large wave height (simulation 3): $H_{m0} = 2.11$ m and $T_p = 8.16$ s

Calibration of bottom friction

The bottom friction formulation of Chezy was used (also used by Stockdon et al. (2014)). The formulations is given below:

$$c_{f,Chezy} = \frac{g}{C^2} \tag{C.1}$$

For Chezy 6 different values of the C parameter were tested. The values can be found in table C.1. A typical value for sandy beaches for C is 55 $m^{1/2}/s$ (Roelvink et al., 2010). A value for γ of 0.42 (used by Stockdon et al. (2014)) was used.

Table C.1: Overview of used values for the bottom friction parameters

Simulation	C ($m^{1/2}/s$)
C1	55
C2	56
C3	57
C4	58
C5	59
C6	60

Calibration of the breaker parameter

With the best performing value for the bottom friction different values for γ were tested. The values tested can be found in table C.2. M1, M2 and M3 were tested as these values were also tested in the calibration of Stockdon et al. (2014). M4 was tested to rule out that a higher value of γ did not perform better.

Table C.2: Overview of used values for the breaker parameters

Simulation	γ
M1	0.32
M2	0.42
M3	0.52
M4	0.60

Results of the calibration

Results of the bottom friction calibration

In table C.3 the results of the bottom friction calibration can be found. For every calibration simulation and every value of the C parameter the root mean square error (over all 36 measuring locations) is given. For each value of the C parameter also the root mean square error for the three calibration simulations together is given. A value for C of 56 $m^{1/2}/s$ performs the best with a root mean square error of 0.0726 m.

Results of the breaker parameter calibration

The results of the breaker parameter calibration are given in table C.4. For every calibration simulation and every value of the γ parameter the root mean square error (over all 36 measuring locations) is given. For each value of the γ parameter also the root mean square error for the three calibration simulations together is given. When looking at this overall root mean square error M2 performs the best. However, as in this measure of error all 36 measurement points are included and consequently the points nearest to the shore get a relatively small weight, also the root mean square error for the measuring locations closest to shore are included in table C.4. At this location the waves are always breaking, irrespective of tidal water level and wave height, and therefore the choice for the breaker parameter will have the largest influence here. When looking at the root mean square error for location 6, M2 still performs performs the best with a root mean square error of 0.1090 m. This is the same value for γ as was found in the calibration of Stockdon et al. (2014).

As the value of γ which turns out to perform best is the same as the value of γ used in the bottom friction calibration it is not necessary to do an extra bottom friction calibration (to check whether the chosen value of C still performs best after calibrating the breaker parameter).

Conclusion

The optimal set of parameter values has been investigated in the calibration. The values which will be used in the validation can be found in table C.5.

Table C.3: Root mean square errors (over all 36 measuring locations) for different values of the C parameter, both the three calibration simulations seperately and overall.

Calibration simulation	C value ($m^{1/2}/s$)	RMSE (m)
1	C1	0.0867
	C2	0.0792
	C3	0.0877
	C4	0.0923
	C5	0.0806
	C6	0.0792
2	C1	0.0786
	C2	0.0731
	C3	0.0736
	C4	0.0786
	C5	0.1671
	C6	0.1618
3	C1	0.0637
	C2	0.0654
	C3	0.0625
	C4	0.0663
	C5	0.0622
	C6	0.060
Overall	C1	0.0764
	C2	0.0726
	C3	0.0746
	C4	0.0791
	C5	0.1033
	C6	0.1003

Table C.4: Root mean square errors (over all 36 measuring locations) for different values of the breaker parameter γ, both for the three calibration simulations and overall. Also the root mean square error at the measuring location closest to shore ($x = 605m$) is given.

Calibration simulation	Value of γ	RMSE
1	M1	0.0484
	M2	0.0769
	M3	0.1286
	M4	0.1673
2	M1	0.1592
	M2	0.0574
	M3	0.0958
	M4	0.1489
3	M1	0.3676
	M2	0.1528
	M3	0.1085
	M4	0.1893
Overall	M1	0.1917
	M2	0.0967
	M3	0.1110
	M4	0.1685
Location 6	M1	0.1091
	M2	0.1090
	M3	0.2399
	M4	0.3505

Table C.5: Values of parameters, resulting from the calibration, which will be used in the validation.

Parameter	Value
C	$56 \ m^{1/2}/s$
γ	0.42

D
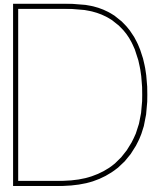
Formulations of statistical parameters

Introduction
In this appendix the formulations of the statistics as used in the calibration and validation are given.

Root mean squared error
The root mean square error is calculated in the following way (with $y_1 - y_i$ the data and $f_1 - f_i$ the model results:

$$rmse = \sqrt{\frac{1}{i}\sum_i (f_i - y_i)^2}$$

Coefficient of determination
The coefficient of determination R^2 indicates the amount of variance of the model's results which is explained by the data variance (Wikipedia, 2017b). It is calculated in the following way (with $y_1 - y_i$ the data and $f_1 - f_i$ the model results):

$$SS_{reg} = \sum_i (f_i - \bar{y})^2$$

$$SS_{res} = \sum_i (y_i - f_i)^2$$

$$SS_{tot} = SS_{reg} + SS_{res}$$

$$R^2 = \frac{SS_{reg}}{SS_{tot}}$$

Bias
The bias is the difference between the computed and measured results and is calculated as follows (with $y_1 - y_i$ the data and $f_1 - f_i$ the model results) (Wikipedia, 2017a):

$$B = \frac{1}{n}\sum_{i=1}^{n} (f_i - y_i)$$
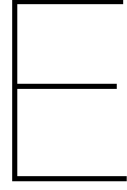
Splitting incoming and outgoing waves with the method of Guza

Introduction

This appendix describes the methodology used to seperate the total wave field into incoming and outgoing waves. This is done with the Guza method.

The Guza method

Guza et al. (1984) gives the following formulations for the incoming and outgoing water level timeseries, η_{in} and η_{out} respectively:

$$\eta_{in} = \frac{\eta \cdot c_{out} + Q}{c_{in} + c_{out}} \tag{E.1}$$

$$\eta_{out} = \frac{\eta \cdot c_{out} - Q}{c_{in} + c_{out}} \tag{E.2}$$

η is the total water level timeseries, c_{in} and c_{out} the wave celerities of the incoming and reflected waves and $Q = u \cdot h$ with u the depth averaged velocity. When the waves are in shallow water this reduces to (van Thiel de Vries, 2009):

$$\eta_{in} = \frac{\eta + u \cdot \sqrt{\frac{h}{g}}}{2} \tag{E.3}$$

$$\eta_{out} = \frac{\eta - u \cdot \sqrt{\frac{h}{g}}}{2} \tag{E.4}$$

This can be solved in time space. However, when the waves are not in shallow water and propagate with c_g instead of $\sqrt{gh}$ it has to be solved in Fourier space. In that case it is assumed that all frequencies propagate freely except for the frequencies with $f < f_{split}$. These are the bound infragravity waves travelling with c_g of the peak frequency.

$$c_{in} = \begin{cases} \frac{\omega}{k} & f \geq f_{split} \\ c_g & f < f_{split} \end{cases} \tag{E.5}$$

$$c_{out} = \frac{\omega}{k} \tag{E.6}$$

Use

The waves are split on 17 different places in the cross shore. The incident waves generally start to break around $x = 575m$. Prior to this point the frequencies with $f < f_{split}$ are considered bound to the incident waves and after they are considered free. f_{split} is defined as $0.5f_p$. The chosen option for each location can be found in table E.1. The infragravity wave height transformation is not sensitive to the point where the propagation is changed from bound to free.

Table E.1: Propagation type for each cross shore point.

X-coordinate (m)	Propagation type
5	bound
10	bound
30	bound
60	bound
100	bound
200	bound
300	bound
400	bound
500	bound
575	bound
605	free
610	free
615	free
620	free
625	free
630	free
635	free

Over the largest part of the cross shore the waves are not in shallow water and the Guza method has to be used in Fourier space. On the swash zone border it can be done in time space as long as enough waves are in shallow water. The fraction of waves which is in shallow water on the swash zone border was determined. The mean water depth at the swash zone border is around 0.5 m. When taking the shallow water limit as $h < \frac{L}{20}$ and defining L with the zero down crossing method, it was shown that for the XBeach Non-hydrostatic model 35% of the waves at the swash zone border are not yet in shallow water. This is considered a fraction too large and the Guza method was used in Fourier space.

When using the Guza method in Fourier space c_g is determined with f_p. However, while the water level output from XBeach Non-hydrostatic consists of all frequencies, the water level output from XBeach Surfbeat only consists of infragravity frequencies. This would lead to a higher group velocity than XBeach Non-hydrostatic and therefore a different propagation. To solve this problem the peak frequency from XBeach Non-hydrostatic is used to calculate the group velocity of XBeach Surfbeat with. On average this increases the incoming infragravity wave height predicted by XBeach Surfbeat with 0.0014 m and maximum 0.0166 m. On an incoming infragravity wave height of order 0.10 m this can make a significant difference. The above is only done for the locations in the cross shore where the infragravity waves are considered bound.

Examples

In figure E.1 an example can be seen from the Guza method in Fourier space. The original water level timeseries is shown together with the incoming and reflected water level timeseries. To check whether the incoming and reflected water level timeseries together still match the original water level timeseries, this is plotted as well.
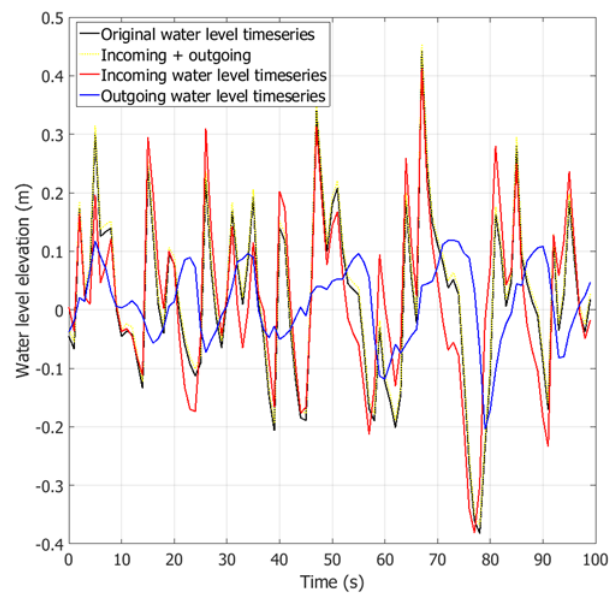
Figure E.1: Example of a water level timeseries seperated in incoming and outgoing waves. The original water level timeseries and the incoming and reflected water level timeseries resulting from the Guza method in Fourier space are shown. To check whether the incoming and reflected water level timeseries together still match the original water level timeseries, this is plotted as well.

$$\text{F}$$
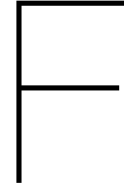
The Hilbert-Huang transformation

Introduction

In this appendix the method of the Hilbert-Huang transformation is described. For a more extensive description one is referred to (Huang and Chen, 2005). The Hilbert-Huang transform is an emperically based data-analysis method which is suitable for nonlinear and non-stationary processes. It consists of two parts: empirical mode decomposition (EMD) and Hilbert spectral analysis (HSA).

Empirical mode decomposition

The empirical mode decomposition is based on the assumption that any data consists of different simple intrinsic modes of oscillation, each mode having the same number of extrema as zero crossings and being symmetric with respect to the local mean. Each of the modes is represented by an intrinsic mode function (IMF). An IMF is more general than a simple harmonic function: it can have a frequency and amplitude which are varying in time.

The original data ($x(t)$) can be decomposed into IMFs as follows:

1. Identify all the local extrema.

2. Connect all local maxima with each other by a cubic spline line. This is the upper envelope.

3. Do the same for the local minima. This is the lower envelope.

4. Take the mean m_1 of the upper and lower envelope.

5. Take the difference between the original data and m_1: $h_1 = x(t) - m_1$.

h_1 is a proto-IMF. In the next step it is treated as data and the above steps are executed again. After repeated siftings $h_{1,k}$ becomes an IMF:

$$h_{1,k} = h_{1(k-1)} - m_{1,k} = c_1 \tag{F.1}$$

c_1 is the first IMF component from the original data x(t). The amount of siftings needed is determined by the stoppage criterion: if the squared difference SD_k between two subsequent proto-IMFs is smaller than a predetermined value, the sifting process stops.

$$SD_k = \frac{\sum_{t=0}^{T} \mid h_{k-1}(t) - h_k(t) \mid^2}{\sum_{t=0}^{T} h_{k-1}^2} \tag{F.2}$$

This formulation of the stoppage criterion poses two problems. First, how to choose the value SD_k should be smaller than. Second, SD_k might be small but the function might not have the same amount of extrema and zero crossings. Another stoppage criterion is the following: the sifting process will stop after S times when the number of zero crossings and extrema stay constant and are equal (or differ
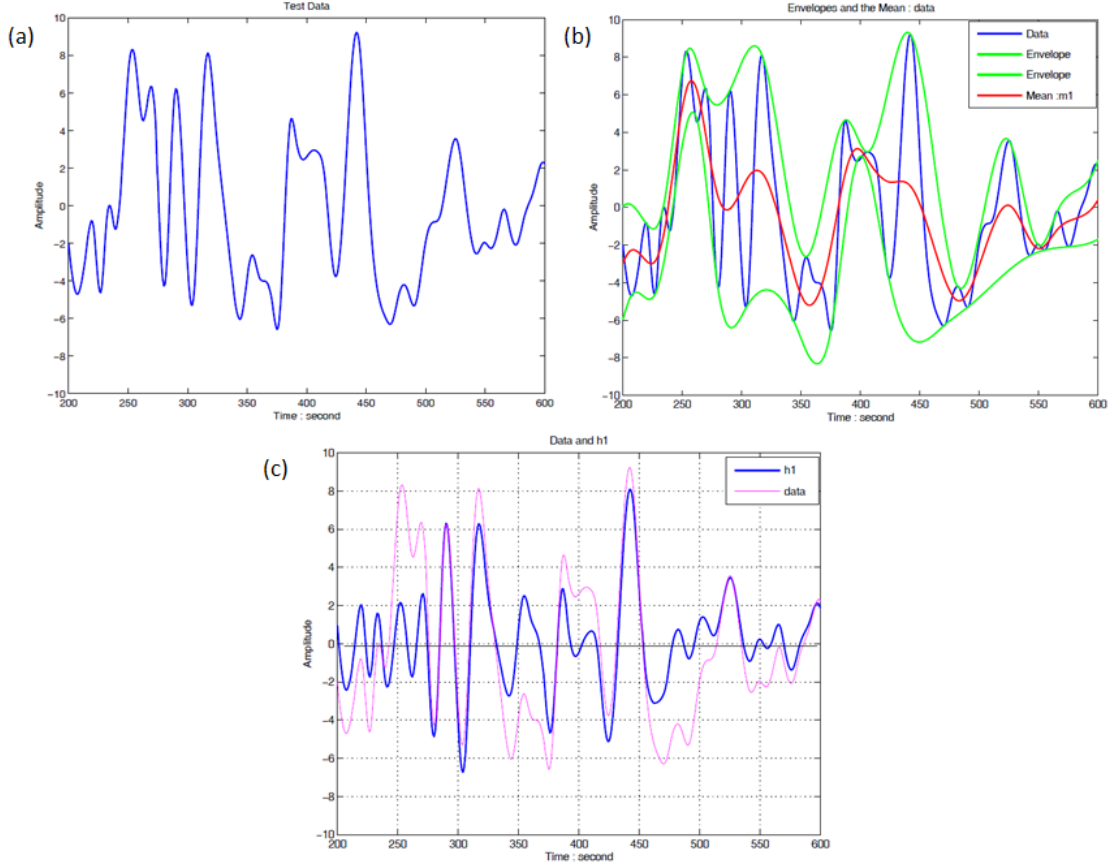
Figure F.1: Method of the Hilbert-Huang transform. (a) The original data timeseries. (b) The original data timeseries with the upper and lower envelope and the envelope mean m_1. (c) The original data timeseries and the first proto-IMF h_1. (Huang and Chen, 2005)

by at most 1). For an optimal sifting process, S should be between 4 and 8.

The first IMF c_1 contains the component with the shortest time scales and can be seperated from the rest of the data, creating the residue r_1:

$$r_1 = x(t) - c_1 \tag{F.3}$$

The residue is treated as the new data and the same sifting process is done again until the second IMF is found, and so on. Finally a decomposition of the original data into n empirical modes is found, together with a residue r_n (with r_n being either a constant or a trend):

$$x(t) = \sum_{j=1}^{n} c_j + r_n \tag{F.4}$$

Hilbert spectral analysis

After having acquired the IMFs the Hilbert transform can be applied to each IMF, resulting in the envelope of each IMF timeseries. First the analytic signal is computed from the input signal (the IMF c_j) and its Hilbert transformation h(t):

$$Y(t) = c_j(t) + i \cdot h(t) \tag{F.5}$$

This can be rewritten as:

$$Y(t) = A(t) \cdot e^{i \cdot \psi(t)} \tag{F.6}$$

A(t) is the envelope of the analytic signal and $\psi(t)$ the phase. The envelope is thus the absolute value of the analytic signal. From the different envelopes the total envelope can be computed as follows:

$$A_{tot}(t) = \sqrt{\sum_{j=1}^{n} A_j(t)^2} \tag{F.7}$$

In figure F.2 an example can be found. A certain timeseries (the incident water level timeseries from figure F.3) has been decomposed into 9 IMFs and for each IMF the envelope has been computed. The original timeseries along with its total envelope can be seen in figure F.3.
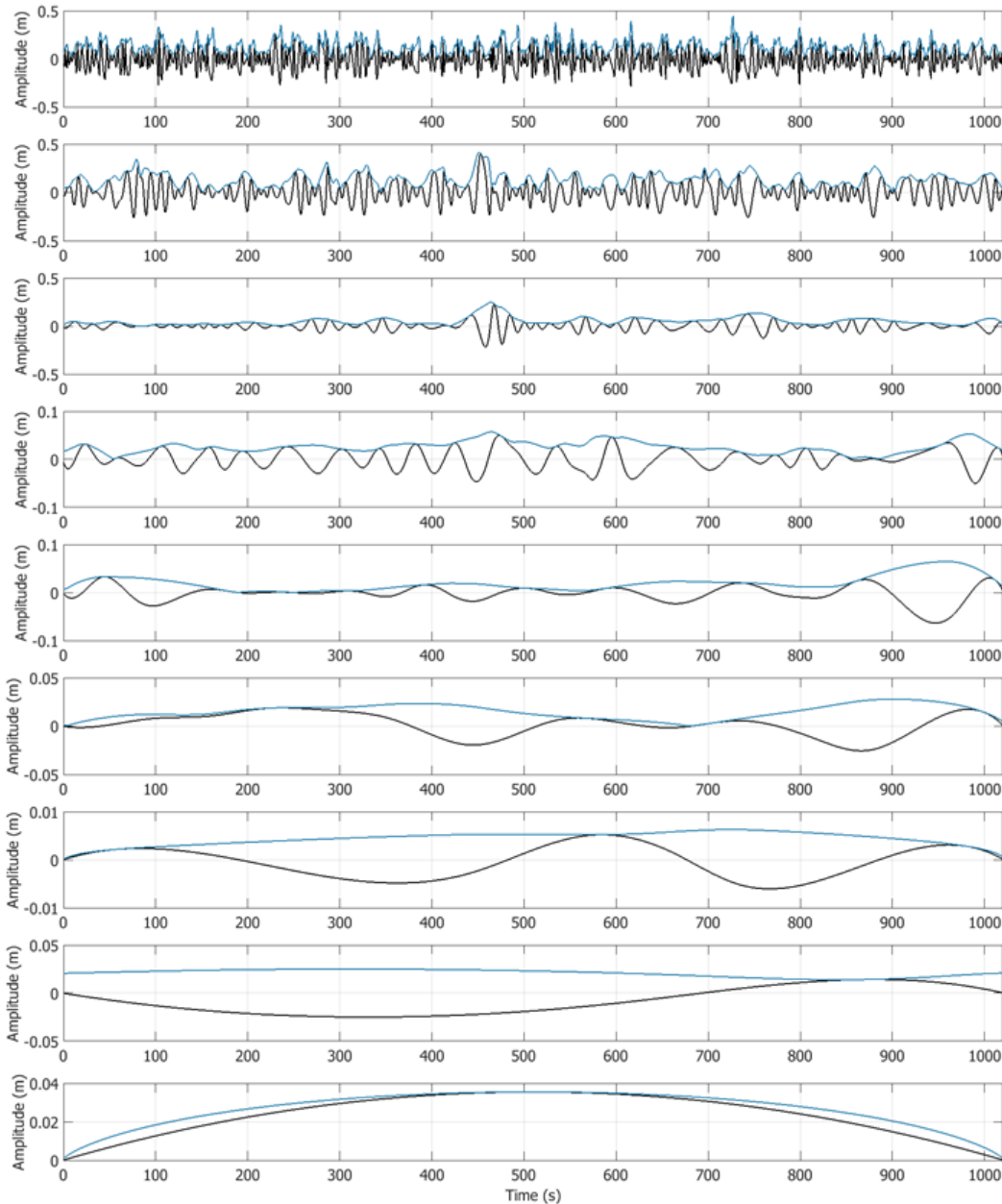
Figure F.2: The timeseries of the different IMFs (in black) and their envelopes (in blue). The first IMF has the shortest time scales, the last the largest.
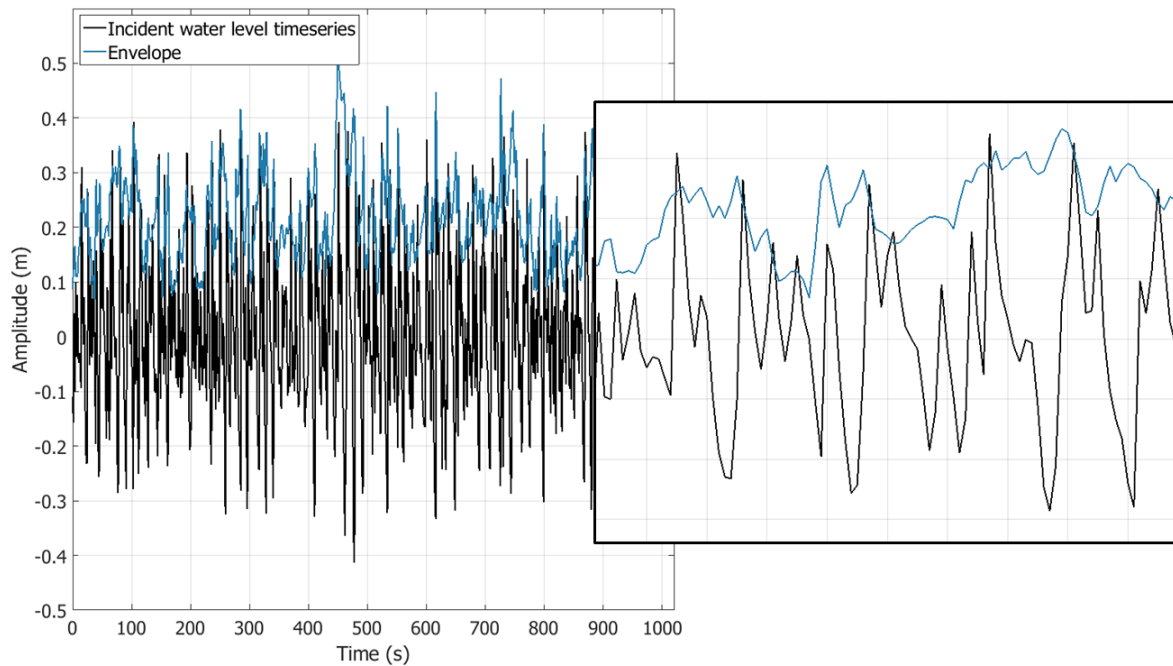
Figure F.3: The original timeseries with the total envelope.

The difference between the Hilbert and the Hilbert-Huang transformation

Offshore
The difference between the Hilbert-Huang and the Hilbert transformation at relatively deep water was examined. An example can be seen in figure F.4. For both methods the envelope and the low-pass filtered envelope can be seen: according to List (1990) the envelope resulting from the Hilbert transformation should be low-pass filtered to get the envelope on the wave group timescale. Especially the unfiltered envelope resulting from the Hilbert transformation follows the water level timeseries well, buth both the unfiltered and low-pass filtered envelope look quite similar for both transformation methods. However, this is only one example and on average the groupiness factor GF computed with the unfiltered Hilbert-Huang transformation is 0.18 lower than for the Hilbert transformation, with a standard deviation of 0.0625.

Swash zone border
Close to shore the Hilbert-Huang transformation is a more suitable method as the waves are highly nonlinear here. In figure F.5 it can be seen that the low-pass filtered envelope follows the incident water level better for the Hilbert-Huang than the Hilbert transformation. At the swash zone border the Hilbert-Huang transformation also predicts a lower groupiness factor GF than the Hilbert transformation, with a mean difference of 0.30 and a standard deviation of 0.07. When using the Hilbert transformation over the entire cross shore no decrease in groupiness close to shore is visible at all, in that way indicating the bad performance of the Hilbert transformation close to shore.
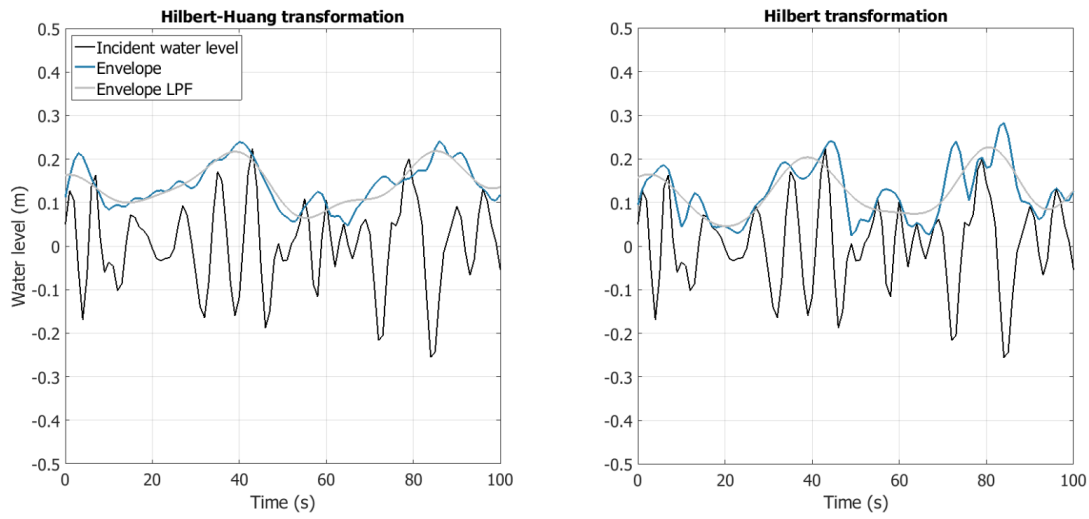
Figure F.4: Comparison of the incident wave envelope for the Hilbert-Huang and the Hilbert transformation at relatively deep water.
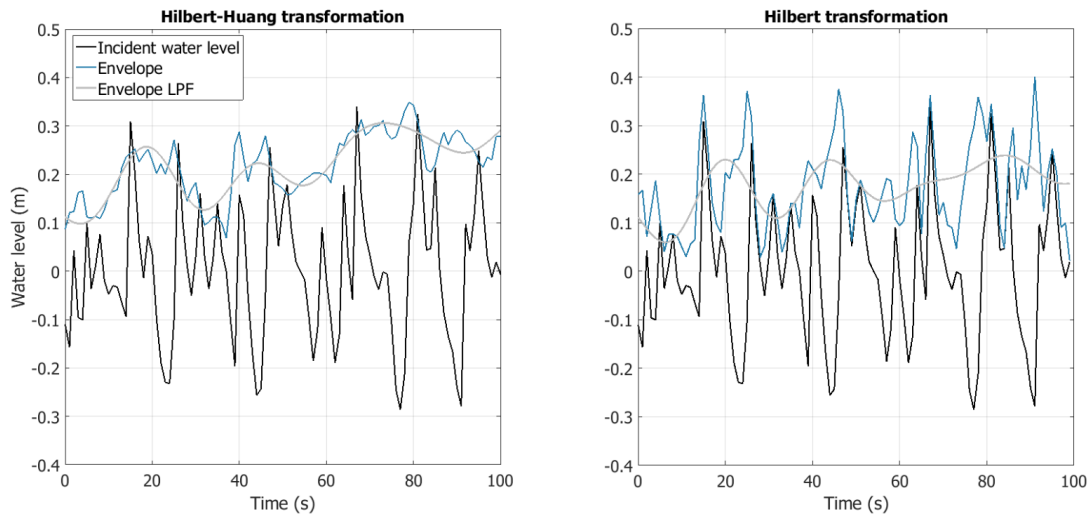
Figure F.5: Comparison of the incident wave envelope for the Hilbert-Huang and the Hilbert transformation at the swash zone border.

G

Determining directional and frequency spreading from a frequency-directional spectrum

Introduction

The method for determining frequency and directional spreading from a frequency-directional spectrum is given in this appendix, following Long (2017).

Directional spreading

The frequency-directional spectrum is integrated along all frequencies for each direction:

$$E_\theta(\theta) = \int_0^\infty E_{f,\theta} df \tag{G.1}$$

The peak of the directional spectrum is found and the half power is defined as half of the peak value. The directional spreading θ_{spread} then is the distance between the two intersection points of the directional spectrum and its half power. For a bimodal spectrum the outer intersection points are used. When the directional spectrum lies completely above the half power, $\theta_{spread} = 180°$. When only one intersection point is found and the other half of the spectrum stays above the half power the other intersection point is equal to the maximum direction (-90 or 90 °, depending which side of the spectrum). A visualisation of the method can be seen in figure G.1.

Frequency spreading

The frequency-directional spectrum is integrated along all directions for each frequency:

$$E_f(f) = \int_{-180}^{180} E_{f,\theta} d\theta \tag{G.2}$$

The peak of the frequency spectrum is found and the half power is defined as half of the peak. The frequency spreading f_{spread} then is the distance between the two intersection points of the frequency spectrum and its half power. For a bimodal spectrum the outer intersection points are used. When the frequency spectrum lies completely above the half power, $f_{spread} = 0.5$ Hz. When only one intersection point is found and the other half of the spectrum stays above the half power the other intersection point is equal to the maximum frequency (0 or 0.5 Hz, depending which side of the spectrum). A visualisation of the method can be seen in figure G.2.
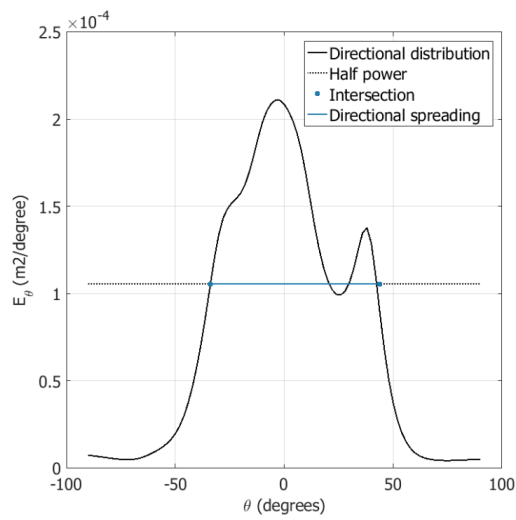
Figure G.1: Example of determination of directional spreading (in this case the directional spectrum is defined between -90 and 90 degrees).
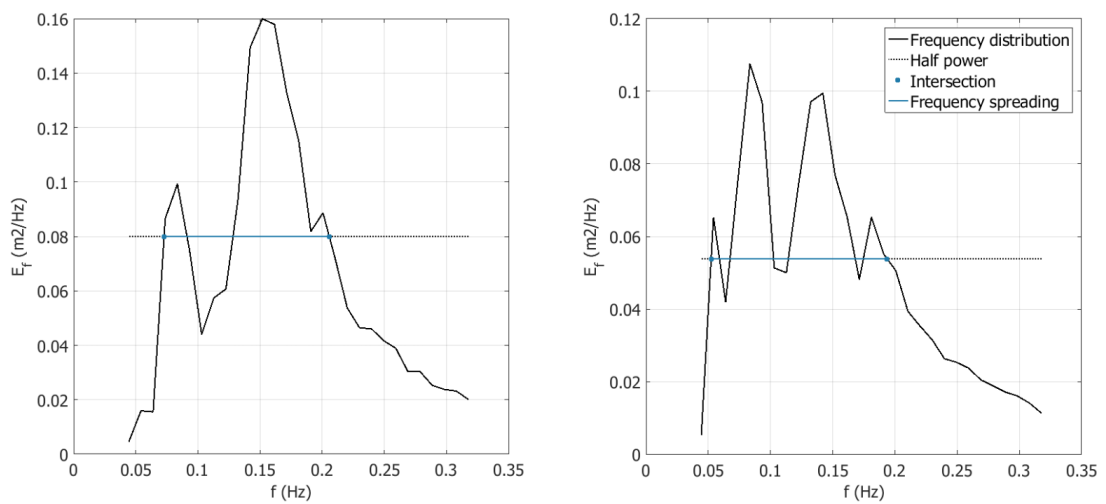
Figure G.2: Example of determination of frequency spreading.

H
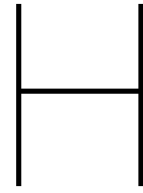
Validation of the low-pass filter

Introduction

To generate a timeseries of infragravity water level the original water level timeseries is low-pass filtered. Its performance has been checked and will be described in this appendix.

Performance of the low-pass filter

In figure H.1 an example of the low pass filter is given: both the incident frequency timeseries, the infragravity timeseries and the total timeseries is shown for both XBeach Non-hydrostatic and XBeach Surfbeat. It can be seen that the water level timeseries of XBeach Non-hydrostatic has a much larger excursion than the one from XBeach Surfbeat. This is because the water level timeseries from XBeach Surfbeat contain mostly infragravity energy and only a small higher frequency tail.
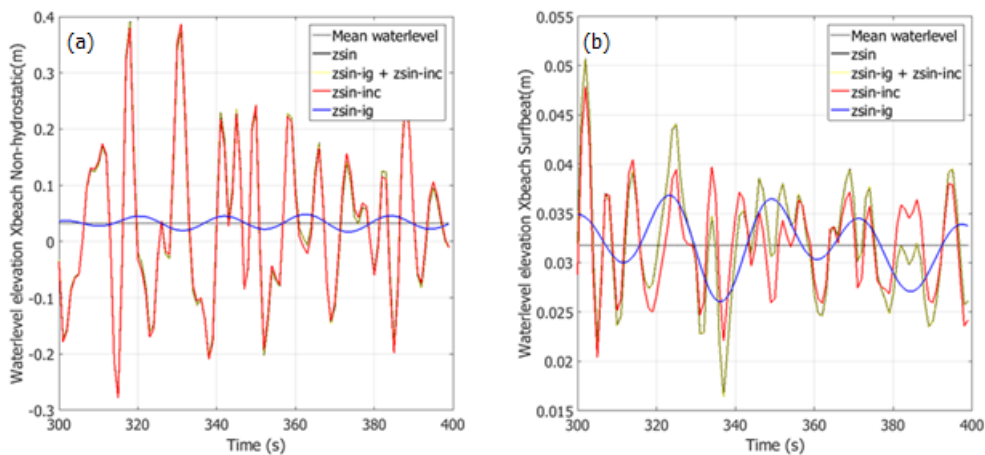
Figure H.1: Low-pass filtered water level timeseries. The total incoming water level timeseries is plotted just as the incident and infragravity water level timeseries. To check whether the incident and infragravity water level timeseries still match the total incoming water level timeseries, this is plotted as well. The results for XBeach Non-hydrostatic can be seen in a, for XBeach Surfbeat in b.

To check whether the low pass filter performs well H_{m0} of the low-pass filtered infragravity waterlevel timeseries is compared to $H_{m0,ig}$ as computed from the full spectrum. The filter performs well (and the right frequencies have been filtered out) when the two H_{m0}'s are comparable. The results can be seen in figure H.2. The mean difference between the two $H_{m0)}$'s for all XBeach Non-hydrostatic simulations is 0.0019 m (-0.0017 m for XBeach Surfbeat). On a mean H_{m0} of 0.16 m (0.11 m for XBeach Surfbeat) this gives an error of 1.19 % (1.55 % for XBeach Surfbeat) and this is considered small enough.
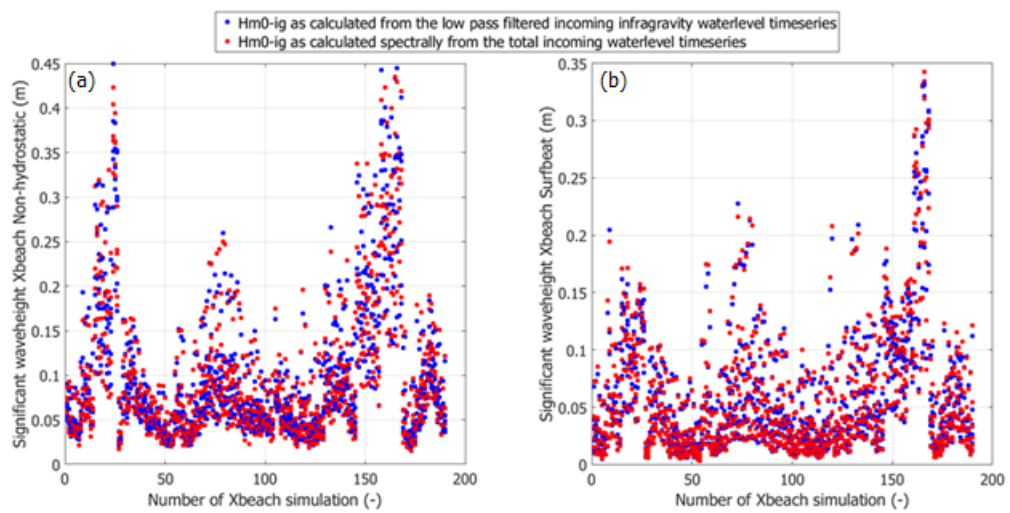
Figure H.2: Check of the functioning of the low-pass filter. For the XBeach Non-hydrostatic model (a) and the XBeach Surfbeat model (b) the significant infragravity wave height as computed from the total incoming water level timeseries and from the low-pass filtered infragravity water level timeseries are compared for all XBeach simulations. When they are comparable it means the low-pass filter functions well and filters out the right frequencies.

Determination of the swash zone border

Introduction
To determine whether the difference in hydrodynamics which causes the runup difference between the XBeach models originates from within or outside the swash zone, the difference in hydrodynamics between the XBeach models is determined on the swash zone border. This appendix describes in detail how the swash zone border is determined.

Method
The location of the border of the swash zone is different for all XBeach simulations due to the changing tide. Therefore it is not possible to define a swash zone border position fixed in space. For each XBeach simulation, both the Non-hydrostatic version and the Surfbeat version, the location of the swash zone border is determined as follows (assuming the swash zone border is at the point of maximum rundown):

- At all x grid points at the chosen alongshore location the minimum waterlevel elevation is determined during the simulation. For XBeach Non-hydrostatic this follows directly from the waterlevel timeseries. For XBeach Surfbeat the waterlevel timeseries is only the result of the infragravity waves. However, the swash is usually dominated by the infragravity swash and therefore the use of the infragravity swash zone border will be sufficient.
- The bottom level at the grid point is subtracted, this results in the minimum water depth during the simulation.
- At each grid point it is checked whether the minimum water depth is larger or smaller than the value of eps (0.005 m, the threshold water depth above which cells are considered wet (Roelvink et al., 2010)). If the minimum water depth is larger than eps, the grid point is wet during the entire simulation. If the minimum water depth is smaller than eps, the grid point is alternating wet and dry during the simulation.
- The swash zone border is considered to be the grid point x_i which is wet during the entire simulation with the next grid point x_{i+1} being alternating wet and dry. The gridpoint which is wet all the time is chosen because otherwise the XBeach output can be only used parts of the simulation.

The determination of the swash zone border is visualized in figure I.1. The location of the swash zone border may differ between the Non-hydrostatic and Surfbeat version of one simulation. This can be seen in figure I.2. The x-coordinate of the XBeach Surfbeat swash zone border is slightly larger than the x-coordinate of the XBeach Non-hydrostatic swash zone border (average difference of 2.68 m). Therefore the XBeach Non-hydrostatic swash zone border is used for both models, such that the respective grid point is always wet in both models. The variation in the x-coordinate of the swash zone border visible in figure I.2 for both models is due to the changing tide.

The depth at the swash zone border varies but is on average 0.47 m, see figure I.3. To determine how the Guza method for splitting incoming and reflected waves should be applied, see appendix E, it is determined how many waves are in shallow water on the swash zone border:
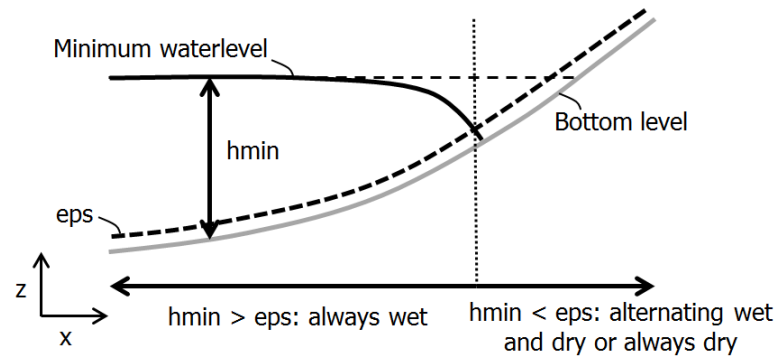
Figure I.1: Visualisation of the determination of the swash zone border. In the chosen cross shore transect at all grid points the minimum depth during a simulation is determined as the difference between the minimum water level and the bottom level. When this value is larger than eps, the threshold water depth above which grid cells are considered wet Roelvink et al. (2010), the grid point is wet during the entire simulation. When it is smaller than eps the grid point is alternating wet and dry or always dry.
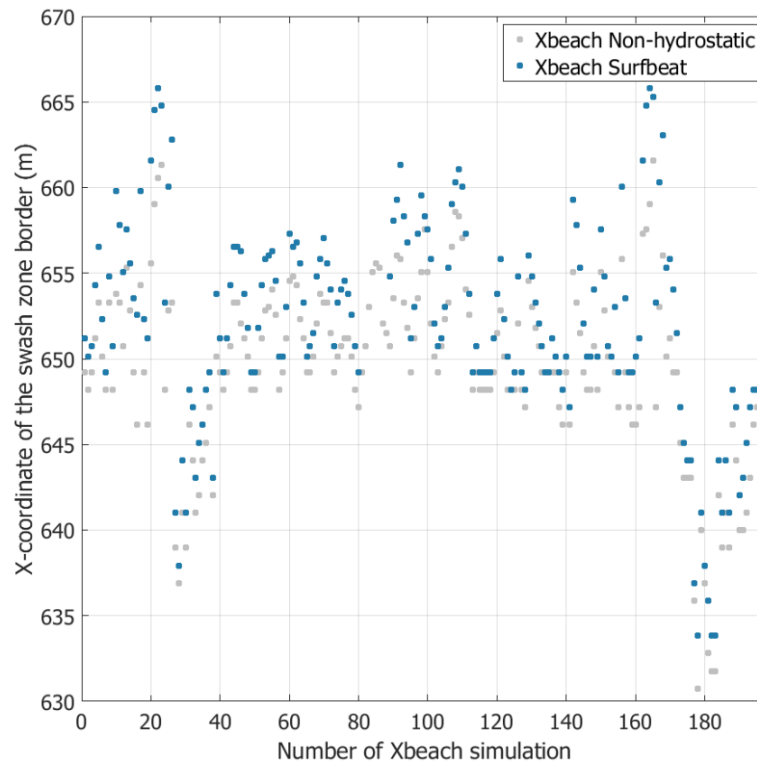
Figure I.2: X-coordinate of the swash zone border for both XBeach models for all simulations.

1. With the zero down-crossing method all waves are identified in the water level timeseries at the swash zone border.

2. The wave period of each wave is determined.

3. With that the radial frequency, wave number and wave length are determined.

4. The shallow water limit is defined as $d \leq \frac{L}{20}$ (Holthuijsen, 2007). The fraction of waves for which

this is true is determined.

It turns out that for the XBeach Non-hydrostatic model 64% of the waves is in shallow water at the swash zone border and 36% is not.
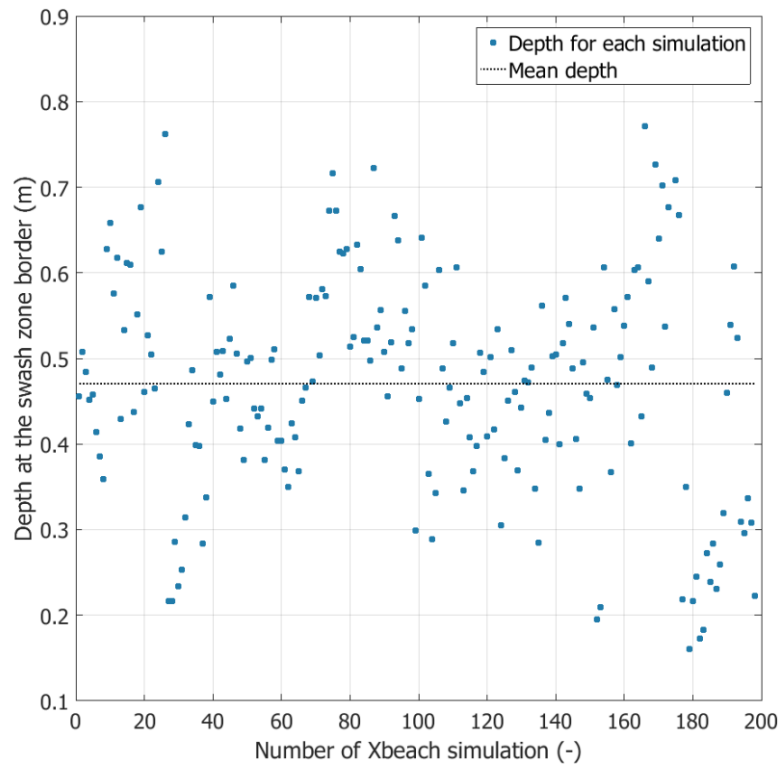
Figure I.3: Depth at the swash zone border for the XBeach Non-hydrostatic model.

J

Isolation of the swash zone

Introduction

In order to prove that a higher infragravity wave height at the swash zone border leads to a higher significant infragravity swash, an isolated XBeach Non-hydrostatic model of the swash zone is made. Its setup will be described in this appendix.

Grid

Two grids are used: a 1D grid of the full cross shore and a 1D grid of the swash zone. The 2D grid for the October 18 16.00 case is transformed into a 1D grid by isolation of one cross shore transect. The same cross shore transect is used as was used for all other analyses (y = 198 m). This grid is the large 1D grid. The 1D grid of the swash zone is constructed by isolating the grid cells from the swash zone onwards.

Boundary conditions

The large 1D grid is used for a XBeach Non-hydrostatic and a XBeach Surfbeat simulation: they are forced with the measured spectrum of October 18 16.00. The border of the swash zone is determined as explained earlier in this thesis, see appendix I. At the location of the swash zone border the water level and cross shore velocity timeseries are extracted, see figure J.1. The isolated model is forced with these water level and velocity timeseries.
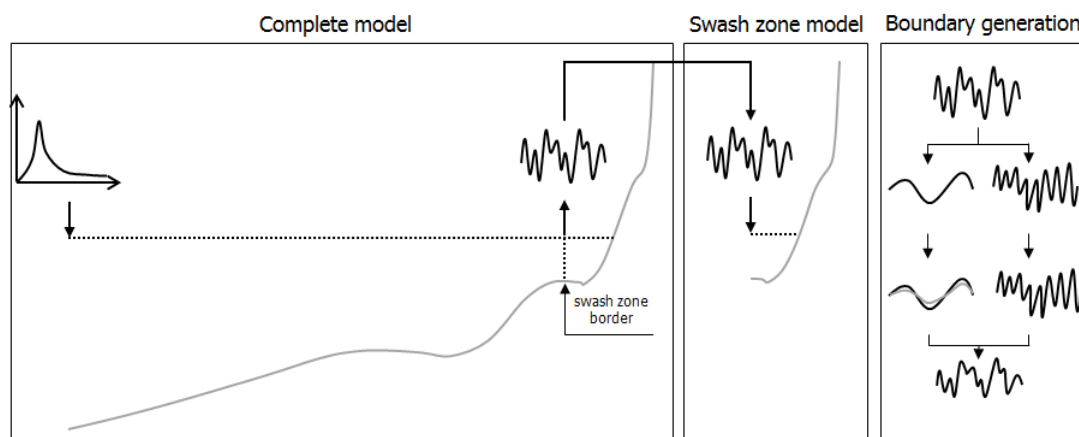
Figure J.1: Visualisation of the isolation of the swash zone.

The swash zone border is forced with multiple infragravity wave heights:

- The infragravity wave height at the swash zone border for the XBeach Non-hydrostatic model at October 18 16.00 (follows from the water level timeseries extracted from the large 1D model).

- The infragravity wave height at the swash zone border for the XBeach Surfbeat model at October 18 16.00, which is lower than for the XBeach Non-hydrostatic model.

- Evenly distibuted infragravity wave heights around the two above.

The starting point is the water level timeseries extracted from the large 1D XBeach Non-hydrostatic model, which gives the infragravity wave height at October 18 16.00 for the XBeach Non-hydrostatic model. For the other cases the infragravity wave height needs to be decreased. This is done in the following way:

1. Both water level and velocity timeseries are split into an incident and an infragravity frequency part (split frequency of 0.05 Hz), using a low-pass filter.

2. The infragravity water level and velocity timeseries are multiplied with a factor to decrease their amplitude, until they represent the required, lower, infragravity wave height.

3. The incident water level and velocity timeseries remain unchanged.

4. The incident and infragravity water level and velocity timeseries are added back together.

An example of the downscaled timeseries can be seen in figure J.2. Downscaling the timeseries with a factor implies using linear wave theory. It should be noted that this is a large assumption as the water is very shallow at the swash zone border.
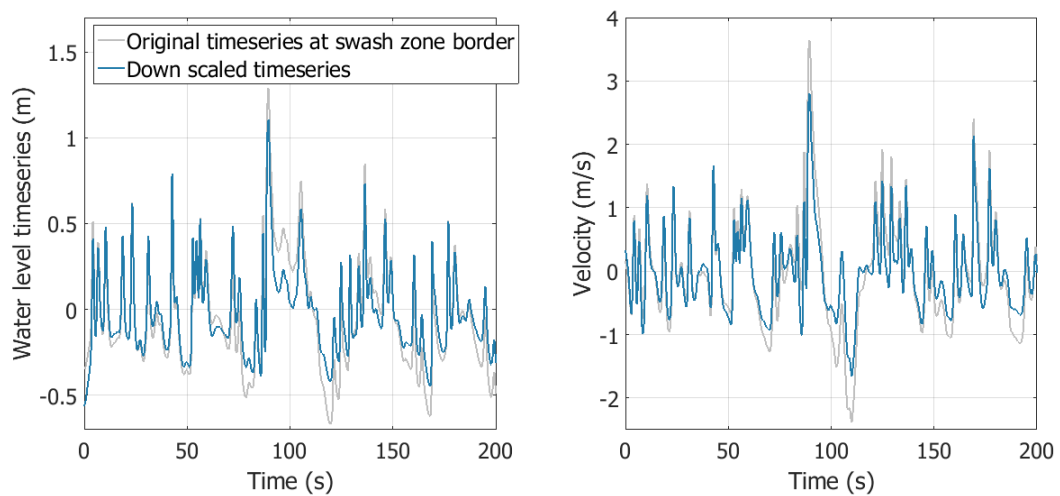
Figure J.2: Resulting water level and velocity timeseries after downscaling the infragravity part.

K
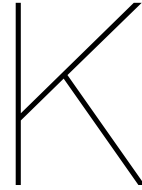
Validation of the infragravity wave height

Introduction

To validate both XBeach models for the infragravity wave height the raw pressure timeseries from the 36 pressure gauges have to be transformed into water level timeseries. The pressure timeseries are available at all moments where runup data is available, which is 85 moments during the measurement campaign. For 72 of these moments 2D XBeach simulations of Duck are available.

Transformation of pressure timeseries into waterlevel timeseries
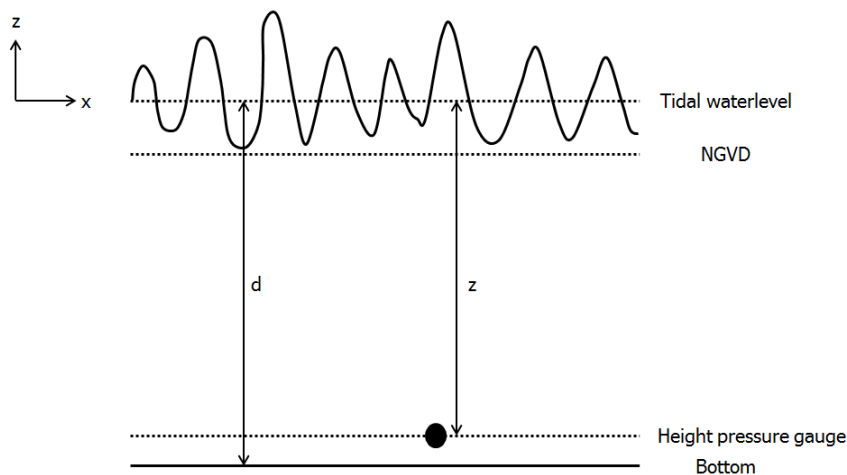
Figure K.1: Definitions used in the transformation from pressure to water level.

The total pressure as a result of wave induced pressure and hydrostatic pressure can be written as follows (Holthuijsen, 2007):

$$p = -\rho g z + \rho g a \frac{cosh(k(d+z))}{cosh(kd)} sin(\omega t - kx) = -\rho g z + p_{wave} \qquad (K.1)$$

In which z is the height in the water column, defined positive upwards, and d is the depth. p_{wave} can be rewritten as:

$$p_{wave} = -\rho g \eta R \qquad (K.2)$$

With $R = \frac{cosh(k(d+z))}{cosh(kd)}$. R is between 0 and 1, a value of 1 corresponding to the hydrostatic pressure. The formulation for the total pressure becomes:

$$p = \rho g(-z + R\eta) \qquad (K.3)$$

To transform the pressure timeseries into a waterlevel timeseries it can be rewritten into:

$$\eta = \frac{p + \rho g z}{\rho g R} \tag{K.4}$$

In this case z is the height in the water column above the pressure gauge. To get the water level timeseries z should be taken at the mean water level, and as this is varying due to the tide, z is different for each moment in time. d is in this case the mean water depth (also varying due to the tide).

The available pressure timeseries are given in centimeters and are transformed to N/m^2 by multiplying with 98.04139432 ($1cm = 98.04139432 N/m^2$). The pressure signal is detrended first. k is computed with the linear dispersion relationship for each frequency in the timeseries. The peak frequency is determined and everything higher than $5 * f_p$ is removed from the pressure signal. The resulting waterlevel timeseries is not sensitive to the choice of this cutoff frequency. The maximum radial frequency is determined as $3 f_p 2\pi$ and the maximum wave number is determined with the linear dispersion relationship from the maximum radial frequency. With a Fourier transform the frequency components in the pressure signal are found and for each frequency component the water level is computed.

A spectrum is made from the waterlevel timeseries and the infragravity wave height is calculated as follows:

$$H_{m0,ig} = 4 \cdot \sqrt{\int_{0}^{0.05} E(f) df} \tag{K.5}$$

Check

To check whether the method works the incident wave height has been computed (between 0.05 and 0.25 Hz) and compared to the wave height data processed by Stockdon et al. (2014). They are almost the same with a mean difference of -0.04 m.

XBeach test cases

Introduction

In order to investigate the difference in generation of boundary conditions for the two XBeach models multiple simple test cases were performed. In this appendix an overview of these test cases is given. Cyclic boundary conditions were not used for the test cases.

Overview of the test cases

Table L.1: Overview of testcases used: their goal, boundary conditions and grid used.

Name case	Goal	Boundary conditions	Grid
1D JONSWAP	Compare infragravity wave height transformation in 1D for a simple spectrum	Narrow JONSWAP spectrum without directional spreading	1D grid of Duck
1D JONSWAP H	As above but with a higher offshore wave height	Narrow JONSWAP spectrum without directional spreading	1D grid of Duck
2D JONSWAP s20 (also s64, s200, s1030)	Investigate the effect of directional spreading on infragravity wave height transformation	Narrow JONSWAP spectrum with different degrees of directional spreading	2D alongshore uniform grid of Duck
2D JONSWAP s20 H (also s64, s200, s1030)	As above but with a higher offshore wave height	Narrow JONSWAP spectrum with different degrees of directional spreading	2D alongshore uniform grid of Duck
2D JONSWAP IG s20 (also s64, s200, s1030)	Compare infragravity wave height when only simulating infragravity waves	Narrow JONSWAP spectrum with different degrees of directional spreading	2D grid with a horizontal bottom and no beach
2D JONSWAP INC s20 (also s64, s200, s1030)	Compare infragravity wave height when only simulating incident waves	Narrow JONSWAP spectrum with different degrees of directional spreading	2D grid with a horizontal bottom and no beach

1D JONSWAP

A 1D testcase on the grid of Duck was set up for both XBeach Non-hydrostatic and XBeach Surfbeat, with the goal to compare infragravity wave heights at the boundary and infragravity wave height transformation for the simplest case possible.

A 1D grid of Duck was generated from the full 2D grid. One alongshore transect was selected: the same was chosen as was used in all other analyses (y = 198 m), which is approximately in the middle of the domain. Instead of the offshore boundary conditions abs 2d abs 1d was used.

The 1D model was forced with a simple JONSWAP spectrum: a narrow spectrum was used without directional spreading (s = 1030). Two significant wave heights of the JONSWAP spectrum were used: 0.96 m (mean offshore wave height during SandyDuck'97) and 1.6 m.

2D JONSWAP

A 2D testcase with an adapted grid of Duck was set up for both XBeach Non-hydrostatic and XBeach Surfbeat, with the goal to compare infragravity wave heights at the boundary and infragravity wave height transformation for a simple 2D case with different degrees of directional spreading imposed on the boundary.

From the 1D grid of Duck used in the 1D JONSWAP test case a 2D alongshore uniform grid was constructed.

The model was forced with a simple JONSWAP spectrum: a narrow spectrum was used with different degrees of directional spreading (s = 1030, s = 200, s = 64 and s = 20). The 2D model with s = 1030 should be similar to the 1D JONSWAP testcase. The directional spread in radians can be computed from the s-value as follows (Roelvink et al., 2010):

$$\theta_{spread} = \sqrt{\frac{2}{s+1}} \tag{L.1}$$

This results in the following values of θ_{spread} in degrees: 2.52, 5.73, 10.31 and 17.76 °. Two significant wave heights of the JONSWAP spectrum were used: 0.96 m (mean offshore wave height during SandyDuck'97) and 1.6 m.

2D JONSWAP IG and INC

A 2D testcase with a horizontal bottom and an absorbing boundary (no beach) with either only enforcing infragravity or incident waves at the offshore boundary was set up for both XBeach Non-hydrostatic and XBeach Surfbeat, with the goal to compare infragravity wave heights at the boundary while excluding reflected waves and shoaling effects.

A 2D grid with a horizontal bottom and a constant depth of 8 meters was used. For the nearshore boundary an absorbing boundary conditions was used, letting through and not reflecting the waves.

The model was forced with a simple JONSWAP spectrum: a narrow spectrum was used with different degrees of directional spreading (s = 1030, s = 200, s = 64 and s = 20). For the 2D JONSWAP IG case a new switch in XBeach was implemented which makes sure only infragravity waves are generated from the spectrum and the incident energy is set to zero. For the 2D JONSWAP INC case order = 1 was used to only have first order wave steering (incident wave energy only).

M
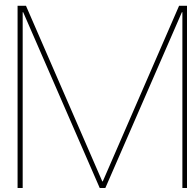
Analyses for the total wave field

Introduction

In chapter 5 all the analyses are done for the incoming waves. To estimate the effect of using the 1D Guza method on a 2D wave field the transformation of the infragravity wave height, the groupiness and the phase difference are shown here for the total wave field.

Infragravity wave height

The same figure as figure 5.1 is shown here for the total wave field, see figure M.1. The mean difference in a is larger than for the incoming infragravity waves, as there is not only a difference in propagation but also in reflection (and propagation back). However, the trends are the same: XBeach Non-hydrostatic generally predicts a larger infragravity wave height over the entire cross shore. Also the transformation for the three specific cases in b looks similar.

Groupiness

The groupiness for the total wave field can only be computed for XBeach Non-hydrostatic, as the incident wave output from XBeach Surfbeat is automatically split into incoming and reflected. For XBeach Non-hydrostatic the groupiness factor is very similar for incoming or total waves, as can be seen in figure M.2 for a few specific cases.

Phase difference

Again $\rho_{lf,hf}$ for the total wave field can only be determined for XBeach Non-hydrostatic. $\rho_{lf,hf}$ is very similar for the total wave field or the incoming wave field, see figure M.3.
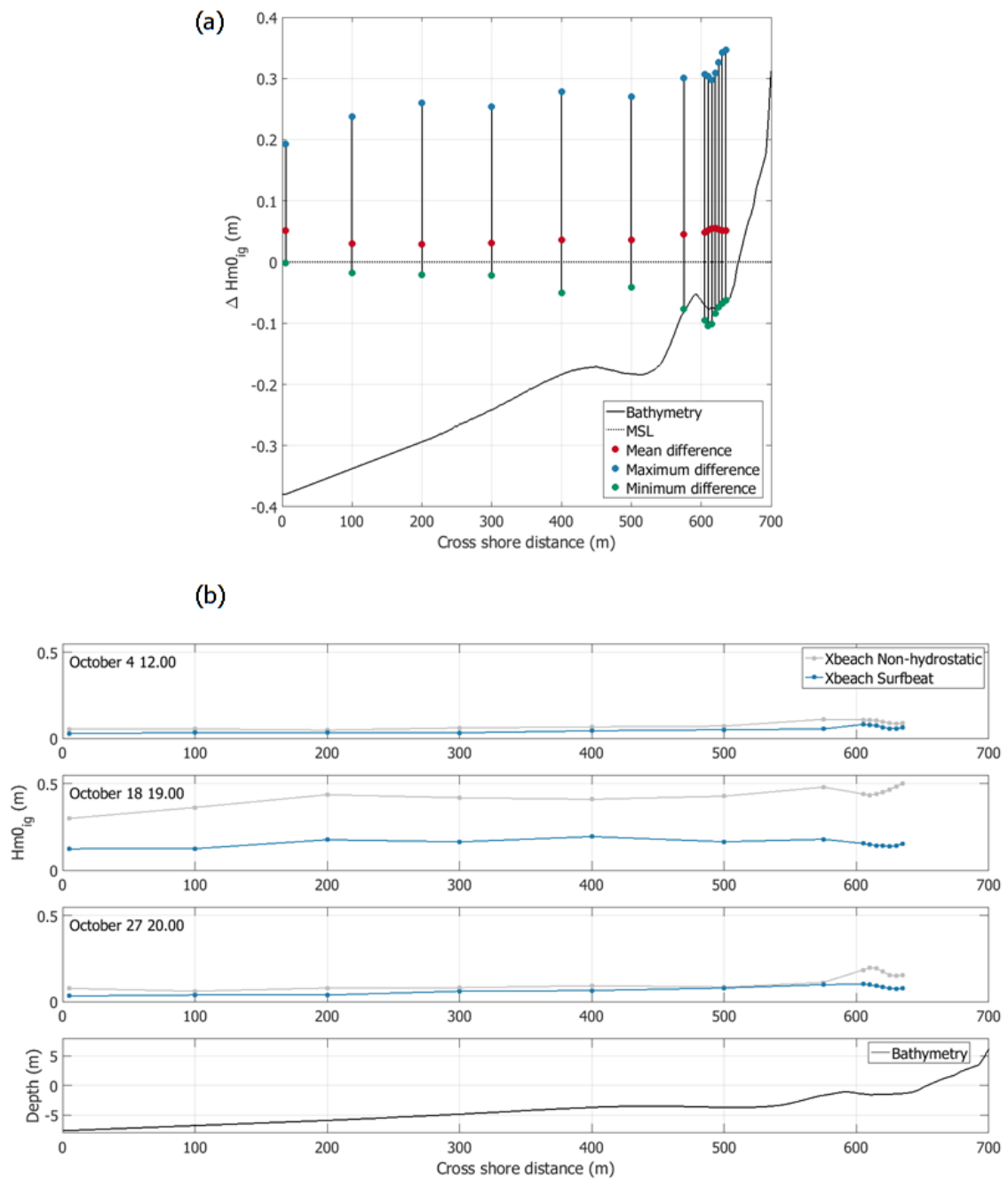
Figure M.1: Transformation of the total infragravity wave heigth over the cross shore for both XBeach models. (a) Transformation of the maximum, mean and minimum difference between XBeach Non-hydrostatic and XBeach Surfbeat over the cross shore. (b) Transformation of the total infragravity wave height over the cross shore for both XBeach models.
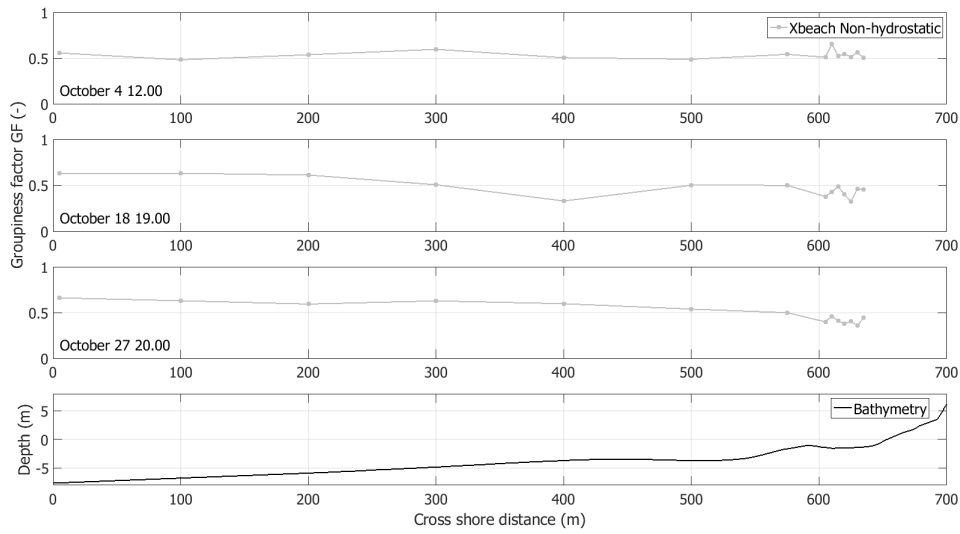
Figure M.2: Transformation of GF over the cross shore for the total wave field of XBeach Non-hydrostatic and a few specific cases.
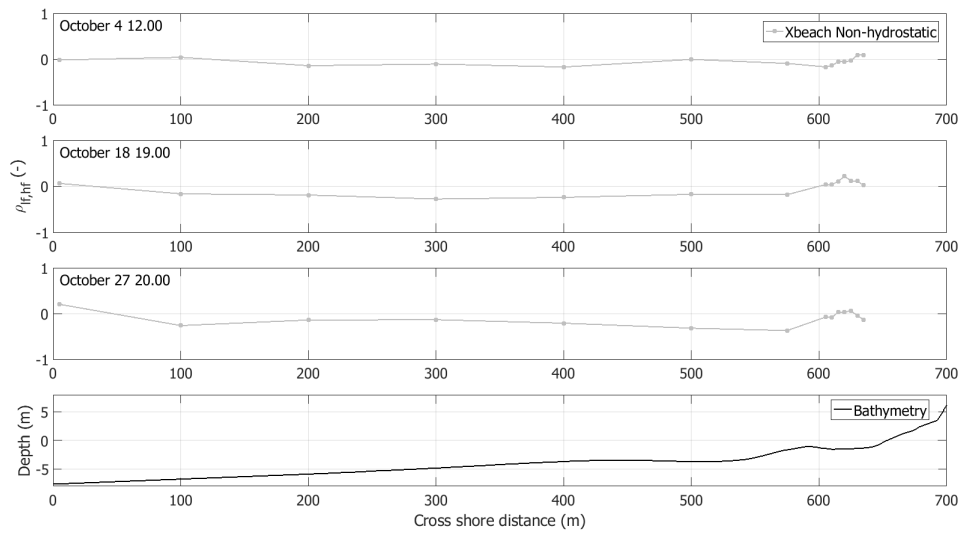
Figure M.3: Transformation of $\rho_{lf,hf}$ over the cross shore for the total wave field of XBeach Non-hydrostatic and a few specific cases.